

**OFFICE OF CIVILIAN RADIOACTIVE WASTE MANAGEMENT
ANALYSIS/MODEL COVER SHEET**

1. QA: QA

Complete Only Applicable Items

Page: 1 of 90

2. ☐ **Analysis** Check all that apply

| | |
|--------------------------|---|
| Type of Analysis | <input type="checkbox"/> Engineering |
| | <input type="checkbox"/> Performance Assessment |
| | <input type="checkbox"/> Scientific |
| Intended Use of Analysis | <input type="checkbox"/> Input to Calculation |
| | <input type="checkbox"/> Input to another Analysis or Model |
| | <input type="checkbox"/> Input to Technical Document |
| | <input type="checkbox"/> Input to other Technical Products |
| Describe use: | |
| | |
| | |

3. ☒ **Model** Check all that apply

| | | |
|---|--|---|
| Type of Model | <input checked="" type="checkbox"/> Conceptual Model | <input checked="" type="checkbox"/> Abstraction Model |
| | <input checked="" type="checkbox"/> Mathematical Model | <input type="checkbox"/> System Model |
| | <input type="checkbox"/> Process Model | |
| Intended Use of Model | <input type="checkbox"/> Input to Calculation | |
| | <input checked="" type="checkbox"/> Input to another Model or Analysis | |
| | <input type="checkbox"/> Input to Technical Document | |
| | <input checked="" type="checkbox"/> Input to other Technical Products | |
| Describe use: | | |
| The abstraction for flow and transport of radionuclides | | |
| in the Engineered Barrier System will be incorporated | | |
| into the GoldSim model for the TSPA-LA. | | |

4. Title:

EBS Radionuclide Transport Abstraction

5. Document Identifier (including Rev. No. and Change No., if applicable):

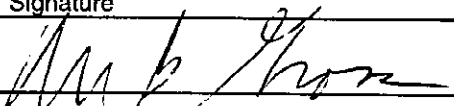
ANL-WIS-PA-000001 REV 00

6. Total Attachments:

Two

7. Attachment Numbers - No. of Pages in Each:

I - 3 pages, II - 3 pages

| | Printed Name | Signature | Date |
|-------------------------|---------------------|--|-----------|
| 8. Originator | Michael B. Gross |  | 4/12/2000 |
| 9. Checkers | David K. Rudeen | Robert MacKinnon for DR | 4/12/2000 |
| | James D Schreiber | Robert MacKinnon for JS | 4/12/2000 |
| 10. Lead/Supervisor | Robert J. MacKinnon | Robert MacKinnon | 4/14/00 |
| 11. Responsible Manager | Robert J. MacKinnon | Robert MacKinnon | 4/14/00 |

12. Remarks:

**OFFICE OF CIVILIAN RADIOACTIVE WASTE MANAGEMENT
ANALYSIS/MODEL REVISION RECORD**

Complete Only Applicable Items

1. Page: 2 of 90

2. Analysis or Model Title:

EBS Radionuclide Transport Abstraction

3. Document Identifier (including Rev. No. and Change No., if applicable):

ANL-WIS-PA-000001 REV 00

4. Revision/Change No.

5. Description of Revision/Change

00

Initial Issue

CONTENTS

| | Page |
|---|------|
| ACRONYMS | 6 |
| 1. PURPOSE | 8 |
| 2. QUALITY ASSURANCE | 9 |
| 3. COMPUTER SOFTWARE AND MODEL USAGE | 9 |
| 3.1 COMPUTER SOFTWARE | 9 |
| 3.2 MODELS | 9 |
| 4. INPUTS | 9 |
| 4.1 DATA AND PARAMETERS | 9 |
| 4.2 CRITERIA | 11 |
| 4.2.1 NRC IRSR Criteria for the ENFE KTI | 12 |
| 4.2.2 NRC IRSR Criteria for the CLST KTI | 15 |
| 4.2.3 NRC IRSR Criteria for the TEF KTI | 17 |
| 4.2.4 YMP Features, Events and Processes (FEPs) | 18 |
| 4.3 CODES AND STANDARDS | 20 |
| 5. ASSUMPTIONS | 20 |
| 5.1 EBS FLOW | 20 |
| 5.2 RADIONUCLIDE TRANSPORT THROUGH THE EBS | 26 |
| 5.3 DRIP SHIELD RESPONSE | 29 |
| 5.4 BATHTUB MODEL | 29 |
| 6. ANALYSIS/MODEL | 30 |
| 6.1 INTRODUCTION AND OVERVIEW | 31 |
| 6.1.1 EBS Flow Abstraction | 33 |
| 6.1.2 EBS Transport Abstraction | 36 |
| 6.1.3 Thermal and Mechanical Abstraction for Drip Shield Response | 38 |
| 6.2 FLUX IN THE BACKFILL & THROUGH THE DRIP SHIELD ($F_1 - F_4$) | 38 |
| 6.2.1 Water Movement Into and Through a Drift (F_1 , F_2 , and F_4) | 38 |
| 6.2.2 Drip Shield Effectiveness | 41 |
| 6.2.3 Drip Shield Breaching | 42 |
| 6.2.4 Water Flux Through and Around a Breached Drip Shield (F_3 and F_4) | 44 |
| 6.3 FLUX INTO AND AROUND THE WASTE PACKAGE ($F_5 - F_9$) | 45 |
| 6.3.1 Breaching of the Waste Package | 46 |
| 6.3.2 Flux Through and Around the WP (F_5 and F_6) | 49 |
| 6.3.3 Evaporation from the Invert and Condensation on the Drip Shield (F_7) | 51 |
| 6.3.4 Flux Into and Through the Invert (F_8 and F_9) | 52 |
| 6.4 TRANSPORT THROUGH THE EBS | 52 |
| 6.4.1 Diffusion Coefficient Abstraction | 53 |

| | | |
|-------|--|------|
| 6.4.2 | Colloidal Transport..... | 57 |
| 6.4.3 | Transport Through Stress Corrosion Cracks | 58 |
| 6.5 | DRIP SHIELD RESPONSE | 59 |
| 6.5.1 | Thermal Expansion..... | 60 |
| 6.5.2 | Floor Heave | 61 |
| 6.5.3 | Rock Fall for the As-Emplaced DS Configuration..... | 61 |
| 6.5.4 | Seismic Response | 64 |
| 6.5.5 | Pedestal Failure..... | 66 |
| 6.6 | BATHTUB MODEL FOR THE WASTE PACKAGE..... | 66 |
| 6.6.1 | Primary Case..... | 67 |
| 6.6.2 | Secondary Cases | 70 |
| 6.6.3 | Summary..... | 76 |
| 7. | CONCLUSIONS..... | 77 |
| 7.1 | CONCEPTUAL MODEL SUMMARY..... | 77 |
| 7.2 | EVALUATION OF NRC ISSUE RESOLUTION STATUS REPORT CRITERIA | 82 |
| 7.3 | RECOMMENDATIONS FOR FUTURE WORK | 83 |
| 7.4 | TO BE VERIFIED (TBV) IMPACT..... | 83 |
| 7.5 | FEPS EVALUATION..... | 84 |
| 8. | REFERENCES..... | 84 |
| 8.1 | DOCUMENTS CITED..... | 84 |
| 8.2 | CODES, STANDARDS, REGULATIONS, AND PROCEDURES | 88 |
| 8.3 | SOURCE DATA, LISTED BY DATA TRACKING NUMBER..... | 89 |
| 9. | ATTACHMENTS | 90 |
| I. | SLIPPAGE AND OVERLAP BETWEEN ADJACENT DRIP SHIELDS | I-1 |
| II. | ANALYTIC SOLUTION FOR THE PRIMARY CASE, $t > T_{fill}$ | II-1 |

FIGURES

| | Page |
|--|-------------|
| Figure 1. Schematic Diagram of a Typical Emplacement Drift and the Major Components of the EBS | 32 |
| Figure 2. Schematic of the Potential Flow Pathways in the EBS | 33 |
| Figure 3. Schematic of the Transport Pathways in the EBS | 36 |
| Figure 4. Schematic of the Dimensions for an Ellipsoidal Crack | 47 |
| Figure 5. Limiting Diffusion Coefficients for Anions and Simple (Non-Complexed) Cations. Selected from Mills and Lobo (1989), Appendix I, Tables 1.1 to 1.6; pgs. 314 to 319 | 56 |
| Figure 6. Schematic of the Bathtub Geometry for the Waste Package | 67 |

TABLES

| | Page |
|--|-------------|
| Table 1. Parameters for EBS Component Analyses and EBS RT Abstraction..... | 10 |
| Table 2. A Listing of YMP FEPs That Pertain to the EBS RT Abstraction..... | 19 |
| Table 3. Summary of Parameters for EBS Flow Pathways..... | 35 |
| Table 4. Summary of Transport Modes and Parameters for the EBS Transport Pathways..... | 37 |
| Table 5. Gap Width for a Range of Residual Stresses at 400°F (~200°C) in a 21-PWR Container | 47 |
| Table 6. Maximum Tilt Angle for the Four Types of Waste Packages. | 50 |
| Table 7. Compilation of Diffusion Coefficients for Molecular Iodine, Yttrium, Technitium, and Lanthanide and Actinide Species..... | 54 |
| Table 8. Summary of EBS Flow Abstraction..... | 79 |
| Table 9. Summary of EBS Transport Abstraction..... | 81 |

ACRONYMS

| | |
|-------|--|
| AMR | Analysis/Modeling Report |
| AP | Administrative Procedure |
| BWR | Boiling Water Reactor |
| CLST | Container Life and Source Term |
| CNWRA | Center for Nuclear Waste Regulatory Analyses |
| CRWMS | Civilian Radioactive Waste Management System |
| DOE | U. S. Department of Energy |
| DS | Drip Shield |
| EBS | Engineered Barrier System |
| EBSO | Engineered Barrier System Operations |
| ENFE | Evolution of the Near-Field Environment |
| FEP | Feature, Event and Process |
| HLW | High Level Waste |
| IRSR | Issue Resolution Status Report |
| KTI | Key Technical Issue |
| LA | License Application |
| M&O | Civilian Radioactive Waste Management System Management and Operating Contractor |
| MTU | Metric Tons of Uranium |
| MYPS | Multi-Year Planning System |
| NFE | Near-Field Environment |
| NRC | U.S. Nuclear Regulatory Commission |
| OCRWM | Office of Civilian Radioactive Waste Management |
| PAO | Performance Assessment Operations |
| PWR | Pressurized Water Reactor |
| QA | Quality Assurance |
| QAP | Quality Assurance Procedure |
| QARD | Quality Assurance Requirements and Description for the Civilian Radioactive Waste Management Program |
| SCC | Stress Corrosion Crack |
| SNF | Spent Nuclear Fuel |
| SR | Site Recommendation |
| TBV | To Be Verified |
| TEF | Thermal Effects on Flow |
| THC | Thermal-Hydrologic-Chemical |
| TSP | Total System Performance |

| | |
|---------|--|
| TSPA | Total System Performance Assessment |
| TSPA-LA | Total System Performance Assessment-License Application |
| TSPA-SR | Total System Performance Assessment-Site Recommendation |
| TSPA-VA | Total System Performance Assessment-Viability Assessment |
| UZ | Unsaturated Zone |
| WAPDEG | Waste Package Degradation Code |
| WP | Waste Package |
| WPO | Waste Package Operations |
| YM | Yucca Mountain |
| YMP | Yucca Mountain Site Characterization Project |

1. PURPOSE

The purpose of this work is to develop the Engineered Barrier System (EBS) radionuclide transport abstraction model, as directed by a written development plan (CRWMS M&O 1999a). This abstraction is the conceptual model that will be used to determine the rate of release of radionuclides from the EBS to the unsaturated zone (UZ) in the total system performance assessment-license application (TSPA-LA). In particular, this model will be used to quantify the time-dependent radionuclide releases from a failed waste package and their subsequent transport through the EBS to the emplacement drift wall/UZ interface.

The development of this conceptual model will allow Performance Assessment Operations (PAO) and its Engineered Barrier Performance Department to provide a more detailed and complete EBS flow and transport abstraction. The results from this conceptual model will allow PAO to address portions of the key technical issues (KTIs) presented in three NRC Issue Resolution Status Reports (IRSRs): (1) the Evolution of the Near-Field Environment (ENFE), Revision 2 (NRC 1999a), (2) the Container Life and Source Term (CLST), Revision 2 (NRC 1999b), and (3) the Thermal Effects on Flow (TEF), Revision 1 (NRC 1998). The conceptual model for flow and transport in the EBS will be referred to as the “EBS RT Abstraction” in this analysis/modeling report (AMR).

The scope of this abstraction and report is limited to flow and transport processes. More specifically, this AMR does not discuss elements of the TSPA-SR and TSPA-LA that relate to the EBS but are discussed in other AMRs. These elements include corrosion processes, radionuclide solubility limits, waste form dissolution rates and concentrations of colloidal particles that are generally represented as boundary conditions or input parameters for the EBS RT Abstraction. In effect, this AMR provides the algorithms for transporting radionuclides using the flow geometry and radionuclide concentrations determined by other elements of the TSPA-SR model. The scope of the EBS RT Abstraction also does not include computational or numerical procedures for solving the process-level equations; rather, it identifies the important processes that must then be evaluated with process-level or component-level software using analytical or numerical solutions.

Three iterations of the TSPA model are referred to in this AMR: (1) the viability assessment (TSPA-VA) that was completed and documented in 1998, (2) the site recommendation (TSPA-SR) that is currently underway, and (3) the license application (TSPA-LA) that will be submitted to the NRC. The text distinguishes between the current models and screening decisions for the TSPA-SR and the potential (future) changes to the EBS RT Abstraction for the TSPA-LA.

The emphasis in the EBS RT Abstraction is on a reasonable approach that bounds the response of the EBS. A reasonably bounding approach is appropriate for this abstraction because of the uncertainty in the response of a very complex engineered system over long periods of time. Areas where additional efforts can reduce the degree of conservatism or add more realism to the model have been identified, when appropriate.

2. QUALITY ASSURANCE

The Quality Assurance (QA) program applies to the development of documentation for the EBS RT Abstraction. A development plan, *Develop the EBS Radionuclide Transport Abstraction Model for TSPA-LA* (CRWMS M&O 1999a), has been completed for this work. The plan identifies the work package MYPS Number for this AMR as 1301213EM1.

The PAO responsible manager has evaluated this technical document development activity in accordance with QAP-2-0, *Conduct of Activities*. The QAP-2-0 activity evaluation, *Engineered Barrier System Performance Modeling* (CRWMS M&O 1999b), has determined that the preparation and review of this technical document is subject to *Quality Assurance Requirements and Description* (QARD) DOE/RW-0333P (DOE 2000) requirements. Preparation of this conceptual model did not require the classification of items in accordance with QAP-2-3, *Classification of Permanent Items*. This activity is not a field activity. Therefore, an evaluation in accordance with NLP-2-0, *Determination of Importance Evaluations*, was not required.

3. COMPUTER SOFTWARE AND MODEL USAGE

3.1 COMPUTER SOFTWARE

No codes or routines were developed for this analysis. No computer software was used to directly generate information for this AMR.

3.2 MODELS

The previous model used for EBS flow and transport is documented in Chapter 6 of the *Total System Performance Assessment-Viability Assessment (TSPA-VA) Analyses Technical Basis Document* (CRWMS M&O 1998a). This conceptual model document is being developed to supersede the concepts presented in Chapter 6 of the Technical Basis Document. More specifically, design changes since the TSPA-VA model was formulated have required reevaluation and, in some cases, substantial changes to the EBS flow and transport abstraction model. These design changes include the presence of a DS, the presence of backfill around the DS, and the use of crushed tuff rather than concrete in the invert.

4. INPUTS

4.1 DATA AND PARAMETERS

For TSPA-Site Recommendation/License Application (TSPA-SR, TSPA-LA) analyses, requests were made by PAO to Waste Package Operations (WPO) and Engineered Barrier System Operations (EBSO) to obtain the appropriate information for EBS conceptual model development. Each organization responded using AP-3.14Q, *Transmittal of Input*, to provide the requested information (CRWMS M&O 1999c; CRWMS M&O 1999d; CRWMS M&O 1999e; CRWMS M&O 1999f; CRWMS M&O 1999g; CRWMS M&O 1999h; CRWMS M&O 2000a). Because these inputs are not all qualified or accepted, they are considered TBV inputs.

However, these inputs do contain some qualified and accepted data. Table 1 summarizes the relevant input parameters and the sources for these values.

Table 1. Parameters for EBS Component Analyses and EBS RT Abstraction

| Model Input | Value | Source |
|---|---|-------------------------------------|
| Angle of repose for Overton sand backfill | 26° | SN9908T0872799.004 |
| Boltzmann constant | 1.380658×10^{-23} J/K | Lide 1997, p. 1-1 |
| Coefficient of linear thermal expansion for titanium | 5.2×10^{-6} °F ⁻¹ = 9.36×10^{-6} °C ⁻¹ | Baumeister 1967, p. 6-10 |
| Cross-sectional area for flow through a patch on the DS | 7.21×10^4 mm ² | CRWMS M&O 2000b, Section 5, page 28 |
| Cross-sectional area for flow through a patch on the WP | 2.346×10^4 mm ² | CRWMS M&O 2000b, Section 5, page 29 |
| Diameter of the drift | 5.5 m | SN9908T0872799.004 |
| Density of quartz sand (grain density) | 2700 kg/m ³ | SN9908T0872799.004 |
| Density of tuff (invert grain density) | 2530 kg/m ³ | SN9908T0872799.004 |
| Density of water at 0°C | 1000 kg/m ³ | Lide 1997, p. 6-3 |
| Distance from edge of DS to edge of lower connector guide | 100 mm | CRWMS M&O 1999c |
| Distance from edge of connector assembly to edge of upper connector guide | 50 mm | CRWMS M&O 1999e |
| Elementary electron charge | 1.602×10^{-19} Coulomb | Lide 1997, p. 1-1 |
| Maximum depth of invert | 606 mm | CRWMS M&O 1999d |
| Length of DS | 5780 mm | CRWMS M&O 1999c |
| Porosity of quartz sand backfill | 0.41 | SN9908T0872799.004 |
| Porosity of crushed tuff rock in the invert | 0.545 | CRWMS M&O 1999d |
| Radius to the midpoint of the DS as a circular shell | 1251 mm | CRWMS M&O 1999d |
| Rib-to-rib separation on top of DS | 1067 mm | CRWMS M&O 1999c |
| Self-diffusivity of water at 25°C | 2.299×10^{-5} cm ² /s | Mills 1973, Table III |
| Surface tension of water at 20°C | 0.0728 N/m | Lide 1997, p. 6-3 |
| Thickness of DS | 15 mm | CRWMS M&O 1999c |
| Viscosity of water at 20°C | 0.001 Pa-s | Lide 1997, p. 6-3 |
| Width of connector assembly | 610 mm | CRWMS M&O 1999e |
| Width of DS | 2250 mm | CRWMS M&O 1999c |
| Width of lower connector guide | 25 mm | CRWMS M&O 1999c |
| Width of upper connector guide | 25.4 mm | CRWMS M&O 1999e |
| WP closure lid gap | 30 mm | CRWMS M&O 1999f |
| WP outer layer thickness | 2 cm or 2.5 cm | CRWMS M&O 1999g |
| WP inner layer thickness | 5 cm | CRWMS M&O 1999g |
| WP outer lid thickness | 2.5 cm | CRWMS M&O 1999g |
| WP inner lid thickness | 8.0 cm or 12.5 cm | CRWMS M&O 1999g |
| Young's modulus of titanium | 14.8×10^6 psi | Baumeister 1967, p. 6-10 |
| 21 PWR Characteristics | | |
| WP outer diameter | 1.564 m | CRWMS M&O 1999g |
| WP length | 5.275 m | CRWMS M&O 1999g |
| Distance from bottom of WP to top of invert | 18.0 cm | CRWMS M&O 2000a |
| Distance from DS to top of WP | 58.8 cm | CRWMS M&O 2000a |
| Distance from DS to top of WP if pedestal collapse | 76.8 cm | Sum of two previous lines |
| WP porosity | 0.672 | CRWMS 1998b Table 5a |
| 44-BWR Characteristics | | |
| WP outer diameter | 1.594 m | CRWMS M&O 1999g |
| WP length | 5.275 m | CRWMS M&O 1999g |

| Model Input | Value | Source |
|--|----------------------|---------------------------|
| Distance from bottom of WP to top of invert | 18.3 cm | CRWMS M&O 2000a |
| Distance from DS to top of WP | 55.6 cm | CRWMS M&O 2000a |
| Distance from DS to top of WP if pedestal collapse | 73.9 cm | Sum of two previous lines |
| 5 HLW/DOE SNF | | |
| WP outer diameter | 2.030 m | CRWMS M&O 1999g |
| WP length | 3.730 m | CRWMS M&O 1999g |
| Distance from bottom of WP to top of invert | 21.6 cm | CRWMS M&O 2000a |
| Distance from DS to top of WP | 8.6 cm | CRWMS M&O 2000a |
| Distance from DS to top of WP if pedestal collapse | 30.2 cm | Sum of two previous lines |
| Naval SNF | | |
| WP outer diameter | 1.869 m | CRWMS M&O 1999g |
| WP length | 5.560 m | CRWMS M&O 1999g |
| Distance from bottom of WP to top of invert | 20.35 cm | CRWMS M&O 2000a |
| Distance from DS to top of WP | 26 cm | CRWMS M&O 2000a |
| Distance from DS to top of WP if pedestal collapse | 46.35 cm | Sum of two previous lines |
| Alloy 22 Parameters | | |
| Modulus of elasticity of Alloy 22 at room temp. | 206 GPa = 29,878 ksi | MO0003RIB00071.000 |
| Modulus of elasticity of Alloy 22 at 93°C | 203 GPa = 29,443 ksi | MO0003RIB00071.000 |
| Modulus of elasticity of Alloy 22 at 204°C | 196 GPa = 28,427 ksi | MO0003RIB00071.000 |
| Poisson's ratio of Alloy 22 | 0.278 | MO0003RIB00071.000 |
| Wetting angle water-Alloy 22 | 0 degrees | CRWMS M&O 1999h |

4.2 CRITERIA

Programmatic requirements for this document are listed in the Development Plan: *Develop the EBS Radionuclide Transport Abstraction Model for TSPA-LA* (CRWMS M&O 1999a). This Development Plan specifies that this document and all analyses described herein must adhere to the requirements of AP-3.10Q, *Analyses and Models*. This Plan also specifies that this AMR must address applicable NRC issue resolution status report (IRSR) acceptance criteria for three Key Technical Issues (KTIs): (1) Evaluation of the Near-Field Environment (ENFE) (NRC 1999a), (2) Container Life and Source Term (CLST) (NRC 1999b), and (3) Thermal Effects on Flow (TEF) (NRC 1998).

The following sections identify the NRC IRSR acceptance criteria for each of the three KTIs applicable to this Development Plan. Evaluations of these criteria are presented in Section 7.2. A listing of features, events and processes (FEPs) that apply to the EBS RT Abstraction is included in Section 4.2.4.

The NRC IRSR acceptance criteria are presented separately for each KTI. This is appropriate because each KTI has a distinct set of acceptance criteria and because only selected subissues within each KTI are applicable to the EBS RT Abstraction. The subissues that apply to EBS RT Abstraction model development for the ENFE KTI are: (a) the effects of coupled thermal-hydrologic-chemical (THC) processes on seepage and flow, and (b) the effects of coupled THC processes on radionuclide transport through engineered and natural barriers. The subissues that apply for the CLST KTI are: (a) subissue 3: the rate at which radionuclides in spent nuclear fuel

are released from the engineered barrier subsystem through the oxidation and dissolution of spent fuel, (b) subissue 4: the rate at which radionuclides in high-level waste glass are released from the engineered barrier subsystem, and (c) subissue 6: the effects of alternate engineered barrier subsystem design features on container lifetime and radionuclide release from the engineered barrier subsystem. The subissue that applies for the TEF KTI is subissue 3: “does the U.S. Department of Energy total system performance assessment adequately account for thermal effects on flow?”

Several task-specific criteria were also used during the EBS conceptual model development. The criterion to evaluate the potential impact of thermal and mechanical processes on DS separation (see Section 6.5) is to compare the calculated separation distance with the possible slippage or overlap between adjacent DSs. This overlap is created by the connector plate attached to each DS. Mechanisms that result in separations that are much less than the overlap have been screened out of the EBS conceptual model for the TSPA-SR. The criteria selected to evaluate the bathtub geometry (see Section 6.6) as an alternative conceptual model are: (1) radionuclide concentration leaving the WP, and (2) radionuclide mass flux leaving the WP. These are reasonable performance measures because they directly effect the concentrations and fluxes of radionuclides released to the EBS and ultimately to the affected population. No other criteria have been used in developing the EBS RT Abstraction.

4.2.1 NRC IRSR Criteria for the ENFE KTI

The acceptance criteria for the ENFE KTI are presented for two of the five major subissues for this KTI. The two subissues that are directly relevant to the EBS RT Abstraction are: (1) IRSR Section 4.1 – The Effects of Coupled Thermal-Hydrologic-Chemical Processes on Seepage and Flow, and (2) IRSR Section 4.4 – The Effects of Coupled Thermal-Hydrologic-Chemical Processes on Radionuclide Transport Through Engineered And Natural Barriers. The subissues in Sections 4.2, 4.3 and 4.5 of the IRSR relate to the waste package chemical environment, to the impact of the chemical environment on radionuclide release (mobilization), and to the potential for nuclear criticality in the near-field, respectively. These subissues are not directly relevant to the EBS RT Abstraction and are not discussed in this AMR.

The following sections present the technical and programmatic acceptance criteria from Sections 4.1 and 4.4 of the IRSR that are applicable to this AMR. Note that a single listing of the acceptance criteria is possible because the criteria in Sections 4.1 and 4.4 are very similar. The main difference between the criteria in Sections 4.1 and 4.4 relates to microbial issues that are not relevant to the EBS RT Abstraction.

4.2.1.1 Applicable Data and Model Justification Acceptance Criteria

1. Consider both temporal and spatial variations in THC effects on EBS flow and transport processes. (NRC 1999a, Sections 4.1.1 and 4.4.1)
2. Consider site characteristics in establishing initial and boundary conditions for conceptual models and simulations of coupled processes that may affect EBS flow and transport processes. (NRC 1999a, Sections 4.1.1 and 4.4.1)

3. Collect sufficient data on the characteristics of the natural system and engineered materials, such as the type, quantity, and reactivity of materials, to establish initial and boundary conditions for conceptual models and simulations of THC coupled processes that may affect EBS flow and transport. (NRC 1999a, Sections 4.1.1 and 4.4.1)
4. Use sensitivity and uncertainty analyses (including consideration of alternative conceptual models) to determine whether additional new data are needed to better define ranges of input parameters. (NRC 1999a, Sections 4.1.1 and 4.4.1)
5. If the testing program for coupled THC processes on the chemical environment for radionuclide release from the engineered barrier system is not complete at the time of license application, or if sensitivity and uncertainty analyses indicate that additional data are needed, DOE has identified specific plans to acquire the necessary information as part of the performance confirmation program. (NRC 1999a, Sections 4.1.1 and 4.4.1)

4.2.1.2 Applicable Data Uncertainty and Verification Acceptance Criteria

1. Use reasonable or conservative ranges of parameters or functional relations to determine effects of coupled THC processes on EBS flow and transport. Parameter values, assumed ranges, probability distributions, and bounding assumptions are technically defensible and reasonably account for uncertainties. (NRC 1999a, Sections 4.1.1 and 4.4.1)
2. Consider uncertainty in data due to both temporal and spatial variations in conditions affecting coupled THC effects on EBS flow and transport processes. (NRC 1999a, Sections 4.1.1 and 4.4.1)
3. Properly consider the uncertainties in the characteristics of the natural system and engineered materials, such as the type, quantity, and reactivity of materials, in establishing initial and boundary conditions for conceptual models and simulations of THC coupled processes that may affect EBS flow and transport. (NRC 1999a, Sections 4.1.1 and 4.4.1)
4. The initial conditions, boundary conditions, and computational domain used in sensitivity analysis involving coupled THC effects on EBS flow and transport processes should be consistent with available data. (NRC 1999a, Sections 4.1.1 and 4.4.1)
5. DOE's performance confirmation program should assess whether the natural system and engineered materials are functioning as intended and anticipated with regard to coupled THC effects on radionuclide release from the engineered barrier system. (NRC 1999a, Sections 4.1.1 and 4.4.1)

4.2.1.3 Model Uncertainty Acceptance Criteria

1. Use appropriate models, tests, and analyses that are sensitive to the THC couplings under consideration for both natural and engineered systems as described in the

following examples. The effects of THC coupled processes that may occur in the natural setting or due to interactions with engineered materials or their alteration products include: (i) Thermohydrologic (TH) effects on gas and water chemistry; (ii) hydrothermally driven geochemical reactions, such as zeolitization of volcanic glass and the precipitation and dissolution of oxides and hydroxides; (iii) dehydration of hydrous phases liberating moisture; (iv) effects of microbial processes; (v) effects of corrosion products on transport of radionuclides in the near field; and (vi) changes in water chemistry that may result from interactions between cementitious or WP materials and groundwater, which, in turn, may affect the environment for EBS flow and transport. (NRC 1999a, Sections 4.1.1 and 4.4.1)

2. Investigate alternative modeling approaches consistent with available data and current scientific understanding, and appropriately consider their results and limitations. (NRC 1999a, Sections 4.1.1 and 4.4.1)
3. Provide a reasonable description of the mathematical models included in analyses of coupled THC effects on EBS flow and transport processes. The description should include a discussion of alternative modeling approaches not considered in its final analysis and the limitations and uncertainties of the chosen model. (NRC 1999a, Sections 4.1.1 and 4.4.1)

4.2.1.4 Model Verification Acceptance Criteria

1. The mathematical models for coupled THC effects on EBS flow and transport should be consistent with conceptual models based on inferences about the near-field environment, field data and natural alteration observed at the site, and expected engineered materials. (NRC 1999a, Sections 4.1.1 and 4.4.1)
2. Appropriately adopted accepted and well-documented procedures to construct and test the numerical models should be used to simulate coupled THC effects on EBS flow and transport processes. (NRC 1999a, Sections 4.1.1 and 4.4.1)
3. Abstracted models for coupled THC effects on EBS flow and transport processes should be based on the same assumptions and approximations shown to be appropriate for closely analogous natural or experimental systems. Abstracted model results should be verified through comparison to outputs of detailed process models and empirical observations. Abstracted model results should be compared with different mathematical models to judge robustness of results (NRC 1999a, Sections 4.1.1 and 4.4.1)

4.2.1.5 Integration Acceptance Criteria

1. Consider all the relevant features, events and processes. The abstracted models should adequately incorporate important design features, physical phenomena, and couplings, and use consistent and appropriate assumptions throughout. (NRC 1999a, Sections 4.1.1 and 4.4.1)

2. The abstracted models should reasonably account for known temporal and spatial variations in conditions affecting coupled THC effects on seepage and flow. (NRC 1999a, Sections 4.1.1 and 4.4.1)
3. Assumptions may be used to simplify PA analyses if certain THC couplings are determined to be unimportant to performance. A firm technical basis will be provided if potentially important couplings are neglected. The technical basis can include activities such as independent modeling, laboratory and field data, or sensitivity studies. (NRC 1999a, Sections 4.1.1 and 4.4.1)
4. The bases used for modeling assumptions and approximations will be documented and justified if simplifications for modeling coupled THC effects on seepage and flow are used for PA analyses instead of detailed process models. (NRC 1999a, Sections 4.1.1 and 4.4.1)

4.2.1.6 Programmatic Acceptance Criteria

1. Data and models should be collected, developed, and documented under acceptable quality assurance (QA) procedures. (NRC 1999a, Sections 4.1.1 and 4.4.1)
2. Deficiency reports should be closed concerning data quality on issues related to coupled THC effects on seepage and flow. (NRC 1999a, Sections 4.1.1 and 4.4.1)
3. Expert elicitations should be conducted and documented in accordance with the guidance in NUREG-1562 (Kotra et al. 1996) or other acceptable approaches. (NRC 1999a, Sections 4.1.1 and 4.4.1)

4.2.2 NRC IRSR Criteria for the CLST KTI

The acceptance criteria for the CLST KTI are presented as a set of general acceptance criteria plus specific acceptance criteria for each subissue under this KTI. All general acceptance criteria are presented in the next subsection, followed by the criteria applicable to EBS flow and transport for the subissues (3, 4 and 6) that are relevant to the EBS RT Abstraction. Subissues 3 and 4 relate to the release of radionuclides from the EBS and subissue 6 relates to the effects of alternate EBS design features on radionuclide release.

4.2.2.1 General Acceptance Criteria For All Subissues

1. The collection and documentation of data, as well as development and documentation of analyses, methods, models, and codes, should be accomplished under approved quality assurance and control procedures and standards. (NRC 1999b, Section 4.0)
2. Expert elicitations, when used, should be conducted and documented in accordance with the guidance provided in NUREG-1563 (Kotra et al. 1996) or other acceptable approaches. (NRC 1999b, Section 4.0)

3. Sufficient data (field, laboratory, and natural analog) should be available to adequately define relevant parameters for the models used to evaluate performance aspects of the sub-issues. (NRC 1999b, Section 4.0)
4. Sensitivity and uncertainty analyses (including consideration of alternative conceptual models) should be used to determine whether additional data would be needed to better define ranges of input parameters. (NRC 1999b, Section 4.0)
5. Parameter values, assumed ranges, test data, probability distributions, and bounding assumptions used in the models should be technically defensible and can reasonably account for known uncertainties. (NRC 1999b, Section 4.0)
6. Mathematical model limitations and uncertainties in modeling were defined and documented. (NRC 1999b, Section 4.0)
7. Primary and alternative modeling approaches consistent with available data and current scientific understanding should be investigated and their results and limitations should be considered in evaluating the subissue. (NRC 1999b, Section 4.0)
8. Model outputs should be validated through comparisons with outputs of detailed process models, empirical observations, or both. (NRC 1999b, Section 4.0)
9. The structure and organization of process and abstracted models should adequately incorporate important design features, physical phenomena, and coupled processes. (NRC 1999b, Section 4.0)

4.2.2.2 Applicable Acceptance Criteria for Subissues 3 and 4

1. Identify and consider the likely processes for SNF or HLW degradation and the release of radionuclides from the EBS, as follows: dissolution of the irradiated UO₂ matrix, with the consequent formation of secondary minerals and colloids; prompt release of radionuclides; degradation in the dry air environment; degradation and failure of fuel cladding; preferential dissolution of intermetallics in DOE SNF and HLW; and release of radionuclides from the WP emplacement drifts. (NRC 1999b, Sections 4.3.1 and 4.4.1)
2. Demonstrate that the numerical models used for SNF/HLW degradation and radionuclide release from the EBS are adequate representations, including consideration of uncertainties, of the expected SNF/HLW performance and are not likely to overestimate the actual performance in the repository environment. (NRC 1999b, Sections 4.3.1 and 4.4.1)
3. Conduct a consistent, sufficient, and suitable SNF/HLW corrosion and radionuclide release testing program at the time of the LA submittal. In addition, identify specific plans for further testing to reduce any significant area(s) of uncertainty as part of the performance confirmation program. (NRC 1999b, Sections 4.3.1 and 4.4.1)

4. Establish an adequate program of monitoring radionuclide release from the WP during the performance confirmation period, to assure that assumptions and calculations of SNF/HLW dissolution and radionuclide release from the WP are appropriately substantiated. (NRC 1999b, Sections 4.3.1 and 4.4.1)

4.2.2.3 Applicable Acceptance Criteria for Subissue 6

1. Identify and consider the effects of backfill, and the timing of its emplacement, on the thermal loading of the repository, WP lifetime (including container corrosion and mechanical failure) , and the release of radionuclides from the EBS. (NRC 1999b, Section 4.6.1)
2. Identify and consider the effects of drip shields (with backfill) on WP lifetime, including extension of the humid-air corrosion regime, environmental effects, breakdown of drip shields and resulting mechanical impacts on WP, the potential for crevice corrosion at the junction between the WP and the drip shield, and the potential for condensate formation and dripping on the underside of the shield. (NRC 1999b, Section 4.6.1)
3. Justify the use of test results for drip shields, ceramic coatings, and backfill materials not specifically collected for the YM side for the environmental conditions expected to prevail at the proposed YM repository. (NRC 1999b, Section 4.6.1)

4.2.3 NRC IRSR Criteria for the TEF KTI

The acceptance criteria for the TEF KTI are presented for subissue 3: “does the U.S. Department of Energy total system performance assessment adequately account for thermal effects on flow?” Subissue 3 has elements that are directly relevant to the EBS RT Abstraction. Subissues 1 and 2 are generally concerned with thermohydrologic flow in the near-field rock environment and hence are less relevant to EBS flow and transport processes.

The following section presents the acceptance criteria for the two programmatic acceptance criteria and for the first three technical acceptance criteria. Technical acceptance criteria 4 through 7 are omitted because they are either covered in other general acceptance criteria or are not directly relevant to the EBS RT Abstraction.

4.2.3.1 Acceptance Criteria For Subissue 3

1. Develop and document analyses under acceptable QA procedures. (NRC 1998, Section 4.3.1).
2. Justify the use of abstracted models in the TSPA. This justification may include, but is not necessarily limited to, the use of expert elicitation. Expert elicitations should be conducted and documented in accordance with NUREG-1563 (Kotra et al., 1996) or other acceptable procedures. (NRC 1998, Section 4.3.1).
3. Abstractions of process-level models may be used if predictions from the abstracted model are shown to conservatively bound process-level predictions. In particular, an

abstracted model for influx of water into an emplacement drift may be used if the abstracted model is shown to bound process-level model predictions of the influx of water as liquid or vapor into an emplacement drift. (NRC 1998, Section 4.3.1).

4. Demonstrate that sufficient data are available to adequately define relevant parameters, parameter values and conceptual models. Specifically, DOE should demonstrate that (NRC 1998, Section 4.3.1):
 - Uncertainties and variabilities in parameter values are accounted for using defensible methods. Provide the technical bases for parameter ranges, probability distributions or bounding values. Derive parameter values (single values, ranges, probability distributions, or bounding values) from site-specific data or an analysis showing that the assumed parameter values lead to a conservative effect on performance.
 - Demonstrate that analyses are consistent with site characteristics in establishing initial conditions, boundary conditions, and computational domains for conceptual models.
5. Provide reasonably complete descriptions of the conceptual and mathematical models for the TSPA (NRC 1998, Section 4.3.1). Further, demonstrate that:
 - Performance affecting processes observed in available thermohydrologic tests and experiments have been identified and incorporated into the TSPA. Specifically, demonstrate that liquid water will not reflux into the underground facility or incorporate refluxing water into the TSPA and bound the potential adverse effects of: (i) corrosion of the WP; (ii) accelerated transport of radionuclides; and (iii) alteration of hydraulic and transport pathways that result from refluxing water.
 - Identify and incorporate Significant Geologic Repository Operations Area underground facility design features, such as the addition of backfill or drip shields, that can result in changes in TSP into the TSPA.
 - Define and document conceptual model uncertainties and assess their effects on conclusions regarding TSP.
 - Ensure that mathematical models are consistent with conceptual models, based on consideration of site characteristics.
 - Consider alternative models and modeling approaches to ensure that they are consistent with available data and current scientific understanding, that their limitations are defined, and that their results are appropriately considered.
 - Compare the results from different mathematical models to judge the robustness of results.

4.2.4 YMP Features, Events and Processes (FEPs)

Table 2 gives a listing of Yucca Mountain Project (YMP) FEPs (CRWMS M&O 1999i) that are relevant to the conceptual model for EBS flow and transport. YMP FEP # and NEA Category are part of the database search properties and are provided for convenience. Any resolution of these FEPs is discussed in Section 7.5.

Table 2. A Listing of YMP FEPs That Pertain to the EBS RT Abstraction

| YMP FEP # | NEA Category | FEP Name | Screening Decision for EBS |
|----------------------|-------------------------|---|---------------------------------------|
| 1.1.02.02.00 | ID-1 | Effects of pre-closure ventilation | Include |
| 2.1.03.01.00 | 2.1.03a | Corrosion of waste containers | Include |
| 2.1.03.10.00 | 2.1.03k | Container healing | Exclude |
| 2.1.03.12.00 | 2.1.03i | Container failure (long-term) | Include |
| 2.1.04.01.00 | 2.1.04u | Preferential pathways in the backfill | Include |
| 2.1.04.02.00 | 2.1.04au | Physical and chemical properties of backfill | Include |
| 2.1.04.04.00 | 2.1.04az | Mechanical effects of backfill | Include |
| 2.1.04.05.00 | 2.1.04b | Backfill evolution | Include |
| 2.1.04.08.00 | 2.1.04t | Diffusion in backfill | Exclude |
| 2.1.04.09.00 | 3.2.07r | Radionuclide transport through backfill | Exclude |
| 2.1.06.05.00 | 2.1.05p | Degradation of invert and pedestal | Include |
| 2.1.06.06.00 | WP-1 | Effects and degradation of DS | Include |
| 2.1.06.07.00 | 2.1.03o | Effects at material interfaces | Exclude |
| 2.1.07.01.00 | 2.1.07a | Rockfall (large block) | Exclude |
| 2.1.07.03.00 | 2.1.03bd | Movement of containers | Exclude |
| 2.1.07.06.00 | 2.1.07ad | Floor buckling | Exclude |
| 2.1.08.04.00 | 2.1.08e | Condensation forms on backs of drifts | Include |
| 2.1.08.05.00 | 2.1.08ad | Flow through invert | Include |
| 2.1.08.06.00 | 2.1.08y | Wicking in waste and EBS | Include |
| 2.1.08.07.00 | 2.1.03ax | Pathways for unsaturated flow and transport in the waste and EBS | Include |
| 2.1.08.09.00 | 2.1.08w | Saturated groundwater flow in waste and EBS | Exclude |
| 2.1.08.11.00 | 2.1.08m | Resaturation of repository | Include |
| 2.1.09.01.00 | 2.1.09k | Properties of the potential carrier plume in the waste and EBS | Include |
| 2.1.09.02.00 | 3.2.01i | Interaction with corrosion products | Exclude in EBS |
| 2.1.09.05.00 | 2.1.09bm | In-drift sorption | Exclude |
| 2.1.09.08.00 | 2.1.09bk | Chemical gradients / enhanced diffusion in waste and EBS | Exclude |
| 2.1.09.15.00 | 2.1.09c | Formation of true colloids in waste and EBS | Exclude in EBS |
| 2.1.09.19.00 | 3.2.04z | Colloid transport and sorption in the waste and EBS | Include |
| 2.1.09.20.00 | 3.2.04y | Colloid filtration in the waste and EBS | Exclude |
| 2.1.09.21.00 | 3.2.08c | Suspensions of particles larger than colloids | Exclude |
| 2.1.11.05.00 | 2.1.11ac | Differing thermal expansion of repository components | Exclude |
| 2.1.11.09.00 | 2.1.11ad | Thermal effects on liquid or two-phase fluid flow in the waste and EBS | Include |
| 2.1.11.10.00 | 2.1.11ag | Thermal effects on diffusion (Soret effect) in waste and EBS | Exclude |
| 2.1.13.02.00 | 2.1.13b | Radiation damage in waste and EBS | Exclude |
| 2.2.07.06.00 | ID-2 | Episodic/pulse release from repository | Include |
| 2.2.08.04.00 | 2.2.08c | Redissolution of precipitates directs more corrosive fluids to containers | Include |

4.3 CODES AND STANDARDS

This AMR was prepared to comply with the DOE interim guidance (Dyer 1999, which directs the use of the proposed NRC high-level waste rule, 10 CFR Part 63. Relevant requirements for performance assessment from Section 114 of that document are: “Any performance assessment used to demonstrate compliance with Sec. 113(b) shall: (a) Include data related to the geology, hydrology, and geochemistry ... used to define parameters and conceptual models used in the assessment. (b) Account for uncertainties and variabilities in parameter values and provide the technical basis for parameter ranges, probability distributions, or bounding values used in the performance assessment. ... (g) Provide the technical basis for models used in the performance assessment such as comparisons made with outputs of detailed process-level models”

The relevant codes, standards, regulations and procedures for the development of the EBS RT Abstraction are listed in Section 8.2.

5. ASSUMPTIONS

The assumptions for the abstraction for EBS flow, for the abstraction for EBS transport, for the DS separation model, and for an alternate conceptual model of flow through the WP (called the bathtub model) are presented in Sections 5.1, 5.2, 5.3, and 5.4, respectively. Note that assumptions are often stated in their most general form to encompass the potential for future design changes or new experimental data, even though certain processes may not occur. For example, corrosive processes for the WP may result in patches, pits or SCCs, although the local chemistry environment or WP fabrication techniques may prevent certain failure modes from occurring in Alloy 22.

5.1 EBS FLOW

The assumptions for the conceptual model for EBS flow are listed below.

5.1.1 Capillary fluxes are estimated assuming pressure equilibrium at the interface between the quartz sand backfill and the host rock.

The high capillarity of the Overton sand backfill relative to the capillarity for flowing fractures in the adjacent host rock results in the potential for backfill to wick water from the host rock. There is speculation as to whether sufficient connection exists between flowing fractures in the adjacent host rock and the backfill for wicking to occur. Simulations with the NUFT code assume sufficient connection for pressure equilibrium between the backfill and the host rock. (The NUFT code (Nitao 1998) provides numerical solutions for the coupled thermohydraulic response of the UZ and emplacement drifts, including the major components of the EBS). Until this issue is studied in more detail, the EBS RT Abstraction assumes a similar connection between the host rock and the backfill and includes a wicking flux in the PA calculations. This assumption is used in the discussions of capillary flow in Sections 6.2.1, 6.2.1.2, and 6.2.1.3.

5.1.2 Condensation on the inside of the DS occurs when the temperature of the DS is less than the temperature of the invert.

The inside of the DS will be filled with a mixture of air and water vapor. The source of the air is the general circulation of atmospheric gas through Yucca Mountain. The water vapor will be generated by evaporation from the invert. Water vapor can also be generated by evaporation from the surface of the WP, although the invert should be the dominant source while the DS is intact and diverts water away from the WP. Liquid water can condense on the inside of the DS when the temperature of the DS, T_{DS} , is less than the dew point of this air/vapor mixture.

Depending on vapor pressure gradients, the evaporated water from the invert can either move laterally away from the DS (i.e., to the right or left of the invert) or it can move upward to the inside of the DS. For example, the water vapor may move toward the drift walls by diffusing rapidly through the porous, high permeability materials in the invert and backfill. If this vapor condenses, it may do so in cooler regions where the relative humidity is high, perhaps on the walls of the drift. This flow pattern would tend to maintain wetter conditions on the outside of the DS, rather than beneath the DS. Note that the DS forms an inverted cap that will tend to trap any water vapor that moves upward.

As a first order approximation, the space between the DS and WP can be treated as a closed system because of the geometry of the DS and invert. The vapor pressure of water beneath the DS will then be close to the equilibrium vapor pressure at the invert temperature, T_{INV} . In this case, comparison of the temperature in the invert (T_{INV}) and the temperature at the top of the DS (T_{DS}) provides a suitable indicator of the potential for condensation on the inside of the DS. That is, condensation will occur if $T_{INV} > T_{DS}$. This is a physically reasonable approximation in terms of providing an indicator for the direction of vapor pressure gradients. This assumption is a reasonably bounding one because the possibility of water vapor transport laterally away from the DS or through gaps in the DS is ignored. This assumption is used in Section 6.3.3.

A more accurate model of the evaporation/condensation process may be used in future TSPAs if experimental data from the ATLAS facility or computational data from NUFT analyses indicate that condensation is occurring.

5.1.3 If condensation occurs, it is assumed that the condensation flux on the DS is equal to the evaporative flux in the invert.

This is a reasonable bounding estimate if thermal conditions are relatively uniform beneath the DSs because some of the evaporative flux from the invert will escape through the backfill and host rock, rather than condense on the DS. If thermal conditions are nonuniform, then the local condensation flux could exceed the evaporation flux at some locations. This issue must be reevaluated for the final TSPA-LA design configuration. This assumption is used in Section 6.3.3.

- 5.1.4 If condensation occurs, it is assumed that all the condensation flux drips from the crown of the DS onto the WP.

This is a reasonably bounding assumption because droplets or thin films of liquid may flow down the sides of the DS, rather than fall on the WP. This assumption is used in Sections 6.3.2 and 6.3.3.

- 5.1.5 The advective flow (of water) in the backfill cannot reach the WPs as long as the integrity of the DS is maintained.

Three lines of reasoning are presented in Section 6.2.2 to defend this assumption.

- 5.1.6 Once the integrity of the DS is compromised, backfill is assumed to fill the axial space surrounding the WP.

This assumption bounds the expected behavior of the EBS, as explained in Section 6.2.3.2.

- 5.1.7 The total flux into the quartz sand is equal to the sum of the seepage flux and the capillary flux multiplied by a factor between 0 and 1.

The capillary flux is calculated in a potentially very conservative framework for two reasons. First, there is speculation as to whether sufficient connection exists between flowing fractures in the adjacent host rock and the backfill for wicking to occur. Simulations with the NUFT code conservatively assume sufficient connection for pressure equilibrium between the backfill and the host rock, but the validity of this equilibrium condition is uncertain. Second, future design changes may specify a coarser backfill that has minimal wicking potential relative to the fractures in the host rock or possibly no backfill at all. Given this situation, the capillary flux will be multiplied by a factor between 0 and 1 to represent the variations in backfill materials, EBS design and the coupling with the fractures in the host rock. The value of this factor will be determined by the PAO for specific analyses and designs in future TSPAs. This assumption is used in Section 6.2.1.

- 5.1.8 Flow of water through the backfill is a quasi-steady process in a homogeneous porous medium.

The overall flow through the backfill approaches a steady state condition because the inflow boundary condition (percolation flux) is generally constant. When the boundary condition does change, such as with a new climate, the flow will move to a new steady state condition. Breaching of the DS or WP can also change the flow geometry, but this effect is considered to be a perturbation to the overall capillary flux through the backfill. Finally, the fine Overton sand backfill should behave as a homogeneous, porous medium in the repository environment. This assumption is used in Sections 6.2.1 and 6.2.4.

- 5.1.9 The fluid flux through a patch or pit in the DS or WP is proportional to the ratio of the length of the penetration in the axial direction to the total axial length of the DS or WP. This assumption is equivalent to assuming that a patch or pit is always

located on the side (90° from the crown) of the DS or WP and that it can collect all fluid that drips or flows from the crown towards the penetration if the axial locations of source and penetration coincide.

Two types of fluxes are considered here: a dripping flux and a capillary-driven flux. A dripping flux may enter the EBS as a point source, either by dripping from fractures (i.e., seepage flux) or by dripping due to condensation. The simplest assumption is that the entire dripping flux could fall exactly at the crown of the DS or WP. This may not be an extreme assumption because preliminary experimental data from the ATLAS test facility seem to show that drips do occur preferentially from the region of the crown. While it is difficult to generalize from preliminary data, it is a reasonable bound to assume that dripping will fall at the crown and that a patch at any azimuthal location on the DS or WP will collect fluid if the axial location of the patch coincides with that of the drip.

A similar assumption is also used for a capillary-driven flux. The capillary flow through the sand backfill will be a complex, multidimensional flow field. Capillary effects should result in a more uniform distribution of effective sources for fluid flow through a penetration in the DS. However, assuming that the penetration is located on the side of the DS will again be a reasonable bounding estimate because any flux can enter the penetration if it is at the same axial location.

This assumption is used in Sections 6.2.4 and 6.3.2.

5.1.10 Fluid flux can pass through any patch on the surface of the WP, independent of its azimuthal location on the WP. Similarly, flow of a thin film through a stress corrosion crack (SCC) on the lid of the WP is independent of the location of the SCC on the lid.

Two general types of openings or breaches can exist in the WP due to corrosion. These are (1) SCCs that penetrate the weld of the lid and (2) patches resulting from general corrosion. Section 6.3.1.2 provides a detailed discussion of these two types of openings.

Fluid flux can pass through any patch on the surface of the WP, independent of its location on the upper or lower surface of the WP. This is a conservative assumption for the patches and pits on the lower half of the WP, where little inflow is expected to occur. Similarly, the dripping flux is assumed to flow through SCCs independent of location on the lid of the WP. This is again a bounding assumption for the SCCs because fluid is unlikely to reach any SCCs on the upper half of the lid. This assumption is used in Sections 6.2.4 and 6.3.2.

The fact that the fluid flux can advect through a single patch or pit is an additional bounding feature in the flow and transport model. This approach is consistent with the analyses showing that a flow-through model provides a bounding estimate with respect to a “bathtub” model for the WP (see Section 6.6).

5.1.11 Patch area on the DS is $7.21 \times 10^4 \text{ mm}^2$ and patch area on the WP is $2.346 \times 10^4 \text{ mm}^2$. The patches are assumed to be square for the purposes of the flux splitting algorithm.

WAPDEG calculates corrosion assuming 500 nodes and 1000 nodes on the DS and WP, respectively (CRWMS M&O 2000b). The equivalent patch area is then calculated as the total surface area divided by the number of nodes. Patches are assumed to be square for the purpose of determining axial length for the flux splitting algorithm. This is a reasonable assumption for large patches on the surface. This assumption is used in Sections 6.2.4 and 6.3.2.

5.1.12 Diversion of flux around a breached DS or WP is based on continuity of liquid flux. This assumption means that the sum of the flux that is diverted and the flux that penetrates the DS or WP equals the incident flux on the DS or WP.

This assumption is reasonable because continuity conserves liquid mass and because it is consistent with the response of a quasi-steady system. This assumption is used in Sections 6.2.1.3, 6.2.4, 6.3.2 and 6.3.4.

5.1.13 SCCs through the welded lid are assumed to be in the radial direction.

Tensile stress is required to drive an SCC through the thickness of the welded lid. Detailed finite-element analyses of the WP and welded lid show that tensile stresses exist for cracks oriented lengthwise in the radial direction. These same analyses also show that circumferentially-oriented cracks are highly unlikely to penetrate the lid because radial stress on the inside surface of the lid is compressive, not tensile. This assumption is used in Section 6.3.1.2.1.

5.1.14 The width of the weld on the inner surface of the outer lid of the WP is assumed to be 0.25 inches.

This is a typical engineering value for a welding operation. This assumption is used in Section 6.3.1.2.1.

5.1.15 The fluid flux onto the closure lid of the WP is reasonably bounded by assuming that the WP is tilted at the maximum angle possible beneath the DS. This flux is given by the ratio of the projected length of the end cap in the axial direction to the projected length of the total WP in the axial direction.

This maximum angle of tilt occurs when the skirt and lid end of the WP is elevated to the height of the inside of the DS while the other end rests on the invert. This assumption is used in Section 6.3.2.

5.1.16 All fluid that flows as a film on the closure lid of the WP is assumed to flow through a SCC, if present.

This is a bounding assumption for several reasons. First, a film that completely spans the opening of a SCC creates a differential in capillary forces that will prevent any further ingress of flowing water into the WP. Second, the presence of corrosion products in the

very small SCC may provide a capillary barrier for advective flux into the WP. In spite of these features, flow through a SCC has not been screened out. The potential for atmospheric pumping, hygroscopic salts in the WP, and the uncertainty about film thickness make it difficult to exclude fluid flow into the WP. The assumption that all the thin film flow can enter the WP is a reasonable bound for the TSPA-SR/TSPA-LA. This assumption is used in Section 6.3.2.

5.1.17 The potential for evaporation in and on the WP is ignored.

The heat released by spent fuel has the potential to evaporate fluid on or in the WP. This is an important process because advective transport is not possible if evaporation eliminates advective fluxes. Detailed calculations of the evaporative process, including the complexities in the internal geometry of fuel pins within the WPs and the small conduits for water vapor to escape through SCCs, are currently being performed. Until these data are available, evaporative processes are ignored. This assumption is used in Sections 6.3.3 and 6.3.2.

5.1.18 The stainless steel components of the WP provide no resistance to corrosion or flow. These components include the inner liner and inner lid of the WP.

Corrosion of the stainless steel inner shell will occur rapidly relative to corrosion of the Alloy 22 outer shell (CRWMS M&O 2000b). In this circumstance, no credit is allowed for the time to corrode any stainless steel component and a pathway through the WP is assumed to exist once the outer shell of Alloy 22 is breached. This assumption is a reasonably bounding assumption that is used in Section 6.3.2.

5.1.19 Seismic damage to the WP has been screened out because of low consequence to EBS performance.

The WP is a simple thick-walled cylindrical structure with end caps. The stainless steel inner shell is 5 cm thick and the Alloy 22 outer shell is 2 cm thick. This massive, compact structure will experience minimal strain and deformation from seismic loading in its “as-designed” condition. Seismic damage can be ignored for the “as-designed” WP.

Corrosion will reduce the structural integrity of the WP over time. At very early times, SCCs may penetrate the welded lids of the WP. SCCs may provide flow pathways into the WP, but should have negligible effect on the structural integrity of the WP. Similarly, general corrosion of the Alloy 22 will gradually reduce the thickness of the outer shell over longer time periods, but the 5 cm inner shell of stainless steel will still provide some strength for a partly corroded WP.

After several patches penetrate the outer shell due to general corrosion, the WP will become increasingly susceptible to damage from a seismic event. A seismic event may even collapse a badly corroded WP, although the consequence for performance will be modest because there are already several patches through the outer and inner shells so that

the changes in fluid flux through the WP and in radionuclide transport out of the WP should also be modest.

It is then reasonable to screen out the seismic response of the WP from the EBS RT Abstraction for Rev 0 of the TSPA-SR. More detailed calculations for the structural response of the WP under seismic loads and in varying states of corrosion will be performed for Rev 01 of the TSPA-SR or for the TSPA-LA. This assumption has been used in Sections 6.3.1 and 6.3.2.

5.1.20 The advective flow for radionuclide transport is a one-dimensional process and always vertically downward.

Advective transport will occur predominantly in the direction of advective flow (lateral dispersion can lead to transport perpendicular to the direction of flow). Advective flow in the backfill follows a complex, multi-dimensional pattern because of capillarity in the finely grained backfill. Similarly, the advective flow field through openings in the DS and onto the WPs can also be multi-dimensional.

In spite of the complex flow patterns outside the WP, fluid must first enter a WP in order to mobilize radionuclides for advective transport. Once the radionuclides are mobilized within the WP, the advective flow will be predominantly directed downward from the WP to the invert and then to the UZ. Since advective transport through the backfill and DS can be ignored (because the radionuclides are not yet mobilized), the assumption of one-dimensional, downward advective flow from WP to the UZ is a physically reasonable assumption for the EBS RT Abstraction. This assumption is inherent in the EBS flow abstraction discussed in Sections 6.2.1.3, 6.2.4, 6.3, 6.3.2, 6.3.3, and 6.3.4.

5.2 RADIONUCLIDE TRANSPORT THROUGH THE EBS

The key assumptions for the conceptual model for radionuclide transport are listed below.

5.2.1 Advective transport is represented as a one-dimensional process in the vertical direction and is always downward.

This assumption is a direct consequence of assumption 5.1.20 and is included here for clarity. This assumption is used in Section 6.4.

5.2.2 There is no transport through the quartz sand backfill.

Upward diffusion, through the backfill, is physically impossible before the DS fails because there is no continuous fluid pathway for diffusion. After the DS fails, advection through the DS and into the WP will be the dominant flow mechanism. In this situation, it is reasonable to neglect any upward or lateral diffusive transport through the quartz sand backfill. Downward diffusive transport from the WP to the invert and UZ is a physically reasonable assumption. This assumption is used in Section 6.4.

5.2.3 The effects of longitudinal and transverse dispersion are ignored.

Longitudinal dispersion is ignored because of the small length of the flow path in the invert and because the representation of WP and invert as single mixing cells implies substantial dispersion in the numerical model. Transverse dispersion is ignored because it is a reasonably bounding assumption for the TSPA-LA. This assumption is used in Section 6.4.

5.2.4 The diffusion coefficient of all relevant radionuclides is bounded by the self-diffusion coefficient for water.

The basis for using the self-diffusion coefficient of water is presented in Section 6.4.1.1. This is a reasonably bounding assumption for the TSPA-SR, as explained in Section 6.4.1.1. The value for the self-diffusivity of water is TBV (MO0002SPASDC00.002).

5.2.5 The diffusion coefficient for a radionuclide in a porous, partly saturated medium is given by the diffusion coefficient in water times the product of porosity and (liquid) saturation of the medium.

The diffusion coefficient for a radionuclide in a porous, partly saturated medium is reduced from the diffusion coefficient in water by the effective cross-sectional area of the wetted liquid pathways. The effective wetted area is proportional to the product of porosity and saturation (ϕs) because the porosity (ϕ) represents the total free volume available for water and the liquid saturation (s) represents the percent of this free volume that is actually filled with liquid. This assumption is an upper bound relative to Archie's law, which predicts that the diffusion coefficient is reduced by $\phi^{1.3}s^2$ for a granular medium like sand or crushed tuff. The more conservative approach is taken here because the data verifying Archie's law are TBV. This assumption is used in Section 6.4.1.2.

5.2.6 The cross-sectional area of a (corroded) patch is $7.21 \times 10^4 \text{ mm}^2$ on the DS and $2.346 \times 10^4 \text{ mm}^2$ on the WP.

WAPDEG calculates corrosion assuming 500 nodes and 1000 nodes on the DS and WP, respectively (CRWMS M&O 2000b). The patch area is calculated as the total surface area divided by the number of nodes. This assumption is used in Sections 6.2.4, 6.3.2, and 6.4.

5.2.7 Sorption of dissolved radionuclides is ignored in the WP and invert. That is, the partition coefficients for all dissolved radionuclides are assumed to be zero. Note that the creation of radionuclide-bearing colloids is allowed in the model.

Corrosion products from the spent fuel and WP have the potential to retard selected radionuclides in the EBS. However, sorption of radionuclides is ignored in the EBS. This is a bounding assumption for the TSPA-SR and TSPA-LA because it maximizes the immediate release of radionuclides. This assumption is used in Section 6.4.

5.2.8 Radionuclide transport through a SCC is limited to diffusive transport through a thin, continuous film that is always present.

There are two cases to consider here: (1) at early times after closure, when SCCs represent the only flow path into the WP, and (2) at later times, after at least one patch appears on the surface of the WP.

At early times, the location of SCCs in the weld of the closure lid and the physical geometry of the WP make it impossible to maintain an advective flux out of the WP. In other words, water can potentially flow in through a SCC by capillary forces, by atmospheric pumping or by hydrostatic head if the lid of the WP is tipped upward. However, these mechanisms and this geometry cannot support flow out of the WP because the SCCs are the only exit path at early times.

Other features of the WP make advective flow through a SCC unlikely. For example, each SCC will fill with corrosion products that will further impede advective flow and the WP is sealed with a double lid configuration, leading to a potentially tortuous advective flow path.

The geometry of the WP and SCCs and the other features of the system make an advective flow path through a SCC physically unrealistic at early times, when no patches exist on the WP.

At late times, there is the possibility that advective flow could enter a SCC and exit through a patch. While this flow path is possible, the cross-sectional area of a typical SCC is orders of magnitude less than that of a patch, so any flow through the SCC is negligible compared to the general advective flux through patches. In addition, corrosion products will further reduce the flux through the SCC. It is then reasonable to ignore advective flux through the SCC at late times in the TSPA-SR model.

In summary, the advective flux through an SCC can be neglected at both early and late times, so the only viable transport mechanism through an SCC is diffusive transport. In addition, the phenomenon of vapor pumping and the presence of hygroscopic salts in the waste make it impossible to eliminate the possibility of thin films forming a continuous liquid pathway that can support diffusive transport from the waste form through SCCs at all times. This assumption is used in Section 6.4.3.

5.2.9 The invert is assumed to be adjacent to the WP for diffusive release calculations.

This is a reasonably bounding assumption when advective fluxes in the EBS are zero. That is, diffusion cannot occur between the WP and invert without a continuous fluid pathway. This pathway does not exist at early times because the WP is supported on a pedestal. However, a diffusive pathway is assumed to exist at all times in the EBS RT Abstraction. This assumption is used in Section 6.4.

5.3 DRIP SHIELD RESPONSE

The key assumptions for the thermal and mechanical analysis of DS response are listed below.

5.3.1 Adjacent DSs can slip freely to relieve thermal stresses and seismic displacements.

Thermal expansion or a seismic event may cause slippage between adjacent DSs. Each DS is not bolted to the invert and is not bolted to its nearest neighbors. In addition, it is assumed that the weld (or other joining process) between the drip shield and the connector plate does not prevent free slippage between adjacent DSs. This assumption is used in Section 6.5.1, Section 6.5.4 and in Attachment I.

5.3.2 The maximum DS displacement from the 1-in-10,000 year earthquake is 250 mm.

A preliminary calculation has been performed to estimate the maximum DS displacement for the 1-in-10,000 year earthquake. This preliminary calculation and the assumptions that it is based on have not been reviewed and accepted by the seismic and structural experts on the CRWMS M&O team. The maximum displacement from this calculation, 250 mm, is data that must be verified by future analyses and will be listed as to be verified (TBV) in the project data set (MO0003SPASEI01.003). This assumption is used in Section 6.5.4.

5.3.3 The sand backfill is effective in spreading the load from a rock fall.

The backfill will act to distribute the load from a fallen block of rock over the full surface area of contact between sand and rock. This assumption is used in Section 6.5.3.

5.3.4 The impact of rock fall on the degraded DS has been screened out from Rev 00 of the TSPA-SR.

Rock fall will produce minor structural response in relation to the potential slippage or overlap between adjacent DSs for the as-emplaced DS configuration (see Section 6.5.3). As the DS degrades under general corrosion, more detailed calculations are required to predict the structural response for a given rock fall.

This impact of rock fall on the degraded DS has been screened out from the TSPA-SR until more detailed structural response calculations for the DS under various rock loads are available. This assumption is used in Section 6.5.3.

5.4 BATHTUB MODEL

The key assumptions for the primary analysis of the bathtub geometry as an alternate conceptual model are listed below.

5.4.1 The seepage inflow rate, waste form dissolution rate, and radionuclide solubility are independent of time.

This is a reasonable approach during the periods between climate changes, when groundwater conditions should be relatively constant. This assumption is used in Sections 6.6.1 and 6.6.2.

5.4.2 Kinetic effects are ignored in determining solubility limits for radionuclides.

This assumption implies that radionuclide concentration is uniform in the WP and determined by a maximum solubility limit or a maximum dissolution rate. This assumption also implies that radionuclide concentration in the WP is well-mixed and hence uniform. This assumption is used throughout Sections 6.6.1 and 6.6.2.

5.4.3 Once the bathtub has filled, steady state conditions prevail in the WP.

This assumption is consistent with the expectation that the groundwater influx equals the outflux after the bathtub has filled. This assumption is used throughout Sections 6.6.1 and 6.6.2.

5.4.4 The WP penetrations (patches or pits) are large enough that they provide no resistance to liquid inflow or outflow.

This assumption is consistent with the expectation that the groundwater influx equals the outflux after the bathtub has filled. This assumption is used in Sections 6.6.1.1, 6.6.1.2, 6.6.2.1, and 6.6.2.2.

5.4.5 The potential depletion of inventory is ignored.

This assumption is used throughout Section 6.6.

Secondary analyses in Section 6.6.2 consider a step change in seepage inflow rate, a step change in groundwater chemistry, or a different flow path geometry (i.e., alternate patch location). These alternatives require selective changes to the assumptions for the primary analyses. For example, the assumption of constant inflow rate for the primary analysis is modified for the alternative of changing inflow rate discussed in Section 6.6.2.1; however, all other assumptions remain the same.

6. ANALYSIS/MODEL

Given the complexity of the EBS and its components, it is useful to provide an overview of the EBS RT Abstraction for the TSPA-LA. This overview begins with a general description of the EBS components and is then divided into three parts: (1) the flow abstraction, (2) the transport abstraction, and (3) an abstraction for the thermal and mechanical response of the DS. Detailed discussion of the flow abstraction for the DS and the WP is provided in Sections 6.2 and 6.3, respectively. Section 6.4 describes the radionuclide transport abstraction. Section 6.5 presents the analyses related to DS separation under thermal and mechanical processes.

Section 6.6 analyzes the response of an alternate conceptual model for flow through the WP. This alternate model, called the bathtub model, allows fluid to collect in the WP before being released. The results in Section 6.6 demonstrate that a “flow through” model is conservative relative to a bathtub model for most cases of interest to repository performance. The detailed discussions of the EBS RT Abstraction are therefore based on the flow through model, with the rationale for screening out the bathtub model given at the end of this section.

6.1 INTRODUCTION AND OVERVIEW

The EBS consists of a *drip shield (DS)*, quartz sand *backfill*, the *waste package (WP)* on a *pedestal*, and an *invert* filled with crushed tuff. Each of these components is designed to prevent or delay the mobilization and release of radionuclides into the geologic environment. For example, the DS is designed to redirect any seepage that flows into the drift away from the WP. This is beneficial for system performance because the WP lifetime is much greater in a dry rather than a wet environment. The quartz sand backfill surrounding the DS is designed to cushion the impact from potential rock falls on the DS and WP. This is important because structural damage from rock falls can impair the integrity of the DS and WP and may accelerate corrosive processes. The quartz sand backfill may also act as a capillary barrier, diverting seepage away from the DS. The invert supports the WP and pedestal. It can act as a barrier to diffusive transport of radionuclides in liquids if the liquid saturation in the crushed tuff is low. Figure 1 presents a typical cross-section of an emplacement drift and the major components of the EBS.

The DS is fabricated from a highly corrosion resistant material (titanium) to provide long-term effectiveness. The WP is (partly) fabricated from another highly corrosion resistant material, nickel-based Alloy 22. The major corrosive processes are stress corrosion cracking in the welded lids of the WP and general corrosion for both the DS and WP.

Before the drip shield fails, the only possible fluid pathway to the WP is from water vapor evaporating from the invert, condensing on the inside of the DS, and then dripping down onto the WP. This pathway is hypothetical because thermal-hydrologic calculations indicate that condensation will not occur; however, it is retained in the EBS RT Abstraction for completeness.

Once the DS fails, the evaporative flux (if condensation occurs) will be augmented by the capillary flux through the backfill. The quartz sand backfill will fall through any gaps or patches of corroded material in the DS, partly filling any space around the WP. Note that the cross-sectional area between the DS and WP is much less than the cross-sectional area of sand backfill. The sand is therefore likely to form a continuous flow path between the backfill outside the DS and the WP inside the DS. When this occurs, water will flow onto the WP because of strong capillary forces in the fine sand backfill.

If the backfill acts as a capillary barrier, then the dominant flux into the EBS will be the seepage flux from the roof of the drift. Again, the DS must fail for this flux to fall or drip onto the WP through gaps between adjacent DSs or through patches in the DS.

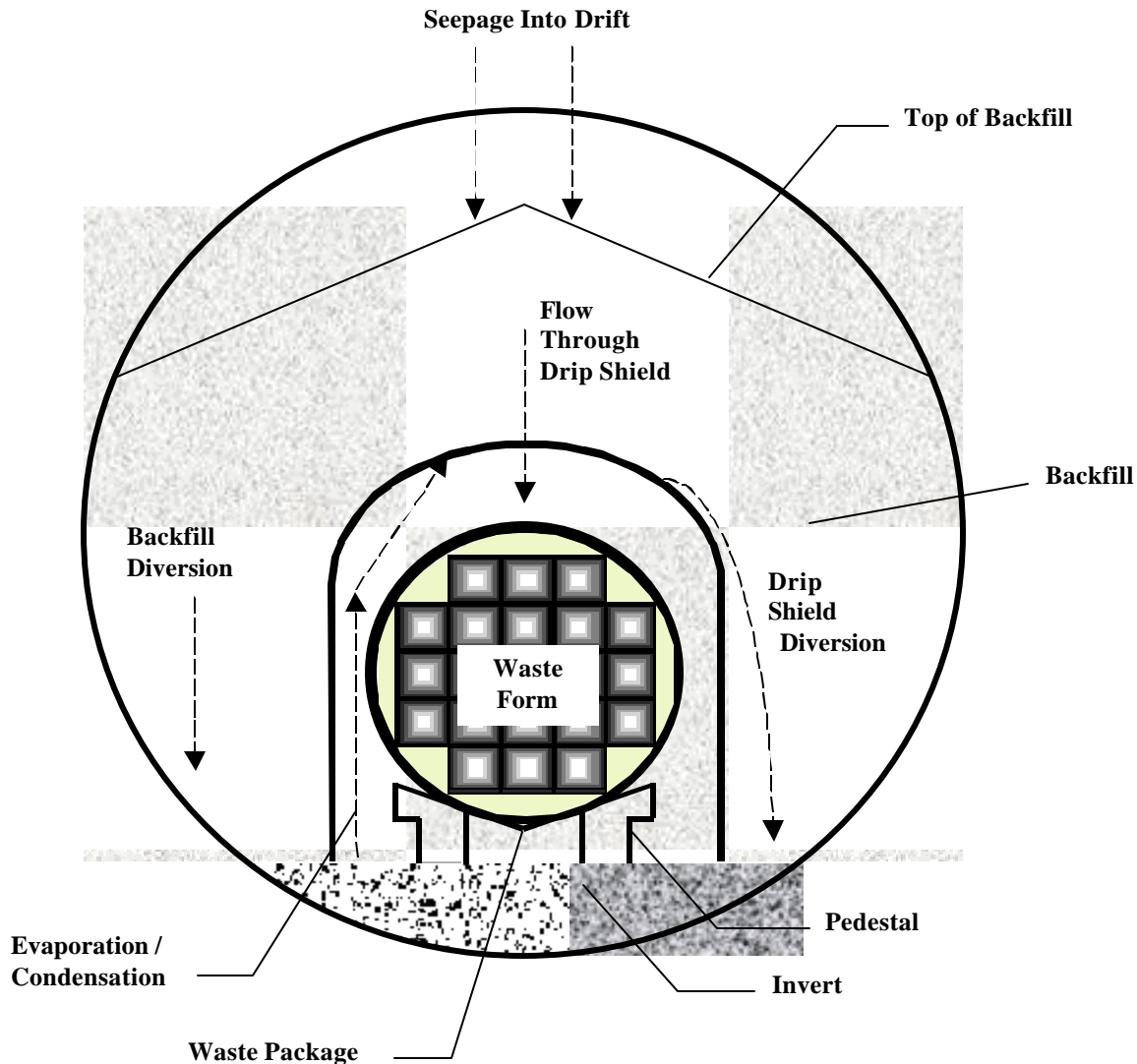


Figure 1. Schematic Diagram of a Typical Emplacement Drift and the Major Components of the EBS

It is possible that DS failure may occur over the gap between adjacent WPs. This is a reasonable scenario because the overlap between adjacent DSs is located over the gap and this overlap is a potential leakage pathway. If the DS fails at the gap, the quartz sand backfill will fall directly to the invert, possibly avoiding the WP and channeling flow directly into the invert. The possibility that DS failure can occur over a gap, allowing fluid to bypass the WP, is conservatively ignored in the EBS RT Abstraction.

After the WP fails, fluid can enter the WP, mobilize radionuclides in the waste form, and transport these radionuclides into the UZ. Diffusion is the primary transport mechanism at early times, when stress corrosion cracks (SCCs) are the only penetrations through the WP. Advective transport is also possible at late times, when substantial advective fluxes can pass through the corroded patches of the DS and WP.

6.1.1 EBS Flow Abstraction

The EBS has two potential sources of inflow. The first source is the seepage flux that drips from the crown (roof) of the drift. The second source is the capillary flux generated by the wicking forces between the rock fractures and the quartz sand backfill. Both fluxes are driven by downward infiltration through the existing fracture system at Yucca Mountain.

The seepage flux is conceptualized to flow from discrete fractures above the roof of the drift, falling vertically downward onto the quartz sand backfill. The seepage flux will be represented in the TSPA-LA model through an existing abstraction (CRWMS M&O 2000c). The capillary flux is conceptualized to be “wicked” from the fractures in the host rock in direct contact with the backfill. In effect, the fine-grained backfill draws the liquid from the fractures on the sides of the drift and passes it into the lower walls and floor of the drift. The capillary flux will be represented in the TSPA-SR and TSPA-LA models through an abstraction of thermal-hydrologic calculations of repository response generated with NUFT (CRWMS M&O 1999j).

These sources of inflow can flow through the EBS along 9 pathways, as shown in Figure 2.

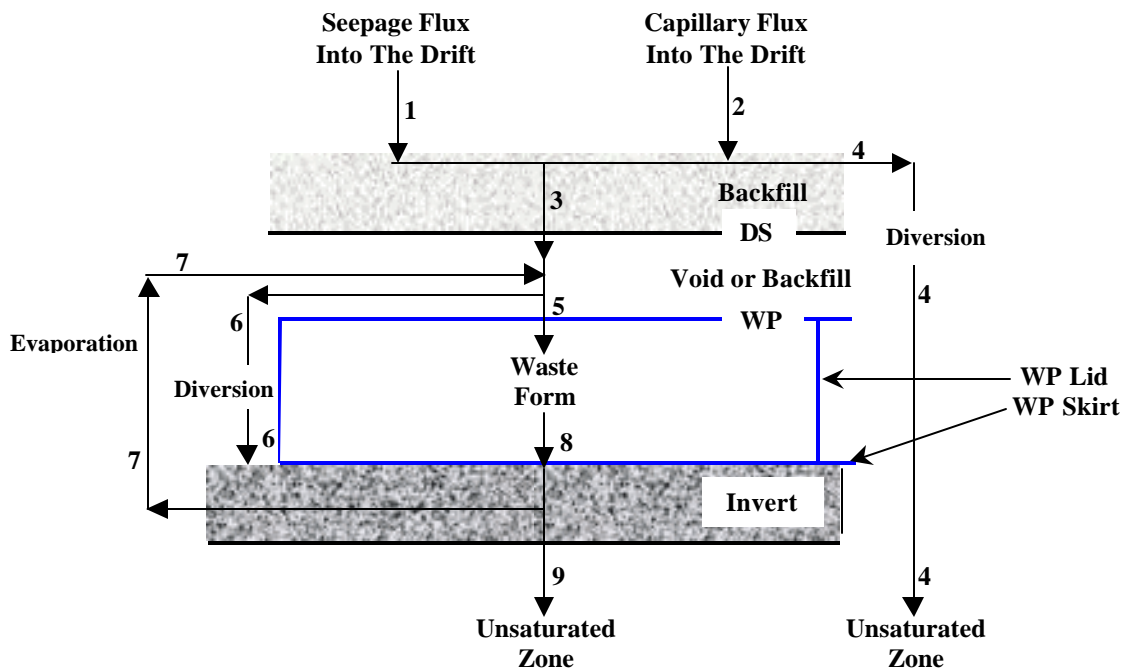


Figure 2. Schematic of the Potential Flow Pathways in the EBS

The nine pathways are:

1. Seepage flux. This is the dripping flux from the crown (roof) of the drift.
2. Capillary flux. This is the flux that is wicked into the drift due to the capillary forces between the fine-grained backfill and the fluid-filled fractures in the host rock.
3. Flux through the DS. The flux through the DS is based on the presence of patches due to general corrosion and gaps between adjacent DSs due to seismic events. The number of patches through the DS is calculated independently of the EBS RT Abstraction by the

WAPDEG code. The size of a patch is fixed for the WAPDEG calculations; it is currently defined to be $7.21 \times 10^4 \text{ mm}^2$, based on the equivalent area of 500 nodes on the surface of the DS (CRWMS M&O 2000b). The size of gaps in the DS due to seismic effects is calculated with the algorithm defined in Section 6.5.4. The fluid flux through any patches or through seismically-induced gaps is given by the ratio of the axial length of the penetration(s) in the DS to the total axial length of the DS (see Section 6.2.4).

4. Diversion around the DS. The portion of the flux that does not flow through the DS is assumed to bypass the EBS, going straight into the UZ (per assumption 5.1.12). This flux is a two-dimensional flow field because of the complex flow pattern through the backfill and around the DS.
5. Flux through the WP. The flux through the WP is based on the presence of SCCs and on patches due to general corrosion. The number of patches and SCCs through the WP is calculated independently of the EBS RT Abstraction by the WAPDEG code (CRWMS M&O 1998c). The size of a patch is fixed for the WAPDEG calculations; it is currently defined to be $2.346 \times 10^4 \text{ mm}^2$, based on the equivalent area of 1000 nodes on the surface of the WP (CRWMS M&O 2000b). The area of each SCC, $4.08 \times 10^{-6} \text{ m}^2$, is calculated in Section 6.3.1.2.1. The flux through patches or SCCs is based on ratios of the appropriate flow lengths for the surface of the WP or for the lid and skirt of the WP, respectively (see Section 6.3.2).
6. Diversion around the WP. The portion of the flux that does not flow into the WP is assumed to bypass the waste form, going straight into the invert (per assumption 5.1.12).
7. Evaporative flux. The magnitude of the evaporative flux from the invert is based on the abstraction of NUFT data. If the DS is cooler than the invert, then all the evaporative flux is assumed to drip on the WP (per assumption 5.1.3). If the DS is hotter than the invert, then there is no dripping on the WP from the evaporative flux.
8. Flux to the invert. All flux from the WP flows to the invert, independent of patch/pit location on the WP. The presence of the pedestal is ignored.
9. Flux to the UZ. All mass flux into the invert is released into the UZ.

It is important to note that these pathways are time dependent, in the sense that DS gaps, DS penetrations, and WP penetrations will vary with time and local conditions in the repository. For example, at very early times there may be no penetrations through the DS, so fluid can reach the WP only if pathway 7, evaporation from the invert and condensation on the DS, is active.

The conceptual model for flow through the EBS also includes two mixing cells: one for the WP (and internals) and a second for the invert. The two mixing cells are conceptualized to have a cylindrical, concentric one-dimensional geometry for volume calculations. The first cell has a diameter given by the diameter of the WP. The second cell (invert) wraps around the lower half of the WP and is 0.606 meters thick (CRWMS M&O 1999d). This is the maximum thickness of the invert directly beneath the WP (see Table 1). This value is appropriate because flow out of the WP is primarily vertically downward, through the thickest part of the invert.

The WP mixing cell represents the source term for the TSPA-LA. Source term abstractions for radionuclide solubility, dissolution rate, cladding response and inventory by waste package type are defined in other AMRs. The source term represents input data or boundary conditions for the EBS RT Abstraction and is not discussed in this document.

The final output from the EBS RT Abstraction is the mass flux of radionuclides from the EBS into the UZ. Note that the diversionary flows from the DS and WP (pathways 4 and 6) are not required outputs from the EBS RT Abstraction and are ignored by the TSPA-SR and TSPA-LA models. The parameters and formulas for calculating the fluxes in the various pathways are summarized in Table 3.

Table 3. Summary of Parameters for EBS Flow Pathways

| Flow Pathway | Flow Parameters | Data Sources & Notes |
|-----------------------------------|--|---|
| 1. Seepage flux, F_1 | Seepage flux is a function of fracture properties, rock properties, and the percolation flux. | (CRWMS M&O 2000c) provides time-dependent and location-dependent values of seepage flux. |
| 2. Capillary flux, F_2 | Capillary flux is a function of the moisture potential, f_m , of the quartz sand backfill, the infiltration flux, and the fracture properties of the host rock. Capillary flux into the EBS is reduced by a factor, α . This factor is chosen between 0 and 1 to reflect the differences in capillary flux for various design options. | f_m , T and RH will be abstracted from calculations with the NUFT code (CRWMS M&O 1999j). T is temperature and RH is relative humidity. |
| 3. Flux through the DS, F_3 | L_{DS_Patch} – axial length of patches due to general corrosion of Ti L_{DS_Pit} – 0 because pH<10 L_{DS_SCC} – probably 0 for Ti L_{DS_Gap} – axial length of total gap in the DS $F_3 = (F_1 + \alpha F_2) \times (L_{DS_SCC} + L_{DS_Patch} + L_{DS_Pit} + L_{DS_Gap}) / L_{DS}$ L_{DS} is the axial length of the DS. α is a factor between 0 and 1 based on the design and backfill properties; Backfill must form a continuous pathway for nonzero flow. | WAPDEG (CRWMS M&O 1998c) will provide the number of patches, pits and SCCs on the DS; Patch size is $7.21 \times 10^4 \text{ mm}^2$ (CRWMS M&O 2000b); $L_{DS_Patch} = (7.21 \times 10^4)^{0.5} = 269 \text{ mm}$ L_{DS_Gap} is calculated from a seismic response model (see Section 6.5.4) Limit F_3 such that $F_3 \leq (F_1 + F_2)$. |
| 4. Diversion around DS, F_4 | $F_4 = F_1 + \alpha F_2 - F_3$ | Continuity of liquid flux. Limit $F_4 \geq 0$. |
| 5. Flux into the WP, F_5 | L_{WP_Patch} – axial length of all patches due to general corrosion of Alloy 22 L_{WP_Pit} – probably 0 for Alloy 22 L_{WP_SCC} – projected axial length of closure lid directly exposed to fluid flux $F_5 = (F_3 + F_7) \times (L_{WP_Patch} + L_{WP_Pit}) / L_{WP} + F_7 (L_{WP_SCC}) / (L_{WP} + L_{WP_SCC})$ L_{WP} is the axial length of the WP. | WAPDEG will provide the number of patches, pits and SCCs on the WP; patch size is constant: $2.346 \times 10^4 \text{ mm}^2$ (CRWMS M&O 2000b); $L_{WP_Patch} = (2.346 \times 10^4)^{0.5} = 153 \text{ mm}$ L_{WP_SCC} is calculated based on the maximum tilt angle of the WP and the diameter of the closure lid (see Section 6.3.2) Limit F_5 such that $F_5 \leq F_3 + F_7$. |
| 6. Diversion around the WP, F_6 | $F_6 = F_3 + F_7 - F_5$ | Continuity of liquid flux. Limit $F_6 \geq 0$. |
| 7. Evaporative flux, F_7 | If $T_{DS} < T_{Invert}$, then F_7 is the evaporative flux calculated by NUFT; else $F_7 = 0$. | Data for temperatures and evaporative flux are based on an abstraction of NUFT calculations (CRWMS M&O 1999j). |
| 8. Flux to the invert, F_8 | $F_8 = F_5$ | Steady state, flow-through assumption for WP (outflow = |

| Flow Pathway | Flow Parameters | Data Sources & Notes |
|--------------------------|-------------------------|---|
| | | inflow in steady state; this is conservative for release; see Section 6.6) |
| 9. Flux to the UZ, F_9 | $F_9 = F_6 + F_8 - F_7$ | Steady state flow-through assumption for invert. Consistent with flow-through assumption for WP. Note that only F_8 can transport radionuclides through the invert. |

6.1.2 EBS Transport Abstraction

The waste form is the source of all radionuclides considered for the EBS. Radionuclides can be transported downward, through the invert and into the UZ, as shown Figure 3. Transport can occur through advection when there is a fluid flux through the WP and invert. Transport can also occur by diffusion, even in the absence of a liquid flux, if there is a continuous liquid pathway via thin films in the waste form, in SCCs in the lid of the WP, and in the invert.

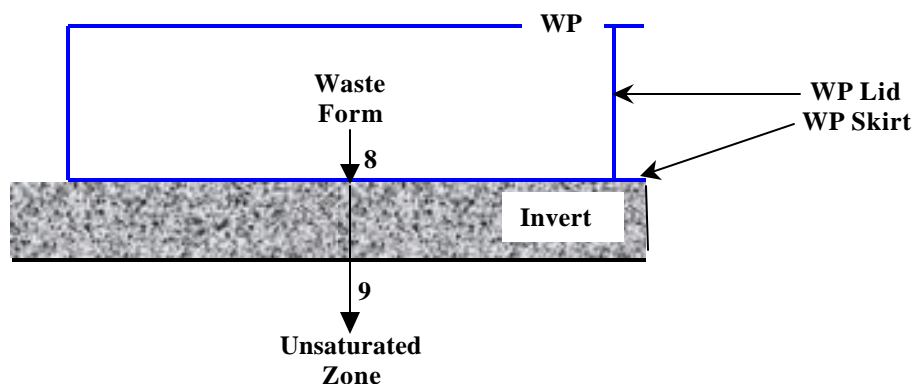


Figure 3. Schematic of the Transport Pathways in the EBS

The advection-dispersion equation for transport of nonreactive constituents in a homogeneous medium with one-dimensional flow is given by (Freeze and Cherry 1979, pp. 389-390 and Appendix X):

$$D^* \frac{\partial^2 C}{\partial x^2} - \bar{v} \frac{\partial C}{\partial x} = \frac{\partial C}{\partial t}, \quad (\text{Eq. 6.1.2-1})$$

where C is the solute concentration [M/L^3], D^* is the diffusivity (or coefficient of molecular diffusion in Freeze and Cherry) [L^2/T], \bar{v} is the average linear water velocity [L/T], and x is the one-dimensional coordinate [L]. This equation assumes that dispersivity and retardation are negligible, consistent with the assumptions 5.2.3 and 5.2.7. The first term on the left-hand side of equation 6.1.2-1 corresponds to transport by diffusion; the second term on the left-hand side corresponds to transport by advection. Table 4 summarizes the transport modes and transport parameters for the two transport pathways in the EBS.

Table 4. Summary of Transport Modes and Parameters for the EBS Transport Pathways

| Transport Pathway | Transport Modes | Transport Parameters and Data Sources |
|---------------------------|---|--|
| 8. WP to invert (F_8) | Diffusion through SCCs (no advective transport through SCCs); Diffusion and advection through patches; Diffusion and advection through pits (no pits are expected in Alloy 22) | Fluid flux for advection = F_8 ; Diffusive area for each SCC is given by $4.08 \times 10^{-6} \text{ m}^2$ (see Sections 6.3.1.2.1 and 6.4.3); Diffusive area for each patch is $2.346 \times 10^{-4} \text{ (mm)}^2$ (1000 nodes on the surface of the WP); Diffusive length in WP is 135 mm to 185 mm depending on WP type (see Section 6.4.3) Diffusion coefficient (all radionuclides): - $2.299 \times 10^{-5} \text{ cm}^2/\text{s}$ at 25°C (see Section 6.4.1.1) - Corrected for porosity and saturation by f_s , where f is porosity and s is the liquid saturation (see Section 6.4.1.2). - Temperature correction defined in Section 6.4.1.3 |
| 9. Invert to UZ (F_9) | Diffusion and advection through the invert; Flow cross-sectional areas given by: $A_{\text{invert}} = p(R_{\text{WP}})L_{\text{WP}}$ $A_{\text{UZ}} = p(R_{\text{WP}} + D_{\text{r}_{\text{invert}}})L_{\text{WP}}$ where R_{WP} is radius of WP, L_{WP} is length of WP, and $D_{\text{r}_{\text{invert}}}$ is the thickness of the invert (0.606 m) | Fluid flux for advection = $F_9 = F_8$; Diffusive length = 0.606 m (max thickness of invert; see Table 1); Diffusion coefficient: - $2.299 \times 10^{-5} \text{ cm}^2/\text{s}$ at 25°C (see Section 6.4.1.1); - Corrected for porosity and saturation by f_s , where f is porosity and s is the liquid saturation (see Section 6.4.1.2). - Temperature correction defined in Section 6.4.1.3; Cross-sectional areas assume a cylindrical geometry, corresponding to the WP lying on the invert. |

There will be no transport through the quartz sand backfill under any conditions. Upward diffusion through the backfill is impossible before the DS fails because a continuous flow path does not exist between the WP and backfill. After the DS fails, upward diffusion will be negligible in comparison to the downward advective flux through the DS.

Colloid-facilitated transport of radionuclides is included as an additional source term for the EBS RT Abstraction. Radionuclide transport from the WP occurs in a fluid containing colloids and dissolved radionuclides. There are three types of colloids in the EBS: (a) waste form colloids, (b) colloids due to corrosion products, and (c) groundwater colloids. The waste form colloids may have irreversibly attached (embedded) or reversibly attached (sorbed) radionuclides. The corrosion and groundwater colloids may have reversibly attached radionuclides.

The diffusion coefficient in the invert is based on the self-diffusivity of water at 25°C as a bounding value for all radionuclides. The effects of porosity, liquid saturation and temperature are also included in calculating the diffusion coefficient.

The corrosion products from the WP and spent fuels have the potential to be strong sorbers for the actinides. Including sorption in the WP and invert will be beneficial to performance because this process can retain radionuclides in the EBS and delay release to the UZ. However, the effects of retardation are conservatively ignored in the EBS RT Abstraction.

6.1.3 Thermal and Mechanical Abstraction for Drip Shield Response

The thermal and mechanical response of the DS has been evaluated for five mechanisms: (1) thermal expansion, (2) floor heave, (3) rock fall, (4) seismic response, and (5) pedestal failure.

Thermal expansion, floor heave and rock fall will produce minor structural response in relation to the potential slippage or overlap between adjacent DSs for the as-emplaced DS configuration. These mechanisms have therefore been screened out from the TSPA-SR, as explained in Sections 6.5.1, 6.5.2, and 6.5.3. Note that the effects of rockfall on the degraded DS configuration, when corrosion may have thinned the structure, is assumed to be screened out for Rev 00 of the TSPA-SR (per assumption 5.3.4) pending more detailed calculations of rock fall block sizes and structural response for the degraded configuration.

Seismic response is the key mechanism that may lead to separation of adjacent DSs, as discussed in Section 6.5.4. The seismic analysis in this AMR is based on the 1-in-10,000 year earthquake. It is a conservative (bounding) analysis in the sense that all the inelastic strain from the earthquake can be concentrated at one or a few locations and that the sand backfill is not represented in the analysis. The sand backfill is important because of its large mass relative to that of the DS. Future analyses will consider less probable but larger earthquakes, such as a 1-in-100,000 year event, and the response of the DS with and without backfill.

Pedestal failure has the potential to shift the DS if the WP falls to the invert and rolls into contact with the shield. Pedestal failure is very likely from general corrosion during long time periods. In addition, failure is even more likely during an earthquake, when the ground motions may increase the load on the pedestal and impart additional momentum to the WP. Given this association and the bounding nature of the analysis for seismic response, the response to pedestal failure is reasonably included in the seismic response for Rev 0 of the TSPA-SR (see Section 6.5.5).

6.2 FLUX IN THE BACKFILL & THROUGH THE DRIP SHIELD ($F_1 - F_4$)

6.2.1 Water Movement Into and Through a Drift (F_1 , F_2 , and F_4)

Water movement from the land surface and down through the UZ at Yucca Mountain is conceptualized to occur through a system of fractures (Liu et al., 1998). Simulations of water movement through the mountain yield estimates of percolation fluxes in the vicinity of the emplacement drifts that are a function of drift location, the geologic unit in which the drift resides, and the climate which varies over time (CRWMS M&O 2000d). Consideration of the interactions between water moving through the mountain and the EBS form the basis of this abstraction for performance assessment.

The basic EBS design concept is shown in Figure 1. The drifts are 5.5 m in diameter. The bottom of the drift, commonly referred to as the invert, is filled with a ballast material of crushed tuff (CRWMS M&O 1999k). The WPs are to be placed on emplacement pallets (formerly referred to as pedestals) that hold them in place above the invert. A titanium DS surrounds the WPs. The space between the WP and the DS, which will be referred to as the axial space, is designed to remain air filled. Backfill is to be placed over the DS to protect it from rock fall

from the roof as the drift degrades over time. The backfill is composed of Overton sand, a fine to medium grained sand.

At early times, any water that enters the drift is vaporized and expelled due to the heat output of the WPs. According to modeling of water movement through the EBS (CRWMS M&O 2000e), much of the water that enters the drift remains as liquid once thermal output has subsided after approximately 3,000 years. This water migrates through the backfill and exits through the bottom portion of the drift.

Water enters the drift by either one of two mechanisms – by seepage from the roof of the drift or by wicking inward from the sides of the drift. In this section, each of these mechanisms is considered in turn, followed by a discussion of water diversion around the DS.

6.2.1.1 Seepage Flux (F_1)

The *Seepage Models for PA Including Drift Collapse* (CRWMS M&O 2000d) presents results of drift-scale UZ flow modeling of the interaction between host rock containing a fracture continuum and a drift for a variety of percolation flux rates and several sets of representative host rock hydraulic parameters. The seepage flux was found to be related to the percolation flux, as expected. However, the air-filled space above the backfill and beneath the roof of the drift acts as a capillary barrier that diverts water around the drift and limits seepage. These findings are consistent with theory for seepage exclusion around cylindrical cavities introduced by Philip et al. (1989). They showed that for given capillary properties of the host rock and a given drift diameter, there exists a critical percolation flux beneath which water will not enter the drift. Indeed, the drift-scale UZ flow modeling results show a propensity for flow to diverge around the drifts.

Seepage Abstraction Analysis (CRWMS M&O 2000c) provides the rationale for calculating the seepage flux into the repository, accounting for thermal effects and spatial variability. Here, the fraction of drifts that allow water seepage as a function of infiltration are given as a function of percolation rate. Across the range of percolation fluxes expected, a large majority of the drifts remain dry.

6.2.1.2 Capillary Flux (F_2)

The high capillarity of the Overton sand backfill relative to the flowing fractures in the adjacent host rock results in the potential for backfill to wick water from the host rock. This capillary wicking effect can result in a focussing of flow through the backfill. In fact, results of thermal-hydrologic simulations of EBS flow using NUFT (CRWMS M&O 2000e) show water fluxes through the backfill that are several times the percolation flux. Further, this modeling yields capillary pressure gradients that indicate flow of water is from the host rock into the backfill. The response to wicking is in marked contrast to the seepage from the roof, where the cylindrical shape of the roof diverts water and only a subset of the drifts permit seepage. With wicking, the effect of the capillarity-induced wicking flux permits appreciable water fluxes through the backfill surrounding every WP.

There is speculation as to whether sufficient connection exists between flowing fractures in the adjacent host rock and the backfill for wicking to occur. The NUFT simulations assume

sufficient connection for there to be equilibrium in regard to pressures between the backfill and the host rock (see assumption 5.1.1). Until this issue is studied in more detail, the potential for wicking flux is included in the PA calculations.

6.2.1.3 Diversion Around The Drip Shield (F₄)

The DS has been designed to divert liquid water that may enter the drift away from the WP. If the DS works as designed (this issue is discussed in detail below), it then acts as a no flow boundary. Any seepage that enters the drift drips onto the backfill and moves downward under the force of gravity. Upon being deflected by the DS, it continues to move downward through the backfill between the DS and the drift wall until encountering the invert or the drift wall. Liquid saturation levels may become elevated at the backfill/invert interface if the (coarse) crushed tuff in the invert acts as a capillary barrier relative to the (finer) sand backfill; however, this is probably a localized effect for the overall capillary flow through the EBS.

Water that enters the backfill by capillary wicking moves laterally under capillary pressure gradients toward the DS, and downward under gravity. In the absence of appreciable seepage from the roof, capillary forces can wick small amounts of water upward into the backfill above the DS. (The flow models are symmetric about the centerline of the drift, so flow cannot cross from the right-hand side to the left-hand side of a drift. Rather, the potential flow path is laterally upward, from the sides of the drift toward the centerline, followed by a turn so flow moves downward along the center line, around the top of the drip shield and downward again along the vertical side of the DS without crossing the centerline.)

This small amount of liquid above the DS will tend to evaporate until the thermal output from the WP becomes negligible. The NUFT simulations show that the flux near the top of the DS is relatively small due to the comparatively long flow path over which the capillary pressure drop is spread. Much higher flux rates are seen along the side of the DS, below the spring line, because of the shorter, more direct flow path from the walls of the drift. (The spring line refers to the line through the two points on the drift wall that are 90° around from the crown (topmost point) of the drift. It represents the widest span across the drift at its mid-height.)

As water migrates downward between the DS and the side of the drift, it encounters the invert. Fine textured backfill overlying the coarse textured invert creates a capillary barrier to flow. Local values for saturation and pressure above the invert increase until sufficient to overcome the capillary forces of the backfill and drive water into the invert. A capillary fringe is then created in the backfill above the invert. The majority of water migrates through the invert although the buildup of the capillary fringe creates sufficient pressure for some portion of the water to migrate back into the host rock directly. Once in the invert, water migrates quickly through, probably as fingered flow into the host rock at the bottom of the drift.

The algorithm for calculating the flux diversion around a breached drip shield is discussed in Section 6.2.4.

6.2.2 Drip Shield Effectiveness

Design drawings for the DS are given in sketch SK-0148 REV01 (CRWMS M&O 1999c). The DS has roughly the shape of a mailbox with vertical sides and a top section that is curved for strength and to shed water. On one end, a guide rib (a 2.5 cm by 2.5 cm square rod) is attached to and extends across the top of the curved top section. On the other end a connector plate is attached. The connector plate contains two ribs, approximately 45 cm apart, that are attached to the underside of the connector plate.

Adjacent DSs are interlocked with one another. This is accomplished by lowering the connector plate of one DS over the upward extending guide rib of the previously emplaced DS such that the two downward extending ribs of the connector plate straddle or bracket the upward extending rib. According to the design specifications, there will be between 200 mm and 635 mm of overlap between adjacent shields (see Attachment I).

The gaps that will exist between DSs in this interlocking design can, potentially, provide a pathway for water to penetrate the DS system. The potential for such leakage under design conditions is considered here, followed by consideration of the ways in which the integrity of the DS might become compromised. This discussion is limited to considering the top of the DS because it is reasonable that any water entering the contact between DSs from the side would simply flow down the vertical sides of the DSs, never contacting the waste.

Three lines of reasoning support the contention that the DS will be successful in excluding liquid water migration from the backfill to the WP under design conditions: analogy, geometry, and experimentation.

Analogy – Consider an extremely simplified and conservative abstraction of the current system, where the DS provides sufficient mechanical support to hold the backfill in place while providing no barrier to water flow. Such a system would be analogous to the top of the drift -- a geologic medium that transmits water above a cylindrical, air-filled cavern. As stated above, such a system diverts water around the air-filled cavern. The extent to which the system completely excludes water is a function of the seepage flux, the capillarity of the geologic medium, and the diameter (Philip et al., 1989). In comparison with the drift roof, the backfill has greater capillarity and the DS has a smaller diameter and receives a smaller flux -- all of which favor the exclusion of water. (Due to diversion of flow, the seepage flux is always less than the focussed percolation flux above the drift. Based on results of the NUFT calculations (CRWMS M&O 2000e), the flux at the top of the drip shield due to capillary wicking tends to be quite small compared to the seepage flux.)

Geometry – Now consider a more realistic system where the titanium walls of the DS form a barrier to flow. Water flux through the DS will now be limited to the gap where adjacent DSs interlock. If extremely high seepage flux conditions exist, then the flow can be driven into this gap. First, the water must travel laterally between 200 mm and 635 mm to get beyond the overlap between the DSs. As this water travels, it must remain precisely along the crown of this gap between the DSs. If there is any deviation, the sloping sides of the DS impose gravity forces that will cause the water to flow down the sides and into the invert. Second, the upward extending guide rib provides a barrier to flow along the crown. Sufficient water pressure must

be provided to push water up and over this barrier. Furthermore, the guide ribs provide surfaces of contact with the DS and the connector plate. These contact surfaces maintain continuity down along the sloping sides of the top portion of the DS. These contacting surfaces will act akin to fractures in the sense that they impart capillarity and are able to transmit water. Any water reaching this point would run down the contact between the DSs. Note also that the air-filled voids (having no capillarity) in between and beyond the guide ribs provide an additional barrier to flow.

Experimentation -- The first quarter-scale test of the DS conducted to date at the Atlas facility (Howard 2000) provide additional evidence. This first test was conducted without backfill; water was dripped onto the DS from the roof of the drift. Without the benefit of the capillarity of the backfill to help divert water and with a simplified DS design (overlapping but not interlocking), water did not penetrate the DS. Some water did, however, flow as a thin film within the overlap between the DSs. Nevertheless, no dripping occurred inside the DS and the WP remained dry.

Some additional inferences can be drawn from the NUFT simulations of the EBS. Even for the relatively high fluxes generated along the side of the DS due to capillary wicking, sufficient pressures for entry through the gaps between DSs are not attained. Additional flow modeling and experimental studies with high seepage fluxes are recommended to provide quantitative evidence demonstrating the effectiveness of the DS.

6.2.3 Drip Shield Breaching

The advective flow of water in the backfill has been shown to be effectively segregated from the WPs as long as the integrity of the DS is maintained. Once holes form in the DS or adjacent DSs separate, the air-filled space between the DS and the WP is assumed to fill with backfill. The consequence of this failure is that a portion of the water flux through the backfill now migrates through the DS and comes into contact with the WP.

6.2.3.1 Breaching Mechanisms

The thermal and mechanical response of the DS may produce gaps between adjacent sections of DS. These breaching mechanisms are analyzed in Section 6.5.

6.2.3.2 Sand Filling of a Breached Drip Shield

Once the integrity of the DS is compromised, the gas-filled space or gap between the DS and the WP may become filled with backfill. While the angle of repose of the backfill might limit its entry into the gap, the potential for repeated seismic events makes it unlikely that backfill will not be able to fill most if not all of the gap volume.

The main reason for assuming that backfill sand fills the gap (per assumption 5.1.6) is to have a bounding model for flow through the EBS. Having sand fill the gap space creates a connected pathway from the backfill through the breaches in the DS to the WP. A connected sand pathway creates a capillary flow path that channels flow through the DS and onto the WP. In addition, the capillary barrier created by having an air-filled gap under the DS no longer exists if there is a connected sand pathway through the DS.

It is also reasonable that at least some of the gap volume will be filled with backfill once the DS is breached. For example, the maximum cross-sectional area of the gap is 3.42 m^2 , based on design drawings of the DS (CRWMS M&O 1999c) and the WPs (CRWMS M&O 1999f). Compare this with the cross-sectional area of the backfill, which has been computed to be 13.23 m^2 (CRWMS M&O 1999d, page 3 of 3). The amount of available backfill is almost 4 times greater than the gap volume (per axial unit of length), so there is ample backfill to at least partly fill the gap volume once the DS is breached.

An alternate approach is to consider the mechanistic details of how sand might fall into the gap beneath the DS for the purpose of exploring potential limits to the connectedness between sand above the DS and sand that has fallen through the DS. The attempt to limit connectedness might include arguments about the height of the penetrations in the DS relative to the elevation of the WP, the presence of separations between WPs that could allow backfill to fall directly to the invert, the angle of repose for sand (especially wet sand), or arguments considering the minimum dimensions for breaches to the DS required for sand to fall through. Further, geologic cementation processes in the backfill might limit the ability of sand to fall through the breached DS if breaching were to occur at sufficiently late times after closure.

However, the likelihood of recurring seismicity over the long time scales of the performance assessment will help to shake sand through any opening in the DS and make arguments about angles of repose for sand untenable. It is then unlikely that the sand backfill will be unable to fall through the penetrations from general corrosion. The significant uncertainties regarding rates of cementation make it difficult to limit sand migration into the gap beneath the DS due to cementation. Finally, the randomness of patch location on the DS and the relatively small separation between adjacent WPs relative to their length imply that patch location and WP separation are unlikely to prevent at least some connectivity across the DS.

Furthermore, angle of repose arguments are a double-edged sword because slope in the backfill created by the angle of repose may also be used to support a focussing of water flow. The process of spilling sand through a breach in the DS creates crossbedding (similar to that seen on the lee side of a sand dune). This crossbedding (micro-scale laminations of alternating coarse and fine textures aligned parallel to the slope) creates, in effect, a series of small-scale capillary barriers. This results in a preference for flow to occur parallel to slope and toward the breached feature. McCord et al. (1991 and 1997) have demonstrated the effect of hillslope and crossbedding under stable flow conditions. Also, Glass and Nicholl (1996) used a lab experiment to show the effect of crossbedding for fingered (unstable) flow. The strength of texture variations across laminae is inversely proportional to the degree of sorting. The well-sorted nature of the Overton sand (CRWMS M&O 2000f) implies that the capillary effect of crossbedding will be somewhat minimized.

In summary, attempting to limit the connectedness of sand through the DS and to maintain the capillary barrier of the gap is not defensible and might require adding significant complexity to the analysis. In contrast, invoking the assumption of sand completely filling the axial space upon DS breaching (per assumption 5.1.6) is a reasonable bound and makes the analysis of water flux through the DS relatively straightforward, as discussed in Section 6.2.4.

Future TSPA-SR and TSPA-LA models will consider the response without an engineered backfill material (the “no backfill” case). In this case, the portion of the seepage flux that passes through the DS can fall or drip directly onto the waste package. The flux splitting algorithm for the no backfill case is identical to that for the backfill case, as described in the next section.

6.2.4 Water Flux Through and Around a Breached Drip Shield (F_3 and F_4)

Once the DS has been breached and the axial space filled with sand, then a portion of the water flux through the backfill (F_3) will pass through the DS and have access to the WP. The flux through the backfill is assumed to be the sum of the seepage flux (F_1) and the flux due to capillary wicking (F_2) (per assumption 5.1.7). The seepage flux is supplied according to the *Seepage Abstraction Analysis* (CRWMS M&O 2000c). The capillary wicking flux is supplied from the NUFT abstraction as the flux at the side of the DS. (Actually, since NUFT invokes symmetry and simulates flow over one half of the drift, the capillary wicking flux is twice the calculated flux at the side of the DS.)

The total calculated flux onto the DS is probably conservative. Since both the seepage flux and the capillary wicking flux are calculated in separate simulations, summing them can result in overestimating the flux through the backfill. For example, a non-negligible seepage flux entering from the top of the backfill will change the flow field, at least partly satiating the capillarity of the backfill and reducing the capillary wicking flux. However, this effect is not included in this EBS RT Abstraction.

- *A Note about the Seepage Flux* – Because fracture flow is the dominant mechanism for flow in the host rock, water will necessarily come into the drift as point sources. In an extreme case, the entire seepage flux enters the drift through a single point source. Carrying this extreme case still further, it is possible that density unstable flow conditions prevail and the seepage flux entering the backfill migrates as fingered flow. Conditions required for fingered flow are a function of the seepage flux, the capillarity of the backfill material, and the initial moisture content. The lower the seepage flux, the less capillarity, and the lower the initial moisture content, the higher the propensity for fingering. In comparison with uniform flow, the occurrence of fingered flow lowers the probability that the seepage flux will encounter multiple breaches in the DS, but the fluxes through the DS would be much higher if a finger encounters a breach.

The low probability/high consequence fingered flow events are likely to be averaged over the total repository for several reasons. First, the seepage flux is conceptualized to vary spatially over the approximately 10,000 WPs in the repository so that it is not always a single point source at a fixed location throughout time. Second, the presence of engineered backfill or natural backfill from rockfalls will tend to produce more uniform flow conditions with higher initial saturation in the backfill, reducing the likelihood of focussed flow. Third, the preliminary data on general corrosion of titanium shows that this process is not a function of direct liquid contact with the DS. Given these factors, the low probability/high consequence fingered flow events will be averaged out since seepage and breaches will vary spatially over the approximately 10,000 WPs in the repository. It therefore seems reasonable to consider uniform fluxes encountering the DS.

- *A Note about the Capillary Wicking Flux* – As a first order approximation, the flux at the side of the DS is used as a surrogate for the flux that would reach the WP due to capillary wicking in the absence of a DS. This is probably an overestimation. Extending the flow lines farther laterally to intersect the WP would likely result in fluxes lower than those seen at the side of the DS. Additional NUFT simulations could be undertaken to demonstrate this point. However, until such simulations are undertaken, the best surrogate available for flow is capillary flux through the DS.

As a reasonable approximation, the flux through the DS is assumed to be scaled by the axial length of the DS penetration as compared to the total axial length of the DS. This approximation is conservative because it is equivalent to assuming that the penetration is at the side of the DS and intercepts fluid flux over all azimuthal angles at the relevant axial location (per assumption 5.1.9). The flux through the DS (F_3) is then given by:

$$F_3 = (F_1 + \alpha F_2) \frac{L_{DS_SCC} + L_{DS_Patch} + L_{DS_Pit} + L_{DS_Gap}}{L_{DS}}, \quad (\text{Eq. 6.2.4-1})$$

where F_1 is the seepage flux, F_2 is the capillary flux, L_{DS_SCC} is the total axial length of all SCCs in the DS, L_{DS_Patch} is the total axial length of all patches in the DS, L_{DS_Pit} is the total axial length of all pits in the DS, L_{DS_Gap} is the axial length of any gaps between adjacent DSs, and L_{DS} is the axial length of the DS. The parameter α is a factor between 0 and 1 based on the design and backfill properties; the rationale for including this parameter is discussed in Section 5.1 (see assumption 5.1.7).

Once the flux through the DS is known, the flux diverted around the DS is calculated assuming continuity of flow:

$$F_4 = F_1 + \alpha F_2 - F_3. \quad (\text{Eq. 6.2.4-2})$$

This quasi-static approach is consistent with assumption 5.1.12.

6.3 FLUX INTO AND AROUND THE WASTE PACKAGE ($F_5 - F_9$)

The conceptual model for the TSPA-SR is based on the presence of continuous flow paths through the patches, SCCs and pits that penetrate the WP. More specifically, the TSPA-SR conceptual model assumes that vertical flow of seepage into the WP, through the waste form and out of the WP is not impeded by the location of patches, SCCs and pits on the surface of the WP (see assumption 5.1.10). In other words, there is no long-term build-up and retention of liquid within the WP for flow and transport. There is also no significant resistance to the flow through the waste form. The TSPA-SR approach attempts to maximize the immediate release and mobilization of radionuclides, as explained in Section 6.6.

Radionuclides cannot be released from the WP if there are no openings through either the wall or lid of the WP. Section 6.3.1 describes the types of openings that can form, how and where they form, the timing of their formation, and the flow through these openings. The dimensions of these openings have implications for whether water is able to flow into or through the WP or whether transport out of the WP will be by advection and/or diffusion. Section 6.3.2 describes the flux of liquid around or through the WP. Section 6.3.3 describes the alternate pathway for

liquid to reach the waste package; namely, evaporation from the invert and condensation on the inside of the DS can provide a source of liquid even when there are no openings in the DS. Section 6.3.4 describes the flux of liquid through the invert.

6.3.1 Breaching of the Waste Package

6.3.1.1 Waste Package Design

Although WPs vary depending on the waste form they contain, the majority of design features are shared in common. These commonalities are described here. The cylindrical WP is constructed with a double-shelled wall. The inner shell is a 5 cm thick shell of stainless steel that provides structural integrity for the WP. The outer shell is a 2 cm or 2.5 cm thick layer of Alloy 22 that provides resistance to corrosion. This cylinder is sealed with two lids that are welded onto the open end. The inner lid is composed of stainless steel and the outer lid is composed of Alloy 22. There is a 3 cm air gap between the inner and outer lids. All WPs also have a protective skirt that extends at least 24 cm beyond the lids. This skirt is an extension of the Alloy 22 outer shell. The design of the WPs is detailed in (CRWMS M&O 1999f).

The stainless steel inner layer of the WP is assumed to have no resistance to corrosion, forming an immediate flow pathway once the outer (Alloy 22) shell has been breached (per assumption 5.1.18). Similarly, it is assumed that the closure weld on the inner stainless steel lid has no resistance to corrosion and the inner lid has failed once the outer lid has failed.

6.3.1.2 Types of Openings

Two general types of openings can exist in the WP due to corrosion. These are (1) radial SCCs that penetrate the weld of the lid and (2) patches resulting from general corrosion. Each of these types of openings is discussed in turn below.

6.3.1.2.1 Stress Corrosion Cracks

SCCs can appear because of the residual tensile stresses generated during the process of welding the lids in place (it is not possible to anneal the final closure welds). SCCs may be important at early times because they can occur relatively quickly relative to the formation of a penetrating patch from general corrosion.

SCCs will typically form along two orientations. Radial stresses can generate circumferential cracks while hoop stresses can generate radial cracks. Only radial SCCs are considered in the EBS RT Abstraction because the formation of circumferential cracks that penetrate the thickness of the lid is highly unlikely. Cracks require the presence of tensile stress for initiation and propagation. Detailed finite-element analyses of the welding process demonstrate that only compressive radial stresses exist at the inner surface (CRWMS M&O 2000g, Fig. 11 - Profile 1-1). In this condition, circumferential cracks cannot propagate through the thickness of the lid weld and are therefore not considered in the EBS RT Abstraction.

Radial cracks are transverse to the weld and cannot be much longer than the weld width. A radial crack opening has an elliptical shape with length “ $2a$ ” and a gap “ d ” (CRWMS M&O

2000g, Section 5). The equation given by Tada et al. (1973) can be used to calculate the gap, d [L], for a crack with length $2a$ in an infinite sheet under plane stress load:

$$d = \frac{2(1-\nu^2)s_a 2a}{E}, \quad (\text{Eq. 6.3.1-1})$$

where E is the modulus of elasticity [M/L/T²], ν is Poisson's ratio [-], $2a$ is the crack length [L] and s_a is the applied stress [M/L/T²]. Appropriate values for E and ν for Alloy 22 are given in Table 1.

The residual tensile stress is higher on the outside surface than on the inside surface (CRWMS M&O 2000g, Fig. 13, Profile 1-1). The resulting shape of the crack is then an ellipsoidal cone where $2a$ is the length of the long axis and d_o and d_i are the short axis lengths for the outside and inside surfaces, respectively. The depth d of the crack is taken to be the lid thickness. Figure 4 is a schematic diagram of the geometry of the ellipsoidal cone crack.

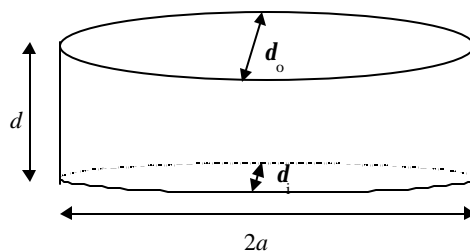


Figure 4. Schematic of the Dimensions for an Ellipsoidal Crack

Values of s_a , the residual stress, and $2a$ are still subject to design changes and improved calculations; however a range of values can be estimated. One approach is to estimate the maximum length $2a$ of a radial crack based on the width of the heat-affected zone around the weld between lid and WP. The width of the heat-affected zone is estimated to be about twice the width of the weld or 0.50 inches (1.27 cm). A second approach is to identify the region of high residual stress from finite-element simulations. The width of the region of high residual stress on the outer surface of the lid is approximately 4 cm (Tang et al., 1999). Table 5 gives the calculated gap width, based on Equation 6.3.1-1, for both approaches based on typical residual stresses at the inner and outer surface of the lid for a 21 PWR WP (CRWMS 2000g, Fig. 13). The second approach is recommended for the EBS RT Abstraction because it is conservative relative to the first approach.

Table 5. Gap Width for a Range of Residual Stresses at 400°F (~200°C) in a 21-PWR Container

| Parameter | Inner Surface | Outer Surface |
|------------------------------------|---------------|---------------|
| Hoop stress | 40 ksi | 50 ksi |
| Gap width for a 1.27 cm long crack | 33 μm | 41 μm |
| Gap width for a 4 cm long crack | 104 μm | 130 μm |

*1 ksi = 1,000 psi

The cross-sectional area of the SCC is important for transport by diffusion. The bounding (largest) cross-sectional area is defined by conditions at the outer surface of the 4 cm long crack. The area of this ellipse is πab , where $2a$ is 4 cm and b is one-half of the larger gap width on the last line in Table 5. The cross-sectional area is then $\pi(0.02 \text{ m})(65 \times 10^{-6} \text{ m})$ or $4.08 \times 10^{-6} \text{ m}^2$.

The width (gap) of the SCCs can also be used as an indicator to determine whether or not water can flow into the WP through a SCC. However, the potential for flow through a SCC may vary with dust or corrosion products in the crack and with the effects of temperature and mineral content on viscosity and surface tension. Given the complexity of this situation, it is reasonable to bound the response by assuming that any fluid that contacts a crack will flow through the crack and into the WP (per assumption 5.1.10 and 5.1.16). This fluid is also assumed to form a continuous liquid pathway for diffusive transport of radionuclides out of the WP (per assumption 5.2.8).

Film flow on the WP exists if condensation generates droplets on the inner surface of the DS or if the EBS design has no quartz sand backfill. This dripping water is assumed to be capable of contacting an SCC only if the drip falls inside the skirt of the WP (see Figure 2 or 3). This is a reasonable limitation because of the effect of gravity and because all WPs are conservatively assumed to be tilted at their maximum angle to provide a bounding estimate of the dripping flux inside the skirt (per assumption 5.1.15). Once a drop or thin film is inside the skirt, it will flow around and down the skirt into any SCCs. The EBS RT Abstraction conservatively assumes that all dripping flux inside the skirt enters the SCCs and WP, independent of film thickness (assumption 5.1.16).

The dripping flux has the greatest potential to fall inside the skirt if the WP is tilted upward. Possible mechanisms for tilting are pedestal collapse due to corrosion or a seismic event that causes one end of the WP to fall off its pedestal. The EBS RT Abstraction conservatively assumes that all WPs become tilted, lid-end upward, at the maximum angle possible. This maximum angle of tilt occurs when the skirt end of the WP is elevated to the height of the inside of the DS while the other end rests against the invert.

Crack apertures will fill with corrosion products over time. The capillary forces in these corrosion products may then act as a Richard's barrier, preventing advective inflow through the crack if there is no fluid pathway through fine granular material between the two lids of the WP. The formation of corrosion products is conservatively neglected in considering flow into SCCs.

6.3.1.2.2 Patches from General Corrosion

The EBS design includes two corrosion-resistant materials, titanium and Alloy-22. The main corrosion mechanism for both materials is expected to be general corrosion, although research is continuing into the potential for pitting corrosion due to extreme near-field geochemical environments and for SCC due to damage from rockfall or seismic events.

The timing and location of patches from general corrosion is predicted by the WAPDEG software. These predictions are based on discretizing the response of the DS with 500 nodes and the WP with 1,000 nodes (see assumption 5.1.11). The equivalent area per patch for the EBS RT Abstraction is calculated as the total surface area divided by the number of nodes on the surface.

The axial length of each patch is calculating assuming a square geometry for each patch. The data on timing, location (upper or lower surface of WP), size and length of patches is available as a boundary condition for the EBS RT Abstraction.

6.3.1.3 Impact of Heat Generation

Heat generated by the waste form has the potential to evaporate water within the WP. In this situation, water cannot collect inside the WP and cannot support advective transport of radionuclides. Preliminary estimates indicate that the available heat can evaporate incoming water for several thousand years and possibly longer. However, complexities in the internal geometry of the WPs (particularly the response of any water pooled at the bottom of the package and the presence of small conduits for water vapor to escape through SCCs) make it difficult to say definitively that all incoming water will be evaporated.

Since the temperature of the WP drops relatively rapidly in the first 3,000 years (CRWMS M&O 2000e), the potential for evaporation in the WP has been ignored in Rev 0 of the TSPA-SR. This approach is conservative because evaporation might stop advection as a transport mechanism. It is potentially nonconservative if evaporation from the surface of the WP is followed by condensation on the DS, resulting in a refluxing of water that could accelerate corrosion of the WP. The current approach (no evaporation) is considered reasonable for the Rev 0 of the TSPA-SR until additional results become available.

6.3.2 Flux Through and Around the WP (F_5 and F_6)

The flux into the waste package, F_5 , is conceptualized to be the sum of two parts: the flux through SSCs and the flux through patches and/or pits in the WP. The flux through SSCs currently has only one source: evaporation from the invert and condensation on the inside of the DS (F_7). (Future models may also include a dripping flux from seepage if the engineered backfill material is removed from the EBS.) The advective (capillary) flux around the WP (F_3) cannot contribute to flow through a SCC because the small size of the SCC excludes individual grains of sand so that the SCC and any corrosion products inside the SCC are anticipated to be a barrier to capillary flow from the backfill. The sources of flux through patches and pits includes the condensation on the DS (F_7) and the advective (capillary) flux thorough the backfill around the WP (F_3). The flux through SCCs and the flux through patches/pits are described in turn.

The value of the SCC flux into the WP is not required by the model because transport through the SCCs is solely by diffusion and because the presence of water vapor and hygroscopic salts on the waste form are assumed to generate a continuous, thin film pathway for diffusive transport (per assumption 5.2.8). However, it is useful to provide an abstraction of the dripping flux for future use. The flux through the SCC is proportional to the ratio of the length of the exposed lid within the skirt to the length of the exposed WP (per assumption 5.1.15). Length is appropriate here, rather than area, because only the dripping flux from condensation can fall within the skirt and this dripping flux is conceptualized to fall from the crown of the invert. In effect, the flux is a line source so a ratio of lengths is used to partition the dripping flux between the WP and the skirt. The calculation is as follows:

$$F_{SCC} = F_7 \frac{\ell_{LID} \sin(\mathbf{j})}{L_{WP} + \ell_{LID} \sin(\mathbf{j})}, \quad (\text{Eq. 6.3.2-1})$$

where F_{SCC} is the flux through the SCC, F_7 is the condensation flux (if present), ℓ_{LID} is the diameter of the lid within the skirt, L_{WP} is the total axial length of the WP, and \mathbf{j} is the maximum tilt angle of the WP.

The maximum tilt angle is defined as the angle of the WP when the top edge of the skirt touches the crown of the DS and the bottom corner of the WP is in contact with the invert. This angle can be calculated from simple trigonometry and the data for the four types of WPs in Table 1. The equation for calculating the maximum tilt angle, \mathbf{j} , is given by

$$L_{WP} \sin(\mathbf{j}) + D_{WP} \cos(\mathbf{j}) = D_{WP} + \Delta h, \quad (\text{Eq. 6.3.2-2})$$

where L_{WP} is the length of the waste package [L], D_{WP} is the outer diameter of the waste package [L], and Δh is the distance from the DS to the top of the WP if the pedestal collapses [L]. This equation can be rewritten into a form suitable for iterative solution on a hand calculator:

$$\sin(\mathbf{j}) = \frac{D_{WP}(1 - \cos(\mathbf{j})) + \Delta h}{L_{WP}}. \quad (\text{Eq. 6.3.2-3})$$

With a given (or old) value of \mathbf{j} , evaluate the right-hand side of Equation 6.3.2-3 to determine the new values of $\sin(\mathbf{j})$ and then of \mathbf{j} itself. Repeated substitutions of the latest value for \mathbf{j} into the right-hand side of Equation 6.3.2-3 and calculation of a new value for \mathbf{j} results in an iterative process that converges to 3 significant places in about 4 iterations. The values of \mathbf{j} for the four types of WPs are presented in Table 6. Note that the maximum tilt angles are relatively small, so only a small fraction of any dripping flux will fall within the lid of the WP.

Table 6. Maximum Tilt Angle for the Four Types of Waste Packages.

| Type of WP | Length of WP, L_{WP} (meters) | Outer Diameter of WP, D_{WP} (meters) | Distance from DS To Top of WP, Δh (meters) | Maximum Tilt Angle, \mathbf{j} (degrees) |
|--------------|------------------------------------|--|---|---|
| 21-PWR | 5.275 | 1.564 | 0.768 | 8.56 |
| 44 BWR | 5.275 | 1.594 | 0.739 | 8.23 |
| 5 HLW/DOE SF | 3.73 | 2.030 | 0.302 | 4.75 |
| Naval SNF | 5.56 | 1.869 | 0.4635 | 4.85 |

The fluid flux through patches and pits in the WP is proportional to the total axial length of all patches and pits to the total axial length of the WP (per assumption 5.1.9). The presence of a gap between adjacent WPs is conservatively neglected in the TSPA-SR model. The calculated flux through the WP is then given by:

$$F_5 = (F_3 + F_7) \frac{L_{WP-Patch} + L_{WP-Pit}}{L_{WP}} + F_{SCC}, \quad (\text{Eq. 6.3.2-4})$$

where F_5 is the flux into the WP, F_3 is the flux through the DS, F_7 is the condensation flux (if any), L_{WP_Patch} is the total axial length of all patches on the WP, L_{WP_Pit} is the total axial length of all pits on the WP, and L_{WP} is the total axial length of the WP. F_{SCC} is given by Equation 6.3.2-1.

Finally, the flux that is diverted around the WP, F_6 , is calculated using continuity of the quasi-static flow (assumption 5.1.12) around and into the WP:

$$F_6 = F_3 + F_7 - F_5. \quad (\text{Eq. 6.3.2-5})$$

6.3.3 Evaporation from the Invert and Condensation on the Drip Shield (F_7)

Liquid water may reach the WP due to condensation on the inside of the DS. A substantial portion of the water draining through the backfill migrates through the invert. In proximity to thermal output from the WP, some of this water will evaporate. This water vapor convects following temperature gradients. In the high humidity environment of the subsurface, this water will condense once it moves away from the heat source. If the water vapor convects downward and laterally away, then the interior of the DS will remain dry. If, however, convection proceeds upward toward the DS, then condensation could occur. The manner in which convection proceeds will be a function of the thermal conductivities of the various media in the vicinity (invert, backfill, and host rock) and the geometry of the system (for instance, the relative proximity of the WP to the invert and the top of the DS).

The inside of the DS will be filled with a mixture of air and water vapor. Liquid water can condense on the inside of the DS when the temperature of the DS, T_{DS} , is less than the dew point of this air/vapor mixture at the DS surface. Note that the DS forms an inverted cap that will tend to trap any water vapor that moves upward from the invert.

As a first order approximation, the space between the DS and WP can be treated as a closed system because of the geometry of the DS and invert. The vapor pressure of water beneath the DS will then be close to the equilibrium vapor pressure at the invert temperature, T_{INV} . In this case, comparison of the temperature in the invert (T_{INV}) and the temperature at the top of the DS (T_{DS}) provides a suitable indicator of the potential for condensation on the inside of the DS. That is, condensation will occur if $T_{INV} > T_{DS}$. This is a physically reasonable approximation in terms of providing an indicator for the direction of vapor pressure gradients and the potential for condensation on the DS.

The potential for condensation is abstracted very simply using the output of NUFT. A NUFT calculation is supplied for each group of WPs in the repository. The NUFT calculations and abstraction provide the average temperature in the invert and the temperature at the crown of the DS as a function of time. The criterion for condensation is then

- If $T_{DS} > T_{INV}$, then $F_7 = 0$ (no condensation occurs),
- Otherwise, the condensation flux is equal to the evaporative flux, F_7 .

Note that all the evaporative flux from the invert drips from the inside of the DS onto the WP. This approach provides a reasonable bound because the possibility of water vapor transport laterally away from the DS is ignored.

It is also possible that liquid will evaporate from the WP; however, the invert is envisioned as the main source of water vapor, particularly during the main thermal pulse. The main thermal pulse occurs during the first 3,000 years after repository closure (CRWMS M&O 2000e), when failure of the DS will be quite infrequent. In this situation, seepage and capillary fluxes will be diverted away from the WP and into the invert, so the invert will be the main source for the evaporative flux.

6.3.4 Flux Into and Through the Invert (F_8 and F_9)

The flux leaving the WP, F_8 , is equal to the flux entering the WP, F_5 . Similarly, the liquid flux leaving the invert, F_9 , is equal to the sum of the diversion around the WP, F_6 and the flux leaving the WP, F_8 , minus any evaporative flux leaving the invert, F_7 . That is,

$$F_8 = F_5, \quad (\text{Eq. 6.3.4-1})$$

and
$$F_9 = F_6 + F_8 - F_7 = F_3. \quad (\text{Eq. 6.3.4-2})$$

The equality of F_8 and F_5 is based on quasi-static flow (i.e., outflow equals inflow). The equality of F_9 and F_3 is consistent with the definitions of F_6 and F_8 and with the quasi-static assumption, which implies that the flux through the DS equals the flux out of the invert. Note that only the flux leaving the WP, F_8 , can transport radionuclides through the invert.

6.4 TRANSPORT THROUGH THE EBS

The waste form is the source of all radionuclides in the repository system. Radionuclides can be transported downward, through the invert and into the UZ, as shown in Figure 3. Transport can occur through advection when there is a fluid flux through the WP, and by diffusion through continuous fluid pathways in the WP. These two transport processes (diffusion and advection) may not be active simultaneously because they are a function of the type of penetrations through the DS and WP. For example, diffusion would be the only viable transport mechanism if SCCs are the only penetrations through the WP. Alternately, diffusion may be negligible once patches form because the cross-sectional flow area for patches ($2.346 \times 10^4 \text{ mm}^2$) is much greater than that for SCCs (4.08 mm^2).

The emphasis in this AMR is on flow and transport of radionuclides through the EBS after the radionuclides are mobilized. This AMR does not define elements of the TSPA, such as corrosion processes, radionuclide solubility limits, waste form dissolution rates and concentrations of colloidal particles, that are generally represented as boundary conditions or input parameters for the EBS RT Abstraction. In effect, this AMR provides the algorithms for transporting radionuclides using the flow geometry and radionuclide concentrations determined by other elements of the TSPA-SR.

Transport through the quartz sand backfill is expected to be negligible. Upward diffusion through the backfill is unlikely before the DS fails for two reasons. First, a direct, continuous flow path does not exist between the WP and the backfill. Second, transport through a more circuitous flow path, such as laterally across the invert and up into the backfill is unlikely given

the downward (capillary) flux through the backfill. After the DS fails, upward diffusion will be negligible in comparison to the downward advective flux through the DS.

The diffusion coefficient for radionuclide transport is based on the self-diffusivity of water at 25°C. This is a bounding value for all radionuclides, as discussed in Section 6.4.1.1. The effects of porosity and liquid saturation on the diffusion coefficient are incorporated using the formulation in Section 6.4.1.2. The effects of temperature on this bounding value are corrected using the formulation in Section 6.4.1.3.

Advective transport is very straightforward in the EBS RT Abstraction because of the conservative assumptions for the TSPA-SR model. In particular, mobilized radionuclides will be transported with the local fluid flux from the WP (F_8) through the invert to the UZ (F_9). (Note that the \bar{v} in Equation 6.1.2-1 can be interpreted as a flux rate per unit cross-sectional area, or $[L^3/T/L^2] = [L/T]$). There are no corrections for dispersive effects or chemical sorption because horizontal dispersion is conservatively ignored in the EBS RT Abstraction and because the partition coefficients for all radionuclides are conservatively set to zero in the WP and invert (see Section 5.2). Given the simplicity of the advective transport model, the discussion in this section focuses on the calculation of the diffusion coefficient for diffusive transport.

6.4.1 Diffusion Coefficient Abstraction

The TSPA-LA model requires an abstraction for the diffusion coefficient in the WP and invert as a function of radionuclide, porosity, saturation, temperature, and concentration. The recommended abstraction for diffusion coefficient is as follows:

- Use the free water diffusion coefficient for self-diffusion of water, $2.299 \times 10^{-5} \text{ cm}^2/\text{sec}$ (Mills 1973, Table III), as a bounding value for all radionuclides at 25°C. The rationale for choosing this value is presented in Section 6.4.1.1. The value of the self-diffusivity of water is TBV (MO0002SPASDC00.002).
- Correct the diffusion coefficient for the porosity and (liquid) saturation of the invert. The correction for porosity and saturation is conservatively represented as the product of porosity times the liquid saturation in a granular medium like the crushed tuff in the invert. The rationale for this approach and its conservatism is presented in Section 6.4.1.2.
- Correct the diffusion coefficient for temperature variation using the formulation in Section 6.4.1.3 (CRWMS M&O 2000h).
- Ignore the effects of concentrated solutions for Rev 0 (see Section 6.4.1.4). The maximum correction for a highly concentrated solution of potassium iodide is a factor of 1.27. This factor is almost within the bounding approximation inherent in using the self-diffusion coefficient for all radionuclides. It will be neglected for the TSPA-SR.

6.4.1.1 Self-Diffusion Coefficient of Water

The self-diffusion coefficient of water provides a conservative bound for the diffusion of ionic and neutral inorganic, and organo-metal species that may be released from a WP. This assertion is based on:

1. A survey of compiled diffusion coefficients at 25°C shows that simple cation and anion species (excluding the proton and hydroxyl species, which are not appropriate analogs to diffusing radionuclide species) have diffusion coefficients that are smaller than that of water.
2. The self-diffusion coefficient for water at 90°C is larger than compiled diffusion coefficients for simple inorganic species at 100°C.
3. Diffusion coefficients for simple lanthanide and actinide cations are much smaller than the self-diffusion coefficient of water and are expected to be even smaller for their hydroxyl and carbonate complexes.

In a compilation of diffusion coefficients for 99 ionic species, only 3 species, H^+ , OH^- , and OD^- have diffusion coefficients that are larger than the self-diffusion of water at 25°C (Mills and Lobo, 1989; Appendix I, Tables 1.1 to 1.6, pages 314 to 319). Of the 33 ionic species for which Mills and Lobo list diffusion coefficients at 100°C in Tables 1.1 through Table 1.7, only 2 species, H^+ and OH^- , have diffusion coefficients larger than the self-diffusion of water (H_2^{18}O) at 90°C (Mills and Lobo, 1989; Table 1, page 17). The fact that the self-diffusion of H_2^{18}O is less than that of H_2O , and that the self-diffusion of H_2O at 90°C would be greater than that of various ionic species at 100°C, further supports the contention that the self-diffusion of water is conservative.

The compilation below (Table 7) lists a selection of diffusion coefficients for some trivalent lanthanides and actinides. Table 7 also includes some anions not listed in most compilations but relevant and/or analogous to those expected for radionuclides released from the WP. The listing shows that, except for I_2 and TcO_4^- , the diffusion coefficients for these species are far smaller than the self-diffusion of water, and that the hydroxyl and/or carbonate complexes of the metal species would be expected to have even smaller diffusion coefficients.

Table 7. Compilation of Diffusion Coefficients for Molecular Iodine, Yttrium, Technitium, and Lanthanide and Actinide Species

| Species | D, cm^2/s | Comments | Reference |
|-------------------|---------------------------|--|---|
| Y^{3+} | 5.7×10^{-6} | 25°C | (Mills and Lobo, 1989); pg. 220. |
| TcO_4^- | 1.48×10^{-5} | 25°C | (Mills and Lobo, 1989); pg. 105. |
| I_2 | 1.36×10^{-5} | 25°C; 0.075 M H_2SO_4 | (Cantrel, Chaouche, and Chopin-Dumas, 1997); Table 5. |
| La^{3+} | 5.42×10^{-6} | 25°C; 0.1 M NaClO_4 | (Rosch and Khalkin, 1990); calculated from mobility data reported in Table 1; pg. 103. ^a |
| La^{3+} | 6.18×10^{-6} | 25°C | (Mills and Lobo, 1989); pg 93. |
| Ce(III)-carbonate | 2.68×10^{-6} | 5.5 M K_2CO_3 , pH 13, presumably at 25°C. | (Haltier, Fourest, and David, 1990); pg 111. |
| Ce(IV)-carbonate | 1.56×10^{-6} | 5.5 M K_2CO_3 , pH 13, presumably at 25°C. | (Haltier, Fourest, and David, 1990); pg 111. |
| Eu^{3+} | 4.38×10^{-6} | 25°C; 0.1 M NaClO_4 | (Rosch and Khalkin, 1990); calculated from mobility data reported in Table 1; pg. 103. ^a |
| Gd^{3+} | 5.24×10^{-6} | 25°C; 0.1 M NaClO_4 | (Rosch and Khalkin, 1990); calculated from mobility data reported in Table 1; pg. 103. ^a |

| Species | D, cm ² /s | Comments | Reference |
|---|-------------------------|---|---|
| Tb ³⁺ | 5.01 x 10 ⁻⁶ | 25°C; 0.1 M NaClO ₄ | (Rosch and Khalkin, 1990); calculated from mobility data reported in Table 1; pg. 103. ^a |
| Tm ³⁺ | 5.10 x 10 ⁻⁶ | 25°C; 0.1 M NaClO ₄ | (Rosch and Khalkin, 1990); calculated from mobility data reported in Table 1; pg. 103. ^a |
| Yb ³⁺ | 5.23 x 10 ⁻⁶ | 25°C; 0.1 M NaClO ₄ | (Rosch and Khalkin, 1990); calculated from mobility data reported in Table 1; pg. 103. ^a |
| Lu ³⁺ | 5.01 x 10 ⁻⁶ | 25°C; 0.1 M NaClO ₄ | (Rosch and Khalkin, 1990); calculated from mobility data reported in Table 1; pg. 103. ^a |
| UO ₂ (CO ₃) ₃ ⁴⁻ | 3.6 x 10 ⁻⁶ | 1 M total carbonate, 22 °C | (Perry, Phillips, and Chung, 1988); pg. 302. |
| UO ₂ (CO ₃) ₃ ⁴⁻ | 3.0 x 10 ⁻⁶ | 0.2 M total carbonate, pH 9.8, 25°C | (Perry, Phillips, and Chung, 1988); pg. 302. |
| UO ₂ (CO ₃) ₃ ⁵⁻ | 3.81 x 10 ⁻⁶ | 0.75 M Na ₂ CO ₃ , 0.6 M NaClO ₄ , pH 11.5, presumably at 25°C | (Haltier, Fourest, and David, 1990); pg 110. |
| UO ₂ ⁺⁺ | 6.8 x 10 ⁻⁶ | 25°C | (Millard and Hedges, 1996); pg. 2141. |
| UO ₂ -carbonate | 1.9 x 10 ⁻⁶ | Calculated using Stokes-Einstein with a radius of 8 Å at 10°C | (Millard and Hedges, 1996); pg. 2141. |
| Np(V)-carbonate | 7 x 10 ⁻⁶ | Calculated using Stokes-Einstein with a radius of 3.4 Å at 25°C | (Tsukamoto, Ohe, et al., 1994); pg. 469. |
| Am ³⁺ | 5.78 x 10 ⁻⁶ | 25°C; 0.1 M NaClO ₄ | (Rosch and Khalkin, 1990); calculated from mobility data reported in Table 1; pg. 103. ^a |
| Am ³⁺ | 5.95 x 10 ⁻⁶ | 25°C, in 0.0002 M Nd(ClO ₄) ₃ | (Mills and Lobo, 1989); pg 131. |
| Cf ³⁺ | 4.39 x 10 ⁻⁶ | 25°C; 0.1 M NaClO ₄ | (Rosch and Khalkin, 1990); calculated from mobility data reported in Table 1; pg. 103. ^a |
| Cf ³⁺ | 5.50 x 10 ⁻⁶ | 25°C, in 0.0002 M Nd(ClO ₄) ₃ | (Mills and Lobo, 1989); pg 132. |
| Es ³⁺ | 5.50 x 10 ⁻⁶ | 25°C, in 0.0002 M Nd(ClO ₄) ₃ | (Mills and Lobo, 1989); pg 132. |

^aCalculation of diffusion coefficients from reported ionic mobilities (Rosch and Khalkin 1990; Table 1). The mobilities were measured in 0.1 M NaClO₄ at various pHs (below the pH of hydrolysis). The mobilities were slightly larger at pHs greater than 5, and these are the data that were used for the calculation. The equation used to calculate the diffusion coefficient is: $D = (kT/(|z|e)) u$, where k is Boltzmann constant, T is the temperature in Kelvin, z is the valence of the ion, e is the elementary charge, and u is the mobility (Atkins 1990, Box 25.1, Einstein relation, page 765).

Future TSPA_SR or TSPA-LA models might use four diffusion coefficients to provide a more realistic model. One coefficient could be used for each charge (mono-, di-, and tri-valent species) and one for the hydroxyl and carbonate complexes of the actinides and lanthanides. At 25°C, the mono-, di-, and trivalent species have bounding values of 2.2 x 10⁻⁵ cm²/s, 1.2 x 10⁻⁵ cm²/s, 0.7 x 10⁻⁵ cm²/s, respectively, as shown in Figure 5.

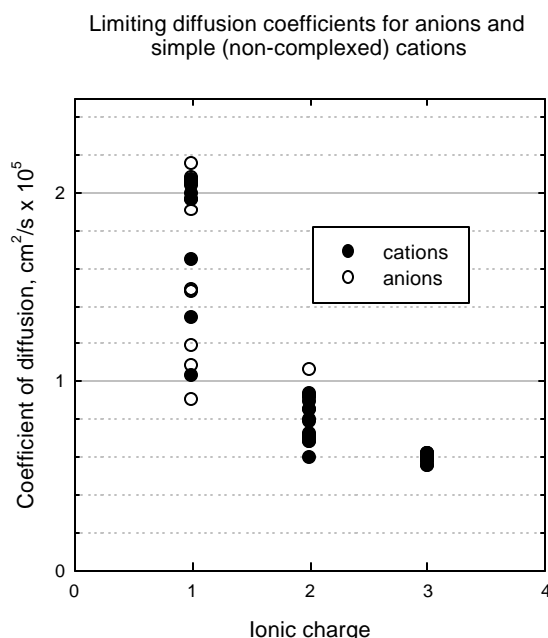


Figure 5. Limiting Diffusion Coefficients for Anions and Simple (Non-Complexed) Cations. Selected from Mills and Lobo (1989), Appendix I, Tables 1.1 to 1.6; pgs. 314 to 319

6.4.1.2 Correction for Porosity and Saturation

The reduction in the free water diffusion coefficient for a partly saturated porous medium can be estimated from Archie's law (CRWMS M&O 2000h). Archie's law gives the diffusion coefficient, D , as a function of porosity and saturation in a partly saturated, granular medium as:

$$D = D_0 f^{1.3} s^2, \quad (\text{Eq. 6.4.1-1})$$

where D_0 is the value of the free water diffusion coefficient (porosity of 1 and saturation of 1), f is the porosity, and s is the (liquid) saturation of the porous medium. The exponents on f and s are estimates based on experimental data that are TBV. Given this uncertainty, the correction for porosity and diffusion is conservatively stated as:

$$D = D_0 f^{1.0} s^{1.0}, \quad (\text{Eq. 6.4.1-2})$$

This latter formula is a reasonable bound because it reduces the free water diffusion coefficient by the effective wetted cross-sectional area of the liquid pathways. The effective wetted area is proportional to the product of porosity and saturation ($f s$) because the porosity represents the total free volume available for the liquid pathway and the liquid saturation represents the percent of this pathway that is actually filled with liquid.

6.4.1.3 Correction for Temperature

The following equations correct the diffusion coefficient for temperature:

$$\frac{D_T}{D_0} = \frac{\frac{T}{T_0}}{\frac{\mathbf{h}_T}{\mathbf{h}_0}}, \quad (\text{Eq. 6.4.1-3})$$

where D_T is the diffusion coefficient at temperature T , D_0 is the free water diffusion coefficient at temperature T_0 , \mathbf{h}_T is the viscosity of water at temperature T , and \mathbf{h}_0 is the viscosity of water at temperature T_0 . The temperature dependence of viscosity is given by:

$$\log_{10} \left(\frac{\mathbf{h}_T}{\mathbf{h}_{20}} \right) = \frac{1.3272(293 - T) - 0.001053(T - 293)^2}{T - 168}, \quad (\text{Eq. 6.4.1-4a})$$

$$\text{or} \quad \mathbf{h}_T = (1.002 \times 10^{-3}) 10^{\left[\frac{1.3272(293 - T) - 0.001053(T - 293)^2}{T - 168} \right]}, \quad (\text{Eq. 6.4.1-4b})$$

where $\mathbf{h}_{20} = 1.002 \times 10^{-3}$ Pa-s.

All temperatures are in Kelvin. Equations 6.4.1-3 and 6.4.1-4 correspond to Equations 13 and 24 in CRWMS M&O 2000h, respectively.

6.4.1.4 Correction for Concentrated Aqueous Solutions

Data in the AIP Handbook (Gray 1972, Table 2p-2) show that the majority of the diffusion coefficients increase with increasing solution strength. For example, the diffusion coefficient of sodium iodide increases from 1.616 in a dilute solution to 1.992 for a 3 molar solution and the coefficient for potassium iodide increases from 2.00 in a dilute solution to 2.533 at 3.5 molar. The percent increase for potassium iodide, 26.7%, is the greatest of any in Table 2p-2, excluding HCl. HCl has been excluded from consideration because it is not representative of the type of radionuclides released from the WP.

This correction factor is partly contained in the conservatism inherent in using the self-diffusion coefficient for water as a bounding value for all radionuclides. The correction for concentrated aqueous solutions is therefore being neglected in the TSPA-SR.

6.4.2 Colloidal Transport

Radionuclide transport from the WP occurs as dissolved species at the appropriate solubility or dissolution rate limit and as colloidal particles. Three types of colloids are anticipated to exist in the EBS (CRWMS M&O 2000i): (a) waste form colloids, (b) colloids due to corrosion products, and (c) groundwater colloids. The waste form colloids may have irreversibly attached (embedded) or reversibly attached (sorbed) radionuclides. The corrosion and groundwater colloids may have reversibly attached radionuclides only. The stability and mass concentrations of colloids are functions of the ionic strength and pH of the groundwater or local fluid chemistry in the WP and invert.

The mass of radionuclides irreversibly attached to the waste form colloids is determined from reactions within the WP (CRWMS M&O 2000i). The mass of radionuclides reversibly attached to all three types of colloids is determined primarily by three parameters:

- Mass concentration of dissolved (aqueous) radionuclide in the fluid
- Mass concentration of colloid material in the fluid
- Radionuclide distribution coefficient (K_d) of a specific radionuclide on a specific colloid mineralogical type

The concentrations of colloids in the drifts and EBS has also been determined (CRWMS M&O 2000j).

6.4.3 Transport Through Stress Corrosion Cracks

Two cases are considered for transport through SCCs. In the first case, there is a dripping flux on the WP but no backfill is in contact with the WP. This first case can happen if there is a dripping flux due to condensation and the DS is intact so that quartz sand backfill cannot fill the annular space around the WP. This first case is also applicable after the DS fails for a design without backfill. In the second case, backfill is in contact with the lid and SCCs after DS failure for the current design.

6.4.3.1 Dripping Flux Only

Transport through SCCs in the WP is limited to diffusion. Once SCCs form in the lid of the WP, all surfaces inside the WP are assumed to be coated with a thin film of water (per assumption 5.2.8). This thin film provides the medium for diffusion from the waste form, through the SCC, and out of the WP.

This approach is consistent with several features of the EBS RT Abstraction. First, the dripping flux onto the skirt area of the WP will flow into the SCCs, independent of gap size or film thickness. Second, corrosion products will quickly build up within the SCCs, helping to maintain a continuous fluid layer through capillary processes and possible condensation within the crack. Third, the WPs are angled with the lid-end upward to maximize any dripping flux into the SCC. Fourth, the WP configuration (lid-end upward) means that fluid can pool inside the WP. However, there is no pressure or head gradient driving advective flow out of the WP when only SCCs are present, so this will be only diffusive transport.

If both SCCs and patches are present, then fluid can flow in through the SCCs and out through the patch. This advective path will be negligible compared to patch-to-patch advective flow because the cross-sectional area of a single SCC, $4.08 \times 10^{-6} \text{ m}^2$ or 4.08 mm^2 , is about 5,750 times smaller than the cross-sectional area of a single patch, $23,460 \text{ mm}^2$. The advective flow through SCCs is again negligible in this case as in the previous case. Radionuclide transport out through the SCCs is limited to diffusive transport. Once radionuclides are released through diffusion, they will then be transported by advection through the invert.

It is probable that some WPs will be oriented with the lid-end downward. In this situation, the skirt shields the SCCs from vertical drips, making it quite difficult for any droplets or thin films that might be generated by a dripping flux to reach the SCCs. Even considering the potentially

chaotic nature of droplet flow and the possible presence of dust and particulates on the surface of the WP, the flow must wrap around the edges of the skirt and move transverse to the gravitational gradient in a physically significant amount to reach the SCC and affect EBS performance. This behavior is considered unlikely, unless experimental data indicate a strong potential for transverse movement of droplets and thin films.

Within the WP, the diffusive length is taken to be the thickness of the two lids plus the air gap between the lids. This length is 185 mm for the Naval SNF package, 150 mm for the 21-PWR WP and the 44-BWRWP, and 135 mm for the 5-HLW/DOE SNF short CRM WP (CRWMS M&O 1999f). The diffusive area is calculated as the product of the area and number of cracks. The area of each crack is estimated from the data in Table 5. The maximum cross-sectional area of each crack for diffusive transport is calculated to be $4.08 \times 10^{-6} \text{ m}^2$ (see Section 6.3.1.2.1).

6.4.3.2 Transport with Backfill

As discussed in Section 6.2.3.2, breaching of the DS causes backfill to enter the axial space surrounding the WP. Water flux through the backfill surrounding the WP brings water up to, but not into, the SCCs. The backfill itself cannot penetrate a SCC because the low end of the grain size distribution for the Overton sand is 100 μm , about the same size as the maximum crack width. Since a capillary barrier is formed above the invert (fine backfill over coarse invert), the saturation of the backfill in direct contact with the SCCs is expected to be high. The SCCs should also be highly saturated with water because of the presence of corrosion products in the crack.

In this situation, flow may be drawn through the SCC by capillary forces. If SCCs are the only penetrations through the WP, liquid can pool inside the WP if the lid-end is tilted upward. Substantial advective flux out of the SCC is unlikely in this configuration, so radionuclide release through the SCC will then be primarily by diffusion. Once released from the WP, radionuclides will then be transported by advection and diffusion through the invert. Note that the diffusive pathway through the invert is always present because the WP is assumed to be in contact with the invert (per assumption 5.2.9).

If both SCCs and patches are present, then fluid can flow in through the SCCs and out through the patches. This advective path will be negligible compared to patch-to-patch advective flow because the cross-sectional area of a single SCC, $4.08 \times 10^{-6} \text{ m}^2$ or 4.08 mm^2 , is about 5,750 times smaller than the cross-sectional area of a single patch, $23,460 \text{ mm}^2$. The advective flow through SCCs is again negligible in this case as in the previous case. Radionuclide transport out through the SCCs is limited to diffusive transport. Once radionuclides are released through diffusion, they will then be transported by advection and diffusion through the invert.

The diffusive lengths and areas for these cases are identical to the values calculated in Section 6.4.3.1.

6.5 DRIP SHIELD RESPONSE

The thermal and mechanical response of the DS has been evaluated for five mechanisms: (1) thermal expansion, (2) floor heave, (3) rock fall, (4) seismic response, and (5) pedestal failure.

Thermal expansion, floor heave and rock fall will produce minor structural response in relation to the potential slippage or overlap between adjacent DSs. These mechanisms have therefore been screened out from the TSPA-SR as detailed below.

Seismic response is the key mechanism that may lead to separation of adjacent DSs. The seismic analysis in this AMR is based on the 1-in-10,000 year earthquake. It is several conservative features, in the sense that all the inelastic strain from the earthquake is concentrated at one or a few locations and that the sand backfill is not represented in the analysis. The sand backfill is important because of its large mass relative to that of the DS. Future analyses will consider less probable earthquakes, such as a 1-in-100,000 year event, and the response of the backfill and new DS designs.

Pedestal failure has the potential to shift the DS if the WP falls to the invert and rolls into contact with the shield. This scenario is more likely during an earthquake, when the ground motions may increase the load on the pedestal and impart additional momentum to the WP. Given this association and the bounding nature of the analysis for seismic response, the response to pedestal failure is reasonably considered to be included in the seismic response for TSPA-SR. Note that pedestal failure is implied by assumption 5.2.9 that the WP is in contact with the invert for the purpose of calculating diffusive transport.

6.5.1 Thermal Expansion

Thermal expansion will produce a change in the dimensions of the DS, particularly during the first few thousand years when DS and WP temperatures are most elevated over ambient conditions. The change in length due to thermal expansion will be greatest in the axial direction because that is the longest dimension of the DS. The response in the axial direction is also of most interest for DS separation.

The coefficient of linear thermal expansion is defined as the length change per reference length per degree of temperature change. The coefficient for titanium B 120VCA (aged) is given as (Baumeister 1967; p. 6-10):

$$\frac{\Delta \ell}{\ell \Delta T} = 5.2 \times 10^{-6} (^\circ\text{F}^{-1}) = 9.36 \times 10^{-6} (^\circ\text{C}^{-1}) \quad (\text{Eq. 6.5.1-1})$$

The axial length of the DS, L_{DS} , is 5780 mm. Then for a temperature change of 150°C, which should bound the maximum temperature change at the DS for the TSPA-SR, the length change, $\Delta \ell$, is given by:

$$\Delta \ell = (9.36 \times 10^{-6}) (5780) (150) \text{ mm} = 8.1 \text{ mm}. \quad (\text{Eq. 6.5.1-2})$$

The overlap between adjacent DSs provides for a substantial amount of slippage. Slippage allows adjacent DSs to slide freely in the axial direction, without any structural impediment or blockage. In effect, the slippage distance can accommodate some thermal expansion without generating stresses in the structure. This slippage distance can vary between 0 mm and 434 mm, as documented in Attachment I. The 8 mm thermal expansion calculated in Equation 6.5.1-2 is less than the available slippage more than 98% of the time if there is a uniform distribution of

values from 0 to 434 mm. Even if the slippage distance is less than 8 mm, it is likely that the adjoining shield will be able to accommodate the additional displacement, thereby relieving most stress from thermal expansion.

The effect of thermal expansion on DS separation has therefore been screened out from the TSPA-SR model.

6.5.2 Floor Heave

A ground support analysis for the TSPA-VA calculated the vertical and horizontal closure for an unsupported emplacement drift with a thermal loading of 85 metric tons of uranium per acre (MTU/acre). Vertical closure refers to the change in the distance between the top and bottom of the drift. Similarly, horizontal closure refers to the change in distance between the left and right sides of the drift at the springline. Net vertical closure is between 8 mm inward to 7 mm outward for the combined *in situ* and thermal loads at 150 years (CRWMS M&O 1998d, Section 7.6.2.1.2 and Figure 7-15a). Net horizontal closure is of the same order of magnitude. Seismic loading did not have a significant impact on drift closure (CRWMS M&O 1998d, Section 7.6.2.1.3).

The DS will continue to function properly provided that floor heave does not cause a continuous fluid pathway to form through the backfill onto the WP. If this pathway forms, then water will wet the WP through capillary action, negating the DS as an engineered barrier.

The vertical displacements from floor heave are small relative to the overlap between adjacent DSs. The overlap varies between 200 mm and 635 mm, as shown in Attachment I. The length of overlap is then more than 20 times greater than the displacement from floor heave. It is very unlikely that the sand backfill can completely fill the overlap between shields due to floor heave.

The effect of floor heave on DS separation has therefore been screened out from the TSPA-SR model.

6.5.3 Rock Fall for the As-Emplaced DS Configuration

The potential ranges and distributions of rock falls corresponding to different fracture orientations under static and seismic loads have been analyzed by the Drift Degradation Analysis AMR (CRWMS M&O 2000k). The range of block volumes from rock fall under static loads varies from 0.01 m³ to 65.99 m³ (see Tables 11 through 14, CRWMS M&O 2000k). However, the largest block volumes are relatively improbable, particularly for the drift orientation closest to the license application (LA) design layout (i.e., an azimuth of 105°). For example, the 98th percentile block volume ranges from a minimum of 1.77 m³ for the Tptpln stratigraphic unit to a maximum of 5.56 m³ for the Tptpll stratigraphic unit at 105° (see Tables 13 and 14, CRWMS M&O 2000k).

The maximum block volume under Level 3 (1-in-10,000 year) seismic loads for the LA drift orientation with an azimuth of 105 degrees is 55.63 m³ (see Tables 16 through 19). Note that larger block volumes are more probable for seismic rather than static loads, particularly for the Level 3 earthquake.

A full structural analysis of the DS requires a finite-element model because of its complex shape and the presence of ribs that provide added rigidity for the curved top and flat sides. In lieu of calculating the full structural response to rock fall, the DS response has been estimated based on standard, quasi-static solutions for both a cylindrical shell and for a flat plate. The cylindrical shell model estimates the collapse pressure of the DS and the flat plate solution estimates the magnitude of the deflection of the crown of the DS.

The collapse pressure for a circular cylinder with radial external pressure and simply supported edges can be estimated from solutions in a mechanical engineering handbook (Baumeister 1967, Section 5, Figure 63). The collapse pressure, W_c [psi], is given by:

$$W_c = KE \left(\frac{t}{D} \right)^3, \quad (\text{Eq. 6.5.3-1})$$

where E is Young's modulus [psi], t is the thickness of the cylinder [L], and D is the outer diameter [L]. K is a dimensionless numerical coefficient determined from Figure 63 in Baumeister using the ratios of L/R and D/t , where L is the length of the cylinder [L] and R is the outer radius of the cylinder [L]. The values of L/R and D/t are as follows:

$$\frac{L}{R} = \frac{1067 \text{ mm}}{(1251 + 7.5) \text{ mm}} = 0.85, \quad (\text{Eq. 6.5.3-2})$$

and
$$\frac{D}{t} = \frac{2(1251 + 7.5) \text{ mm}}{15 \text{ mm}} = 168. \quad (\text{Eq. 6.5.3-3})$$

The value of R is given by the radius to the midpoint of the DS as a circular shell plus one-half of the thickness of the DS (see data in Table 1). With these ratios, K is approximately 120 [-] from Figure 63 and the collapse pressure, W_c , is then 375 psi.

The collapse pressure can be compared to the effective pressure from the combined loads of the sand backfill and a 100 m³ block of tuff. This block volume is selected because it bounds the maximum rock fall predicted by the Drift Degradation Analysis AMR. The static pressure from the sand can be estimated using an upper bound for the sand depth. This upper bound is given by the drift diameter (5.5 m) minus the air gap above the backfill (0.50 m) minus the thickness of the invert (0.606 m from CRWMS M&O 1999d). The static pressure from the sand is then bounded by:

$$p_{\text{backfill,max}} = (1593 \text{ kg/m}^3) (9.81 \text{ m/s}^2) (5.5 \text{ m} - 0.5 \text{ m} - 0.606 \text{ m}) = 6.87 \times 10^4 \text{ Pa} = 10 \text{ psi}. \quad (\text{Eq. 6.5.3-4})$$

Note that the density of the sand includes the effect of its porosity (41%). The maximum effective pressure from a cubic block of tuff, $P_{\text{block,max}}$ is then given by:

$$p_{\text{block,max}} = \frac{(100 \text{ m}^3)(2530 \text{ kg/m}^3)(9.81 \text{ m/s}^2)}{(\sqrt[3]{100 \text{ m}^3})(\sqrt[3]{100 \text{ m}^3})} = 1.15 \times 10^5 \text{ Pa} = 16.7 \text{ psi.} \quad (\text{Eq. 6.5.3-5})$$

The maximum effective pressure from the rock fall plus the sand backfill, 27 psi, is then a factor of 14 less than the collapse pressure, 375 psi.

There are many factors that can modify this estimate. For example, the thickness of the DS will decrease from corrosion and the static load from the sand will increase with saturation. The strength of the DS will also decrease with temperature, although this is a relatively minor effect with titanium for the modest temperature changes in the repository. Finally, the loading is not truly radial and the top surface is not cylindrical, so the actual collapse pressure will probably be substantially less than the ideal value of 375 psi. However, there still appears to be a very large margin of safety, particularly because of the bounding estimate for block size. In this situation, the DS is unlikely to collapse due to rock fall in its as-emplaced condition.

Although the drip shield will not have a catastrophic collapse, the potential displacement after a large rock fall is still a possible concern. This displacement has been estimated from a standard, quasi-static solution for a flat plate that is either simply supported or fixed on all four edges. These idealized boundary conditions do not match the situation for the curved top of the DS. For example, the DS has ribs on its undersurface to provide structural support. The vertical sides of the structure also support the curved top. These support mechanisms provide less resistance to displacement than a fixed boundary condition but more resistance than a simply supported boundary condition. So the two cases (fixed or simply supported) are anticipated to bound the response of the DS.

The displacement of a flat plate with fixed or simply supported edges can be estimated from solutions in a mechanical engineering handbook (Baumeister 1967, Section 5, pp. 69-70). The maximum deflection, y_M , is given by:

$$y_M = k_1 \frac{wr^4}{Et^3}, \quad (\text{Eq. 6.5.3-6})$$

where E is Young's modulus [M/L/T^2], t is the thickness of the plate [L], r is the length of the smaller side of the plate [L], and w is a uniformly distributed load [M/L/T^2]. k_1 is a dimensionless empirical coefficient [-] whose values (Baumeister 1967, Table 20) are a function of the appropriate boundary condition and the ratio R/r , where R is the length of the longer side of the plate [L]. The value of R/r is calculated as the width of the DS divided by the distance between ribs:

$$\frac{R}{r} = \frac{2250 \text{ mm}}{1067 \text{ mm}} = 2.1. \quad (\text{Eq. 6.5.3-7})$$

The values of k_1 are then 0.0277 for the fixed boundary condition and 0.1106 for the simply supported boundary condition.

The maximum loads from the sand backfill and a 100 m³ block of tuff are 10 psi and 16.7 psi, respectively (see Equations 6.5.3-4 and 6.5.3-5). Then the maximum deflection for the simply supported (free) and for the fixed boundary conditions is:

$$y_{M,free} = (0.1106) \frac{(10\text{psi} + 16.7\text{psi})(1067\text{mm})^4}{(14.8 \times 10^6 \text{psi})(15\text{mm})^3} = 77\text{mm}, \quad (\text{Eq. 6.5.3-8})$$

and

$$y_{M,fixed} = (0.0277) \frac{(10\text{psi} + 16.7\text{psi})(1067\text{mm})^4}{(14.8 \times 10^6 \text{psi})(15\text{mm})^3} = 19\text{mm}, \quad (\text{Eq. 6.5.3-9})$$

respectively. The response of the DS probably lies between these two extremes. Note that the curvature of the top and the support from the internal ribs and vertical sides will tend to reduce the maximum deflection toward the value in Equation 6.5.3-9. Note also that the load from the backfill (10 psi) has been overestimated by more than a factor of 2 because the depth of sand above the crown is more than a factor of two less than the depth to the bottom of the DS.

The DS will continue to function properly provided that the deflection of the crown does not cause a continuous fluid pathway to form through the backfill onto the WP. The vertical displacements from rock fall are small relative to the overlap between adjacent DSs. The overlap varies between 200 mm and 635 mm, as shown in Attachment I. The minimum length of overlap is then between 2.6 and 10.5 times greater than the deflection of the DS. The maximum length of the overlap is then between 8.2 and 33 times greater than the deflection of the DS.

More accurate estimates of the dynamic response of the DS to rockfall require finite-element calculations that account for the strengthening ribs on the DS, the weight of water in the backfill pore space, and the potential reduction of DS thickness from corrosion. The effects of adjacent DSs must also be included because they will restrain the ends of the DS from lifting up during the rock fall. These uncertainties in DS response to rockfall will not be resolved before the TSPA-SR calculations.

The effect of rock fall on the as-emplaced DS has been screened out from the TSPA-SR model when backfill is present. In the as-emplaced condition, there appears to be an adequate margin of safety to ensure that the deflection of the crown does not cause a continuous fluid pathway to form. The effect of rock fall has also been screened out after the DS degrades, pending more complete analyses of DS response.

6.5.4 Seismic Response

Since each DS is not structurally connected with the invert or the adjacent DSs, there is the potential for separation between adjacent DSs during a seismic event. This separation is referred to as the gap between adjacent drip shields, L_{DS_Gap} , in Table 3; it is used to calculate the flux through the drip shield in Equation 6.2.4-1.

A preliminary calculation has been performed to estimate the DS displacement for a seismic event having a frequency of 10^{-4} per year. The preliminary analysis predicts a maximum displacement of 25 cm (250 mm) for the 1-in-10,000 year earthquake. This value for maximum

displacement is highly uncertain because it does not include any effects from the mass of the backfill on the structural response, and because it allows all displacement from a seismic event to occur at one point in the structure. In addition, the most recent designs for the DS include a vertical pin that will inhibit relative motion between adjacent DSs until failure. In this situation, the value for maximum displacement is considered TBV pending more detailed analyses of seismic response.

The following abstraction is recommended for TSPA-SR. All parameters in this abstraction are considered TBV (MO0003SPASEI01.003). Given the uncertainties in structural response and the potential for design changes, it is not possible to state that this is a conservative or bounding model. Structural response calculations with a broader spectrum of seismic events and with the latest DS design parameters will be necessary before finalizing the TSPA-LA model for seismic response of the DS. However, the following abstraction should provide an indication of the sensitivity of repository performance to seismic events.

- Sample the distribution for DS overlap once per realization. This distribution is a uniform distribution from 200 to 635 mm.
See Attachment I for the calculation of the overlap between DSs. The uniform distribution is chosen because only the lower and upper limits for the overlap are well known.
- The seismic event occurs as a Poisson process with a rate of 10^{-4} per year.
This rate is consistent with the preliminary calculation. A Poisson process is consistent with the expectation that earthquakes will occur randomly over time at a constant probabilistic rate.
- When the seismic event occurs,
 - Sample the distribution for seismic displacement. This distribution is a uniform distribution between 0 and 250 mm (TBV).
 - Sample the distribution for number of gaps per emplacement drift. This distribution is a discrete distribution, with equal probabilities (33.3%) for 1, 2 or 3 gaps per emplacement drift. *The number of gaps is a reasonable approximation for the failure of the DS. Note that the choice of fewer gaps is conservative for generating a separation between adjacent DSs.*
 - Calculate the displacement per gap by dividing the seismic displacement by the number of gaps.
 - Add the displacement per gap from the current event to the sum of the displacements from all previous events.
 - If the sum of the displacements is less than the DS overlap, then the DS is intact and there is no gap between DSs.
 - If the sum of the displacements is more than the DS overlap, divide the sum of the displacements by the number of axial gaps to determine the gap size and frequency in each emplacement drift.
- Limit the number of seismic events to 5 total.
A limit on the number of displacement-inducing seismic events is reasonable because the DS design limits the ability of the shields to “telescope” on top of one another. A maximum of

five events has been chosen because these events will occur over a time period of approximately 50,000 years. After 50,000 years, there will be a substantial number of penetrations through the DS from general corrosion, and the seismic response of the DSs will become an increasingly minor component of the total flow area through the shields. This model therefore represents the seismic response when it is most important, during the first 20,000 years after repository closure, and provides a cutoff after 5 events, when the seismic response is less important and it is unreasonable to continue adding displacements.

This abstraction for the drip shield response to a seismic event may not be a bounding model.

6.5.5 Pedestal Failure

Pedestal failure has the potential to shift the DS if the WP falls to the invert and rolls into contact with the shield. This scenario is more likely during an earthquake, when the ground motions may increase the load on the pedestal and impart additional momentum to the WP.

There are likely to be structural deformations and displacements if a WP rolls into the DS. Note that the sand backfill surrounding the DS will tend to distribute the load from the WP over a wide area. The backfill may also dissipate the energy of impact when the sand is pushed back.

The potential displacements from a rolling WP have not been analyzed in detail. Note that the large overlap between adjacent DSs, 200 to 635 mm, will tend to negate the effects of small deformations or displacements in the side of the DS. This fact, combined with the bounding nature of the analysis for seismic response, suggests that any effects from pedestal failure can be reasonably considered to be included in the variability of the seismic response calculations for the TSPA-SR.

An alternate scenario for pedestal failure could occur if only one end of the pedestal fails while the WP is still supported near its midpoint. In this case, the WP could swing upward after pedestal failure, knocking the DS out of alignment and forming a fluid pathway. This alternate scenario is very unlikely because (1) the current pedestal design does not support the WP near its midpoint, only at the ends (see Emplacement Pallet Sketch, CRWMS M&O 1999c), and (2) the 21 PWR, 44 BWR and Naval SNF WPs are emplaced closer to the invert than to the DS, so it is physically impossible to contact the DS. For example, the 21 PWR WP is 18 cm above the invert but 58.8 cm below the drip shield, so that an 18 cm swing upward at one end will not cause contact between DS and WP. In this circumstance, this alternate scenario has been screened out of the seismic response model for the drip shield.

6.6 BATHTUB MODEL FOR THE WASTE PACKAGE

The conceptual model for the TSPA-SR is based on the presence of continuous flow paths through the patches, SCCs and pits that penetrate the WP. More specifically, the TSPA-SR conceptual model assumes that vertical flow of seepage into the WP, through the waste form and out of the WP is not impeded by the location of patches, SCCs and pits on the surface of the WP (see assumption 5.1.10). There is no long-term build-up and retention of liquid within the WP for flow and transport. There is also no significant resistance to the flow through the waste form. The TSPA-SR approach attempts to maximize the immediate release and mobilization of

radionuclides into the local groundwater environment. The TSPA-SR approach will be referred to as the “flow through” geometry.

An alternative conceptual model to the “flow through” geometry is the “bathtub” geometry (Mohanty et al. 1996). The bathtub geometry allows seepage to collect within the WP before being released to the EBS. In theory, a bathtub geometry could result in the sudden release of a large pulse of radionuclides when a package overflows with liquid or when a second patch fails abruptly beneath the water line.

The “bathtub” effect will be most important during the first 20,000 years after repository closure because only a few patches or pits are anticipated to penetrate the DS and WP during this time frame. In this situation, there may be penetrations through the top of the WP while the bottom surface remains intact, leading to retention of liquid. At longer duration, say 100,000 years or greater, the presence of multiple penetrations makes a “flow-through” geometry the more likely configuration.

The response of the bathtub geometry is evaluated for a primary case and for three secondary cases. The primary case includes consideration of two types of radionuclide release mechanisms: dissolution rate limited and solubility limited. Tc-99 is typical of dissolution rate limited radionuclides: the Tc-99 released due to waste dissolution can always be dissolved in the available groundwater because the solubility limit of Tc-99 is very high. Np-237 is typical of the second type of radionuclide, where all the release from dissolution is limited by the low solubility.

The results for the primary case are based on a closed form analytic solution with constant values of inflow rate, dissolution rate, and solubility. The three secondary cases consider a step change in inflow rate, such as would occur from a climatic change, a step change in groundwater chemistry, and a step change in flow geometry, as would occur if a patch suddenly failed beneath the waterline. The basic geometry and flow pattern for the primary bathtub model is shown in Figure 6 (from Mohanty et al. 1996, Figure 2-7). q_{in} is identical with F_5 in Table 3 and in Section 6.3.2.

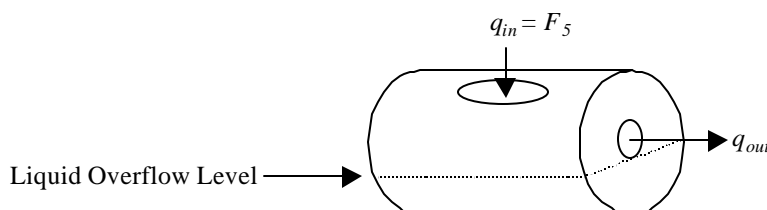


Figure 6. Schematic of the Bathtub Geometry for the Waste Package

6.6.1 Primary Case

6.6.1.1 Dissolution-Rate-Limited Radionuclide

Consider the system shown in Figure 6, with a constant inflow rate, q_{in} , and assume that V_{tub} is the total volume of liquid that can be retained within the WP before it overflows. The response of the WP will be a two step process. During Step 1, the package is filling with liquid and the

outflow rate, q_{out} , is zero. This condition continues until the WP fills with liquid at a time, T_{fill} , given by V_{tub}/q_{in} . After time T_{fill} , the amount of liquid inside the WP remains constant and $q_{out} = q_{in}$. This is a steady state condition, consistent with the assumption that q_{in} is constant and that liquid does not continue to accumulate within the package. Note that the following analysis assumes there is complete contact between the liquid and the waste form within the WP. This assumption is consistent with the use of a single mixing cell to represent the waste package for the TSPA-SR model.

During Step 1, for time t such that $0 < t < T_{fill}$, the release of a radioisotope into the groundwater inside the WP can be represented as

$$\dot{m} = Df, \quad (\text{Eq. 6.6.1-1})$$

where \dot{m} is the rate of release of radionuclide into the liquid [M/T],

D is the dissolution rate of the waste form [M/T], and

f is the mass fraction of radioisotope released per unit mass of waste form (-)
(f is less than one for a waste form with multiple radionuclides).

During the fill period q_{out} is zero, so the mass, $m(t)$, of radioisotope dissolved within the liquid in the WP at time t is given by

$$m(t) = Dft, \quad (\text{Eq. 6.6.1-2})$$

because D and f are constant. Similarly the volume of liquid in the WP at time t , $V(t)$, is given by

$$V(t) = q_{in}t, \quad (\text{Eq. 6.6.1-3})$$

so the concentration of dissolved isotope in the WP, $c(t)$, is

$$c(t) = \frac{m(t)}{V(t)} = \frac{Dft}{q_{in}t} = \frac{Df}{q_{in}}. \quad (\text{Eq. 6.6.1-4})$$

Note that the concentration, $c(t)$, is constant during the fill phase because the values of D , f , and q_{in} are assumed to be constant. This result for $c(t)$ is not surprising because the dissolved mass, m , and the volume of liquid, V , are linear functions of the time, so their ratio remains constant.

The result in Equation 6.6.1-4 will hold for each dissolution-rate-limited radioisotope in the waste form, although the numerical value of c will differ because the mass fraction, f , is different for each isotope. Note that the equations in Section 6.6 generally apply to the i^{th} isotope in the waste form, although the subscript has been dropped for simplicity.

During Step 2, when $t > T_{fill}$, the radioisotope mass within the WP is a balance between the release of radioisotope into the groundwater within the WP and the loss of radioisotope due to outflow from the WP:

$$\dot{m} = Df - q_{out}c(t). \quad (\text{Eq. 6.6.1-5})$$

Substituting for the definition of $c(t)$ from Equation 6.6.1-4:

$$\dot{m} = Df - q_{out} \frac{m(t)}{V_{tub}}, \quad (\text{Eq. 6.6.1-6})$$

a first order differential equation with constant coefficients. The solution to this equation for constant q_{in} , with $q_{out} = q_{in}$, is derived in Attachment II and given by:

$$m(t) = m(T_{fill}) = DfT_{fill}. \quad (\text{Eq. 6.6.1-7})$$

It follows that

$$c(t) = \frac{m(t)}{V(t)} = \frac{DfT_{fill}}{V_{tub}} = \frac{Df}{q_{in}}. \quad (\text{Eq. 6.6.1-8})$$

Note that the dissolved mass in the WP is constant for $t > T_{fill}$. In addition, the concentration of dissolved radionuclide is constant for all time $t > 0$, as shown by Equations 6.6.1-4 and 6.6.1-8. These results are reasonable because the WP is in steady state for $t > T_{fill}$. This means that the inflow rate equals the outflow rate and that any loss of dissolved radionuclide mass in the outflow from the WP is exactly balanced by the addition of dissolved radionuclide mass from dissolution of the waste form.

The response for the comparable flow-through model has the same radionuclide concentration, $c(t)$, and the same release flux, given by $c(t)q_{out}$, as the bathtub geometry. The sole difference between the flow-through and bathtub models is that the flux from the flow-through model starts from $t = 0$ while the flux from the bathtub model is zero until time T_{fill} . The bathtub model introduces a delay in the response but does not change the concentration in the package or the mass flux out of the package.

The flow-through model is conservative relative to the bathtub model for radionuclide transport. The flow-through transport model assumes advective transport with no sorption of radionuclides. These assumptions are consistent with those used elsewhere in this AMR. With these assumptions, the flow-through transport model releases radionuclides with no delay into the invert and UZ, in contrast to the delay inherent in the bathtub model.

6.6.1.2 Solubility-Limited Radionuclide

The response for a solubility-limited radionuclide is similar to that for a dissolution-rate-limited radionuclide, in the sense that the bathtub model delays the release from the WP but does not change the dose rate.

During Step 1, $0 < t < T_{fill}$, the amount of radionuclide dissolved in the groundwater in the WP can be represented as

$$\dot{m} = sq_{in}, \quad (\text{Eq. 6.6.1-9})$$

where s is the solubility limit of the radionuclide. Assuming constant groundwater chemistry (assumption 5.4.1), the solubility will be constant and the mass, m , of radioisotope retained in the WP at time t is

$$m(t) = sq_{in}t. \quad (\text{Eq. 6.6.1-10})$$

The volume of liquid in the WP at time t , $V(t)$, is given by

$$V(t) = q_{in}t, \quad (\text{Eq. 6.6.1-11})$$

so that the concentration of dissolved isotope in the WP is

$$c(t) = \frac{m(t)}{V(t)} = \frac{sq_{in}t}{q_{in}t} = s. \quad (\text{Eq. 6.6.1-12})$$

The concentration is constant during the fill phase and equal to the solubility limit, as would be expected. This is true for each radionuclide in the system, although the numerical values of the solubility limit will vary.

For $t > T_{fill}$, the mass balance within the WP is given by:

$$\dot{m} = sq_{in} - c(t)q_{out} = sq_{in} - \frac{m(t)}{V_{tub}}q_{out}. \quad (\text{Eq. 6.6.1-13})$$

The solution to Equation 6.6.1-13 with $q_{out} = q_{in}$ is given by:

$$m(t) = sV_{tub}, \quad (\text{Eq. 6.6.1-14})$$

with

$$c(t) = s. \quad (\text{Eq. 6.6.1-15})$$

Again the dissolved mass in the WP is constant for $t > T_{fill}$ and the concentration of dissolved radionuclide is constant at the solubility limit for all times $t > 0$ (see Equations 6.6.1-12 and 6.6.1-15).

The comparable flow-through model has the same radionuclide concentration, s , and the same release flux, given by sq_{out} , as the bathtub geometry. The sole difference is that the flux from the flow-through model starts from $t = 0$ while the flux from the bathtub model is zero until time T_{fill} . The bathtub model introduces a delay in the response but does not change the dose rate. Again, the flow-through model is conservative relative to the bathtub model because radionuclides are released with no delay time to the EBS.

6.6.2 Secondary Cases

The secondary cases evaluate the response of the bathtub model when changes occur in the groundwater inflow rate, in groundwater chemistry, or in the flow geometry.

6.6.2.1 Change in Inflow Rate

The response of a bathtub model to a change in inflow rate differs for a solubility-limited or a dissolution-rate-limited radionuclide. The solubility-limited case is simpler because of chemical equilibrium and is discussed first.

Consider a step change in inflow rate after the bathtub has filled for a solubility-limited radionuclide. Since kinetic effects are ignored, the chemical system is always at equilibrium and the concentration within the WP remains unchanged at the solubility limit. The only change in the system is that the radionuclide mass flux out of the WP changes instantaneously from cq_{out} to $cq_{out, new}$. This response is exactly the same as it would be for the flow-through model, so the response of the bathtub model is identical to that for the flow-through model.

Now consider a step change in inflow rate after the bathtub has filled for a dissolution-rate-limited radionuclide. In this case the mass released per unit time remains constant because the dissolution rate remains constant, but the radionuclide concentration will come to a new equilibrium value. This new equilibrium value can be determined by Equation 6.6.1-8, with the product of concentration and liquid inflow remaining constant:

$$c_{new}q_{in,new} = c_{old}q_{in,old} = Df. \quad (\text{Eq. 6.6.2-1})$$

If the inflow rate decreases, the final concentration will increase because their product remains constant. A flow-through model will have an instantaneous increase in concentration, while the bathtub model will show an exponential growth to the new concentration. The flow-through model is then conservative for concentration released into the EBS.

The exponential growth to the new concentration can be seen as follows. The replacement of “old” groundwater with concentration c_{old} with “new” groundwater with concentration c_{new} can be represented through a parameter \mathbf{b} , the volume fraction of old groundwater to V_{tub} , the total liquid volume in the bathtub. The rate of change of the volume of old groundwater, V_{old} , is given by:

$$\frac{dV_{old}}{dt} = -\mathbf{b}q_{out,new} = -\mathbf{b}q_{in,new}. \quad (\text{Eq. 6.6.2-2})$$

Equation 6.6.2-2 represents the loss of old groundwater through outflow, with the factor \mathbf{b} representing the (decreasing) volume fraction of old groundwater that is lost. Since by definition,

$$\mathbf{b} \equiv \frac{V_{old}}{V_{tub}}, \quad (\text{Eq. 6.6.2-3})$$

and substituting this definition into the left-hand side of Equation 6.6.2-2, it follows that:

$$\frac{d\mathbf{b}}{dt} = -\frac{q_{in,new}}{V_{tub}} \mathbf{b}. \quad (\text{Eq. 6.6.2-4})$$

The solution to Equation 6.6.2-4 is an exponential decay of ***b*** from 1 to 0, which corresponds to an exponential decay of *c* from *c_{old}* to *c_{new}*.

If the inflow rate increases, the concentration will decrease. A flow-through model will have an instantaneous decrease in concentration, while the bathtub model will exponentially relax to the new concentration. The flow-through model is then less conservative for concentration released into the EBS. Note that the mass of radionuclide mobilized is identical, as implied by Equation 6.6.2-1; but the dissolved concentration will vary with the amount of fluid flowing through the system. The TSPA-SR model passes mass to the UZ, rather than concentration, so the difference between the flow through model and the bathtub model for this case is probably not critical to performance.

Finally, a change in inflow rate during the initial period, when the bathtub is filling, only affects the value of *T_{fill}* and hence the delay until the bathtub fills, after which it will behave as described in Section 6.6.1.

In summary, the response of the bathtub model to a change in inflow rate is identical to that of the flow-through model for solubility-limited radionuclides. For dissolution-rate-limited radionuclides, the response of the bathtub model is less conservative than the flow-through model when the inflow rate decreases (and concentration increases). If the inflow rate increases (and concentration and probably dose decreases), the bathtub model will be more conservative than the flow-through model.

6.6.2.2 Change in Groundwater Chemistry

Consider a step change in groundwater chemistry after the bathtub has filled. Initially, there will be minor changes in concentration within the bathtub because the bulk of the water retains the original groundwater composition. Eventually the “old” groundwater will be flushed out and replaced with the “new” groundwater, resulting in new concentrations within the bathtub.

The replacement of old with new groundwater can be represented through a parameter ***b***, representing the volume fraction of old groundwater to *V_{tub}*, the total liquid volume in the bathtub. The rates of change of the volumes of old and new groundwater are given by:

$$\frac{dV_{old}}{dt} = -\mathbf{b}q_{out}, \quad (\text{Eq. 6.6.2-5})$$

and

$$\frac{dV_{new}}{dt} = q_{in} - (1 - \mathbf{b})q_{out}, \quad (\text{Eq. 6.6.2-6})$$

where *V_{old}* and *V_{new}* represent the volumes of groundwater with the old and new chemistries, respectively. Equation 6.6.2-5 represents the loss of old groundwater through outflow, with the factor ***a*** representing the volume fraction of old groundwater that is lost. Equation 6.6.2-6 represents the addition of new groundwater through inflow and its partial loss through outflow. Remembering that *q_{out}* = *q_{in}* because of the steady state assumption, it follows that

$$\frac{dV_{old}}{dt} = -\mathbf{b}q_{in}; \quad \frac{dV_{new}}{dt} = +\mathbf{b}q_{in}. \quad (\text{Eq. 6.6.2-7})$$

By definition

$$\mathbf{b} \equiv \frac{V_{old}}{V_{tub}}, \quad (\text{Eq. 6.6.2-8})$$

and substituting this definition into the left-hand equation in 6.6.2-7 it follows that:

$$\frac{d\mathbf{b}}{dt} = -\frac{q_{in}}{V_{tub}} \mathbf{b} = -\frac{1}{T_{fill}} \mathbf{b}. \quad (\text{Eq. 6.6.2-9})$$

The solution to Equation 6.6.2-9 with the boundary condition $\mathbf{b}(0) = 1$, is given by

$$\mathbf{b}(t) = e^{-\frac{t}{T_{fill}}}, \quad (\text{Eq. 6.6.2-10})$$

It follows that the old and new volumes of groundwater are given by:

$$V_{old} = V_{tub} e^{-\frac{t}{T_{fill}}} \quad (\text{Eq. 6.6.2-11})$$

and

$$V_{new} = V_{tub} \left(1 - e^{-\frac{t}{T_{fill}}} \right) \quad (\text{Eq. 6.6.2-12})$$

These equations say that the volume fraction of groundwater with the old chemistry decays exponentially with the characteristic time T_{fill} . Alternately, the volume fraction of new groundwater increases to 1.0 with a characteristic time of T_{fill} for the exponential growth given by Equation 6.6.2-12.

The impact of changing groundwater chemistry on dissolution rate or solubility is much more difficult to predict analytically because chemical interactions are very nonlinear. More specifically, the pH of mixtures of groundwaters will not be proportional to \mathbf{a} because the pH scale is proportional to the log of the hydrogen ion concentration and inherently nonlinear and because potential chemical interactions in mixtures, such as buffering, produce a nonlinear response. In addition, solubility and dissolution rate are often complex nonlinear functions of the pH.

Nonlinear response makes it particularly difficult to predict the time-dependent response for (say) solubility; however, the starting state and the ending state, for $t \gg T_{fill}$, are well defined and can be approximated to first order by

$$s(t) \approx s_{old} e^{-\frac{t}{T_{fill}}} + s_{new} \left(1 - e^{-\frac{t}{T_{fill}}} \right) \quad (\text{Eq. 6.6.2-13})$$

Consider the response when $s_{new} \gg s_{old}$. This condition can easily occur for the actinides, where solubility increases by several orders of magnitude as pH changes from between 7 and 8 to a value below 6 or above 10. In the limit of large s_{new} , Equation 6.6.2-13 becomes

$$(s_{new} \gg s_{old}) \quad s(t) \approx s_{new} \left(1 - e^{-\frac{t}{T_{fill}}} \right) \quad (\text{Eq. 6.6.2-14})$$

In effect the initial solubility is negligible compared to s_{new} , and solubility at late times increases to s_{new} from below. Alternately, if $s_{new} \ll s_{old}$,

$$(s_{old} \gg s_{new}) \quad s(t) \approx s_{old} e^{-\frac{t}{T_{fill}}} + s_{new}. \quad (\text{Eq. 6.6.2-15})$$

Here the solubility will decay towards a much smaller value in the new groundwater mixture.

While the details of the time-dependent behavior are unknown, the starting and ending states must be accurate and Equations 6.6.2-14 and 6.6.2-15 provide a simplified approximation to the transition from one chemical regime to another. Note also that the dissolution rate could replace solubility in Equations 6.6.2-13 through 6.6.2-15, and the same general conclusions would hold.

In summary, the response of the bathtub model to a change in groundwater chemistry will be slower than that for a flow-through model, where the solubility or dissolution rate will change abruptly with a step change in groundwater chemistry. The bathtub damps or delays the response to a change in groundwater chemistry over a time scale on the order of perhaps T_{fill} to $7T_{fill}$. The upper estimate of $7T_{fill}$ corresponds to an exponential factor of e^{-7} or 0.0009, at which point Equation 6.6.2-15 should have asymptoted to s_{new} . The analytic models cannot predict the precise time dependence because of the nonlinear effects of mixing on pH and of pH on solubility and dissolution rate.

The flow-through model is conservative when solubility increases because the bathtub geometry delays the increase in radionuclide concentrations and mass fluxes from the WP to the EBS. Note that the case of increasing solubility or increasing dissolution rate is important because it will increase the peak dose rate. The fact that the flow-through model is not conservative when solubility or dissolution rate decreases is therefore of less importance for performance assessment and is of secondary importance in selecting the conceptual model for flow through the WP.

6.6.2.3 Change in Patch Geometry

The geometry for the bathtub model allows seepage to collect within the WP before being released to the EBS. In the primary model (Figure 6), the patch is positioned such that release is governed by the condition $q_{out} = q_{in}$ after the package fills with liquid.

An alternate conceptual model does not have an existing patch on the side of the package, but instead allows the second patch to fail abruptly beneath the water line. While the radionuclide

concentration within the WP is unchanged by the alternate location, failure will result in the sudden release of a larger pulse (mass) of radionuclides at the failure time of the second patch. Mathematically, the flux of radionuclides leaving the WP in the primary model, F_{pri} , is given by:

$$F_{pri} = cq_{out} = cq_{in} = c \frac{V_{tub}}{T_{fill}}, \quad (\text{Eq. 6.6.2-16})$$

and the flux of radionuclides leaving the WP in the alternate model, F_{alt} , is given by:

$$F_{alt} = c \frac{V_{tub}}{\Delta T}, \quad (\text{Eq. 6.6.2-17})$$

where ΔT is the time to empty the retained liquid through the second patch. In theory, it is possible that $\Delta T \ll T_{fill}$, so that $F_{alt} \gg F_{pri}$.

Equations 6.6.2-16 and 6.6.2-17 have the same value for radionuclide concentration, c , in the retained liquid because the chemistry of the groundwater is independent of patch location. Equations 6.6.2-16 and 6.6.2-17 also assume that the second patch in the alternative conceptual model fails when the volume of liquid is identical to the capacity of the WP in the primary model.

It is worth noting that the flow-through model produces an average release continuously, while the bathtub model with the alternate flow path produces zero release initially, followed by a high pulse that returns to the same flux as the flow-through model. In other words, the flow-through model represents a time average of the response of the bathtub model. From this viewpoint, the potential difference F_{alt} and F_{pri} will be partly mitigated by the sorption and diffusion processes in the unsaturated and saturated zones. The potential difference between F_{alt} and F_{pri} will also be small if the second patch fails shortly after the first penetration because there will be less retained liquid.

This alternate scenario can also be thought of as being equivalent to the appearance of additional penetrations in the WP. This analogy is appropriate because additional penetrations in the WP increase the groundwater flux into the waste form, resulting in higher releases to the EBS. The main effect of the alternate conceptual model is to generate this increase earlier. This is not considered a major difference because there is a very wide range of variability in corrosion rates for the TSPA-SR model (CRWMS M&O 2000b). The effect of the alternate conceptual model can then be reasonably considered to be captured within this variability.

The results and observations in this section (6.6.2.3) and throughout Section 6.6 are appropriate for the general boundary conditions considered here. In other words, this comparison is based on the full fluid flux into the WP having access to all radioisotopes in the waste. An alternate conceptual model, in which radionuclides are mobilized in a rind of corrosion products around the fuel pellets, will partly mitigate the differences discussed here. This mitigation occurs because a large fluid flux will not transport radionuclides at the solubility limit if the mass in solution is limited by the pore volume in a rind of corrosion products. The situation is then

similar to that mentioned at the end of Section 6.6.2.1, where mass transfer to the UZ is the dominant issue, rather than dissolved concentration.

6.6.3 Summary

The response of the bathtub geometry has been evaluated for a primary case, with constant boundary conditions and material properties, and for three secondary cases. Analyses for the three secondary cases consider a step change in inflow rate, a step change in groundwater chemistry, and a change in flow geometry, as would occur if a patch suddenly failed beneath the waterline. All cases include consideration of two types of radionuclide release mechanisms: dissolution-rate-limited and solubility-limited. The comparisons are based on closed form analytic solutions.

The key conclusions from the evaluation follow:

- The bathtub model introduces a time delay in the release of radionuclides from the WP to the EBS in comparison to the flow-through model for the primary case. The flow-through model is conservative in relation to the bathtub geometry for the primary case because there is no delay in release of radionuclides to the EBS.
- The response of the bathtub model to a step change in inflow rate (secondary case 1) is identical to the flow-through model for solubility-limited radionuclides. The response of the bathtub model for dissolution-rate-limited radionuclides is to delay the change in concentration and mass flux associated with the new inflow rate. The flow-through model is conservative with respect to the bathtub geometry for the case of decreasing inflow, when the concentration of radionuclide increases. The case of increasing radionuclide concentration is of primary interest from a performance or regulatory viewpoint.
- The response of the bathtub model to a step change in groundwater chemistry (secondary case 2) is to delay the change in concentration and mass flux associated with the new groundwater chemistry. Analytical models cannot define the exact time delay, which will be sensitive to nonlinear chemical effects when groundwaters mix. Limiting cases, when solubility increases or decreases by several orders of magnitude, have been examined to define a first order approximation to the response of the chemical system.

The flow-through model is conservative with respect to the bathtub geometry when solubility or dissolution rate increase with changing groundwater chemistry. The flow-through model is conservative because it has an instantaneous change to the higher equilibrium value while the bathtub geometry delays the change until the old groundwater is flushed out of the WP. Note that the case of increasing radionuclide concentrations and fluxes is of primary interest from a performance or regulatory viewpoint, so the lack of conservatism of the flow-through model for decreasing solubility or dissolution rate is ignored here.

- The response of the bathtub model when a second patch opens instantaneously beneath the water level in the WP (secondary case 3) has been analyzed. The impact of the

instantaneous opening is to release a pulse (additional mass) of radionuclides in comparison to the flow-through model. The impact of this alternate conceptual model is mitigated by the time delays introduced through sorption and diffusion in the unsaturated and saturated zones. In addition, the higher mass flux from the alternate flow path is similar to the impact from additional patches opening in the WP. Note that there is a wide range of variability in corrosion rates for the TSPA-SR model, and the impact from the instantaneous opening is probably encompassed in the uncertainty in corrosion rates.

The impact of this alternate flow path has therefore been screened out of TSPA-SR analyses because of the potential mitigation from sorption and diffusion and because the variability of corrosion rates provides substantial uncertainty in radionuclide fluxes from the WP.

7. CONCLUSIONS

The EBS RT Abstraction for the flow of water and the transport of radionuclides in the EBS has been defined in this AMR. This model is a reasonably bounding model because it is designed to overestimate flow through the DS and into the WP and transport out of the EBS. Future efforts will refine some of the approximations in the current model in order to have a more realistic yet still conservative approach for licensing calculations.

7.1 CONCEPTUAL MODEL SUMMARY

Radionuclide transport out of the waste form and WP, through the invert, and into the UZ is dependent on a complex series of events in the repository. After the WPs are emplaced, radioactive decay of the waste will heat the drifts and locally perturb the normal percolation of water through the mountain. As the drifts cool, some of the water percolating through the mountain may drip and wick into the drifts and subsequently contact some of the DSs. Over time, the DS, WP, and other components of the EBS are expected to degrade, leading to the mobilization and transport of radionuclides through the EBS to the UZ. The primary transport medium through the EBS is anticipated to be water. Either a thin film or moving water is necessary for radionuclide transport out of the WP and through the invert to the UZ.

A number of key factors will affect the mobilization and transport of radionuclides through the EBS:

- Performance of the DSs
- Performance of the WPs
- Protection provided by cladding
- Waste form degradation rates
- Entry and movement of water through WPs
- Solubilities of radionuclides
- Transport of radionuclides through and out of the WPs
- Transport of radionuclides through the invert below the WPs
- Colloidal transport of radionuclides

Once a DS is breached, water may contact the WP. Once a WP is breached, water may enter the package as water vapor or as drips. If the cladding is also breached, radionuclides may start to dissolve in the water. The dissolved concentration of each radionuclide mobilized from the waste form cannot exceed the radionuclide solubility limit, unless suspended colloids are included. Colloids may be important for two reasons: they may increase the release of radionuclides from the WP, and they may increase the transport velocity of radionuclides. Radionuclides mobilized in water as dissolved or colloidal species may then be transported by advective and diffusive transport from the waste form, through the WP, and out of breaches in the WPs. Once outside the package, the radionuclides will be transported through the invert predominantly by diffusion, if water is not flowing through the invert, or by advection, if an appreciable amount of water is flowing through the invert.

The emphasis in this AMR is on a reasonable approach that bounds the response of the EBS. The use of reasonable bounds is appropriate because of the uncertainty in the response of a very complex engineered system over long periods of time. The EBS RT Abstraction model is valid and appropriate for its intended use because it is designed to be a bounding, conservative model. Following are the noteworthy conservatisms in this abstraction:

- **Seepage through the DS always falls on a WP.** DS placement in the current repository design is such that the overlap between adjacent DSs should be above the small axial gap between adjacent packages. This feature is conservatively ignored because the quartz-sand backfill that falls through the DS separation will probably fill the axial gap and provide a flow path onto the WPs.
- **Seepage is assumed to uniformly wet the DS and WP.** The seepage and flow of droplets tends to be a chaotic process in space and time. Because seepage will vary spatially and temporally over the approximately 10,000 WPs in the potential repository, it seems reasonable to represent the response of groups of WPs as averages for performance assessment. In addition, the flux into a breached DS or WP assumes that the breach is located so that it will collect all fluid dripping onto the DS or WP at the same axial location as the breach. This assumption conservatively ignores the possibility that a dripping flux on the left half of a DS or WP may not be able to reach a breach on the right half. This approach provides a degree of conservatism for a complex, chaotic process.
- **Diffusive transport is maximized because transport is always possible through SCCs and because the WP is in contact with the invert.** The waste form is assumed to be covered with a thin liquid film that supports diffusive transport at all times. In addition, the WP is assumed to be in contact with the invert, providing a continuous liquid pathway for diffusion. Radionuclides will then be released by diffusion through a SCC, even when the DS is intact and there is no advective flux into the WP. Note that this transport pathway will also function when the package is hot and in-package evaporation may be significant enough to dry out the thin liquid films on the waste form.
- **Release of radionuclides through advective transport is independent of the location of breaches on the WP.** Advective transport out of the WP is based on a flow-through model that is independent of the location of penetrations through the WP or the DS. This means that a WP with only one penetration or a WP with one or more penetrations

on its upper surface and none on its lower surface will still have advective transport into the invert.

- **Evaporation within and on the WP is ignored.** Diffusive or advective transport will cease if the heat from the waste form can evaporate any thin liquid films on the waste form or evaporate a small seepage flux on the surface of the WP. The potential for evaporation to eliminate radionuclide transport is conservatively ignored in the EBS RT Abstraction.
- **Bounding value for diffusion coefficient.** The use of a bounding diffusion coefficient for all radionuclides may overestimate the diffusivity of actinide complexes by an order of magnitude. The effect of porosity and liquid saturation on the free water diffusivity has been included in a conservative manner. These assumptions enhance diffusion.

The conceptual model for flow through the EBS identifies nine key flow pathways. These pathways and their relationships are summarized in the following list and in Table 8. Sections 6.1.1, 6.2, and 6.3 contain a detailed technical discussion of the EBS flow abstraction.

- **Seepage Flux and Capillary Flux**—These are the input fluxes or boundary conditions.
- **Through the DS to the WP**—Flux through the DS is based on the ratio of the axial lengths of breaches in the DS to the total axial length of the DS. The number of patches and pits in the DS and WP are calculated by the WP Degradation software (WAPDEG).
- **DS to Unsaturated Zone (Diversion around DS)**—Any seepage flux that doesn't go through the DS is assumed to bypass the EBS and flow straight into the UZ.
- **Through the WP to the WF**—Flux into the WP is proportional to the product of the flux through the DS and the ratio of the lengths of patches and pits in the WP to the total axial length of the WP.
- **WP to Invert (Diversion around WP)**—Flow that doesn't go through the WP is diverted to the invert.
- **Invert to WP (Evaporation)**—If the DS is cooler than the invert, all the evaporative flux from the invert is assumed to drip on the WP. If the DS is hotter than the invert, there is no dripping on the WP from the evaporative flux. Current thermal-hydrologic calculations indicate that condensation does not occur on the underside of the DS.
- **Waste Form to Invert**—All the flux from the WP flows to the invert, independent of patch/pit location on the WP.
- **Invert to UZ**—All the flux into the invert is released into the UZ.

Table 8. Summary of EBS Flow Abstraction

| Flow Pathway | Flow Parameters | Data Sources & Notes |
|-------------------------------|--|---|
| 1. Seepage flux, F_1 | Seepage flux is a boundary condition for the EBS flow abstraction | (CRWMS M&O 2000c) provides time-dependent and location-dependent values of seepage flux. |
| 2. Capillary flux, F_2 | Capillary flux is a boundary condition for the EBS flow abstraction. | Capillary flux will be determined by abstraction of computational results from the the NUFT code (CRWMS M&O 1999j). |
| 3. Flux through the DS, F_3 | $F_3 = (F_1 + aF_2) \times (L_{DS_SCC} + L_{DS_Patch} + L_{DS_Pit} + L_{DS_Gap})/L_{DS}$ a is a factor between 0 and 1 based | WAPDEG (CRWMS M&O 1998c) will provide the number of patches, pits and SCCs on the DS; |

| Flow Pathway | Flow Parameters | Data Sources & Notes |
|-----------------------------------|--|--|
| | on the design and backfill properties; (see Section 6.2.4) | patch size is constant: $7.21 \times 10^4 \text{ mm}^2$ (CRWMS M&O 2000b); $L_{DS \text{ Patch}} = (7.21 \times 10^4)^{0.5} = 269 \text{ mm}$ $L_{DS \text{ Gap}}$ is calculated from a seismic response model (see Section 6.5.4) |
| 4. Diversion around DS, F_4 | $F_4 = F_1 + aF_2 - F_3$ (see Section 6.2.4) | Continuity of liquid flux (quasi-steady flow) |
| 5. Flux into the WP, F_5 | $F_5 = (F_3 + F_7) \times (L_{WP_Patch} + L_{WP_Pit})/L_{WP} + F_7(L_{WP_SCC})/(L_{WP} + L_{WP_SCC})$; (see Section 6.3.2) | WAPDEG will provide the number of patches, pits and SCCs on the WP; patch size is constant: $2.346 \times 10^4 \text{ mm}^2$ (CRWMS M&O 2000b); $L_{WP \text{ Patch}} = (2.346 \times 10^4)^{0.5} = 153 \text{ mm}$ L_{WP_SCC} is calculated based on the maximum tilt angle of the WP and the diameter of the closure lid (see Section 6.3.2) |
| 6. Diversion around the WP, F_6 | $F_6 = F_3 + F_7 - F_5$ (see Section 6.3.2) | Continuity of liquid flux (quasi-steady flow) |
| 7. Evaporative flux, F_7 | If $T_{DS} < T_{Invert}$, then F_7 is the evaporative flux calculated by NUFT; else $F_7 = 0$. (see Section 6.3.3) | Data for temperatures and evaporative flux are based on an abstraction of NUFT calculations (CRWMS M&O 1999). |
| 8. Flux to the invert, F_8 | $F_8 = F_5$ (see Section 6.3.4) | Quasi-steady, flow-through assumption for WP |
| 9. Flux to the UZ, F_9 | $F_9 = F_6 + F_8 - F_7$ (see Section 6.3.4) | Quasi-steady flow-through assumption for invert. Note that only F_8 can transport radionuclides through the invert. |

The waste form is the source of all radionuclides in the potential repository system. Radionuclides can be transported downward, through the invert and into the UZ. Transport can occur through advection when there is a fluid flux through the WP, and by diffusion through thin films in the WP when there are SCCs in the lids of the package. The concentration of each radionuclide during transport is limited by the sum of its (dissolved) solubility limit and the presence of any colloidal particles that may act as reversible or irreversible carriers for the radionuclide.

Transport through the quartz sand backfill is anticipated to be negligible under any conditions. Before the DS fails, upward diffusion through the backfill will be negligible for two reasons. First, a continuous, direct flow path does not exist between the WP and the backfill while the DS is intact. Second, the circuitous pathway that goes down to the invert, laterally across the invert and then upward through the backfill will most likely be dominated by any seepage or capillary fluxes moving through the backfill toward the UZ. After the DS fails upward diffusion will be negligible in comparison to the downward advective flux through the DS.

The diffusion coefficient in the invert is based on the self-diffusivity of water at 25°C as a bounding value for all radionuclides. The effects of porosity and time-dependent saturation in the invert are conservatively incorporated by multiplying the self-diffusivity by the product of porosity and saturation in the invert. The effect of temperature is also incorporated into the abstraction for the diffusion coefficient.

No credit is taken for the potential for sorption in the waste form, WP or invert. Partition coefficients for all radionuclides are conservatively set to zero in the WP and invert.

The conceptual model for transport through the EBS focuses on the flow from the waste form to invert and from the invert to the UZ. The transport pathways and transport processes (advection or diffusion) are summarized in Table 9. Sections 6.1.2 and 6.4 contain a detailed technical discussion of the EBS transport abstraction.

Table 9. Summary of EBS Transport Abstraction

| Transport Pathway | Transport Modes | Transport Parameters and Data Sources |
|---------------------------|--|---|
| 1. Through 7. | None | No transport is expected along pathways 1. through 7. (see Section 6.4) |
| 8. WP to invert (F_8) | Diffusion through SCCs; Diffusion and advection through patches; Diffusion and advection through pits (if present) | Fluid flux for advection = F_8 ; No retardation in waste form/WP; No lateral or forward dispersion; Colloidal particles will transport radionuclides. Diffusive area for each SCC is given by $4.08 \times 10^{-6} \text{ m}^2$ (see Sections 6.3.1.2.1 and 6.4.3); Diffusive area for each patch is $2.346 \times 10^4 \text{ (mm)}^2$ (1000 nodes on the surface of the WP); Diffusive length in WP is 135 mm to 185 mm depending on WP type (see Section 6.4.3) Diffusion coefficient (all radionuclides): - $2.299 \times 10^{-5} \text{ cm}^2/\text{s}$ at 25°C (see Section 6.4.1.1) - Corrected for porosity, saturation and temperature (see Sections 6.4.1.2 and 6.4.1.3) |
| 9. Invert to UZ (F_9) | Diffusion and advection through the invert; | Fluid flux for advection = $F_9 = F_8$; No retardation in waste form/WP; No lateral or forward dispersion; Colloidal particles will transport radionuclides. Diffusive length = 0.606 m (max thickness of invert; see Table 1); Diffusion coefficient (all radionuclides): - $2.299 \times 10^{-5} \text{ cm}^2/\text{s}$ at 25°C (see Section 6.4.1.1) - Corrected for porosity, saturation and temperature (see Sections 6.4.1.2 and 6.4.1.3) Cross-sectional areas assume a cylindrical geometry, corresponding to the WP lying on the invert. |

The thermal and mechanical response of the DS is an important factor in EBS performance. The thermal and mechanical response of the DS has been evaluated for five mechanisms: (1) thermal expansion, (2) floor heave, (3) rock fall, (4) seismic response, and (5) pedestal failure.

Thermal expansion, floor heave and rock fall will produce minor structural response in relation to the potential slippage or overlap between adjacent DSs. These mechanisms have therefore been screened out from the TSPA-SR.

Seismic response is the key mechanism that may lead to separation of adjacent DSs. The seismic analysis in this AMR is based on the 1-in-10,000 year earthquake. This analysis assumes that all the inelastic strain from the earthquake can be concentrated at one or a few locations and that the sand backfill is not represented in the analysis. The sand backfill is important because of its large mass relative to that of the DS. These are conservative features, but it is not possible to state that the seismic response model is a reasonable bound because of the need for more detailed

structural response calculations. Future analyses will consider less probable earthquakes, such as a 1-in-100,000 year event, different excitation models (axial and transverse to the drift), and the response of the other components (i.e., the backfill) of the EBS.

7.2 EVALUATION OF NRC ISSUE RESOLUTION STATUS REPORT CRITERIA

This document defines the abstraction model for flow of liquid and transport of radionuclides through the EBS. Being conceptual in nature, it is not possible to evaluate many of the IRSR acceptance criteria in Section 4.2. For example, sensitivity studies have not yet been performed with the full TSPA-SR model and are beyond the scope of this document.

The relevance of this AMR to the NRC IRSR criteria (NRC 1999a) for the ENFE KTI is as follows:

From Section 4.2.1.1 (Applicable Data and Model Justification Acceptance Criteria), Criteria 1, 2, and 3 are addressed by this abstraction. With regard to Criterion 3, much of the data used in this abstraction needs further work in terms of its completeness and its quality assurance. Criteria 4 and 5 are outside the scope of this AMR.

From Section 4.2.1.2 (Applicable Data Uncertainty and Verification Acceptance Criteria), Criteria 1, 2, and 3 are addressed by this abstraction. With regard to Criterion 2, much of the data used in this abstraction needs further work in terms of its completeness and its quality assurance. Criteria 4 and 5 are outside the scope of this AMR.

For Section 4.2.1.3 (Model Uncertainty Acceptance Criteria), Criteria 2 and 3 are addressed by this AMR. Note that other alternative modeling approaches may be considered in response to future design changes for the EBS. Criterion 1 is outside the scope of this AMR.

For Section 4.2.1.4 (Model Verification Acceptance Criteria), Criterion 1 is addressed by this abstraction. Criteria 2 and 3 require computational testing that is beyond the scope of this AMR.

For Section 4.2.1.5 (Integration Acceptance Criteria), Criteria 1 and 2 are addressed by this abstraction. Criteria 3 and 4 require computational testing and sensitivity studies that are beyond the scope of this AMR.

For Section 4.2.1.6 (Programmatic Acceptance Criteria), Criterion 1 is addressed by this abstraction. With regard to Criterion 2, much of the data used in this abstraction needs further work in terms of its completeness and its quality assurance. Criterion 3 is not applicable to this AMR because expert elicitation has not been used to develop this abstraction.

The relevance of this AMR to the NRC IRSR criteria (NRC 1999b) for the CLST KTI is as follows:

For Section 4.2.2.1 (General Acceptance Criteria for All Subissues), Criteria 1, 3, 5, 6, 7, and 9 are addressed in this AMR. Again, much of the data used in this abstraction needs further work in terms of its completeness and its quality assurance before Criterion 3 can be resolved. Criteria 2, 4 and 8 are outside the scope of this AMR.

For Section 4.2.2.2 (Applicable Acceptance Criteria for Subissues 3 and 4), these criteria are not directly addressed in this AMR. The emphasis in these criteria is on the mobilization of radionuclides from SNF and HLW, rather than transport through the EBS to the UZ. Criteria 2, 3, and 4 involve detailed calculations or testing and are beyond the scope of this AMR. The final element of Criterion 1, release of radionuclides from the WP emplacement drifts, is addressed by this AMR.

For Section 4.2.2.3 (Applicable Acceptance Criteria for Subissue 6), criteria 1 and 2 are addressed by this AMR. Criterion 3 is beyond the scope of this AMR.

The relevance of this AMR to the NRC IRSR criteria (NRC 1998) for the TEF KTI is as follows:

For Section 4.2.3.1 (Acceptance Criteria for Subissue 3), criteria 1, 2, 3, and 4 are addressed by this AMR. With regard to the need for sufficient data in criterion 4, much of the data used in this abstraction needs additional work in terms of its completeness and quality assurance before this criterion can be resolved with the NRC.

7.3 RECOMMENDATIONS FOR FUTURE WORK

Further work is required to refine certain bounding approximations that have been made in developing the EBS RT Abstraction. Specific areas of interest include: (a) modeling the DS separation for the 1-in-10,000 year earthquake and for a less likely (but stronger) earthquake. This seismic analysis should include the DS response for ground motions propagating both axially and transverse to the drift; (b) modeling the DS response for rock fall events, particularly after the DS has degraded from general corrosion; (c) analyzing potential DS failure modes in response to thermal expansion when there is little or no slippage between adjacent DSs; (d) modeling the diffusivity in the invert as a function of saturation and porosity; (e) determining the conditions under which condensation will occur on the inside of the DS in the repository environment; and (f) using the separation between adjacent WPs to split the flux through the DS into a flux that falls on the WP and a flux that falls directly to the invert.

In order to avoid procedural ambiguity in AP-3.10Q with respect to model validation, this conceptual model has not undergone validation. The EBS RT Abstraction will be verified through comparison to outputs of detailed process models, empirical observations, analytic solutions, or hand calculations, as appropriate.

7.4 TO BE VERIFIED (TBV) IMPACT

There can be significant impacts to this conceptual model due to potential changes in TBV inputs. There are two TBV input items defined in this AMR that pertain to these impacts: (1) the self-diffusivity of water at 25°C (2.399×10^{-5} cm²/s) (MO0002SPASDC00.002), and (2) the parameters for the seismic response of the DS (MO0003SPASEI01.003).

The self-diffusivity of water is used as a bounding value for the diffusion coefficient of all radionuclides considered in the TSPA-SR. The numerical value of the self-diffusivity directly impacts the magnitude of diffusive transport through the EBS to the UZ. The

The response of the DS to a seismic event is a key performance issue for the EBS. An intact DS diverts water away from the WP, thereby maintaining a dry environment around the WP. The parameters in the abstraction for the seismic response of the DS are the maximum displacement in a drift (250 mm), the number of gaps in a drift (up to 3), the frequency of seismic events (10^{-4} per year), and the maximum number of seismic events (5). The seismic response of the DS directly impacts advective transport through the EBS to the UZ.

This document may be affected by technical product input information that requires confirmation. Any changes to the document that may occur as a result of completing the confirmation activities will be reflected in subsequent revisions. The status of the input information quality may be confirmed by review of the Document Input Reference System database.

7.5 FEPS EVALUATION

Although the FEPs found in Table 2 are discussed in this document, they cannot be fully resolved until the results with this conceptual model are evaluated through a complete analysis and sensitivity study of results from the TSPA-SR.

8. REFERENCES

8.1 DOCUMENTS CITED

Atkins P.W. 1990. *Physical Chemistry*. 4th Edition. New York, New York: W. H. Freeman and Company. TIC: 245483.

Baumeister, T. and Marks, L.S. 1967. *Standard Handbook for Mechanical Engineers*. 7th Edition. New York, New York: McGraw Hill Book Co. TIC: 231635.

Cantrel, L.; Chaouche, R.; and Chopin-Dumas, J. 1997. "Diffusion Coefficients of Molecular Iodine in Aqueous Solutions." *Journal Chemical Engineering Data*, 42, 216-220. Washington, D.C.: American Chemical Society. TIC: 246757.

CRWMS M&O (Civilian Radioactive Waste Management Services Management and Operations) 1998a. "Waste Form Degradation, Radionuclide Mobilization, and Transport Through the Engineered Barrier System." Chapter 6 of *Total System Performance Assessment-Viability Assessment (TSPA-VA) Analyses Technical Basis Document*. B00000000-01717-4301-00006 REV 01. Las Vegas, Nevada: CRWMS M&O. ACC: MOL.19981008.0006.

CRWMS M&O 1998b. *AREST-CT Parameter Input: Calculation of Spent Fuel Volume Fraction, Porosity, and Radius*. B00000000-01717-0210-00025 REV 01. Las Vegas, Nevada: CRWMS M&O. ACC: MOL.19981030.0236.

CRWMS M&O 1998c. *Software Routine Report for WAPDEG (Version 3.11)*. CSCI: 30074 v 3.11. DI: 30074-2999, Rev. 00. Las Vegas, Nevada: CRWMS M&O. ACC: MOL.19981026.0040.

CRWMS M&O 1998d. *Repository Ground Support Analysis for Viability Assessment*. BCAA00000-01717-0200-00004 REV 01. Las Vegas, Nevada: CRWMS M&O. ACC: MOL.19980512.0714.

CRWMS M&O 1999a. *Develop the EBS Radionuclide Transport Abstraction Model for TSPA-LA*. TDP-WIS-PA-000001 REV 00. Las Vegas, Nevada: CRWMS M&O. ACC: MOL.19991214.0634.

CRWMS M&O 1999b. *Conduct of Performance Assessment*. Activity Evaluation, September 30, 1999. Las Vegas, Nevada: CRWMS M&O. ACC: MOL.19991028.0092.

CRWMS M&O 1999c. *Enhanced Design Alternative (EDA) II Repository Estimated Waste Package Types, Descriptions and Quantities*. Input Transmittal PA-WP-99184.Tc. Las Vegas, Nevada: CRWMS M&O. ACC: MOL.19991209.0053.

CRWMS M&O 1999d. *Request for Repository Subsurface Design Information to Support TSPA-SR*. Input Transmittal PA-SSR-99218.Tb. Las Vegas, Nevada: CRWMS M&O. ACC: MOL.19990901.0311.

CRWMS M&O 1999e. *Request For Input on the Dimensions/Design of Drip Shield Connector*. Input Request PA-WP-99420.R. Las Vegas, Nevada: CRWMS M&O. ACC: MOL.19991217.0212.

CRWMS M&O 1999f. *Waste Package Design Input for Geochemical Analysis*. Input Transmittal PA-WP-99294.T. Las Vegas, Nevada: CRWMS M&O. ACC: MOL.19991014.0108.

CRWMS M&O 1999g. *Waste Package Dimensions for License Application Design Selection, Phase 2, Enhanced Design Alternatives (EDA)*. Design Input Transmittal SSR-WP-99173.T. Las Vegas, Nevada: CRWMS M&O. ACC: MOL.19990421.0166.

CRWMS M&O 1999h. *Waste Package Design and Corrosion Information Engineered Barrier System Organization (EBSO) – Water Diversion Model and Radionuclide Transport Models*. Input Transmittal EBS-WP-99244.T. Las Vegas, Nevada: CRWMS M&O. ACC: MOL.19991018.0167.

CRWMS M&O 1999i. *YMP FEP Database Rev. 00C*. Las Vegas, Nevada: CRWMS M&O. ACC: MOL.19991214.0518; MOL.19991214.0519.

CRWMS M&O 1999j. *Abstraction of NFE Drift Thermodynamic Environment and Percolation Flux (E0130)*. TDP-EBS-HS-000003 REV 00. Las Vegas, Nevada: CRWMS M&O. ACC: MOL.19990831.0080.

CRWMS M&O 1999k. *Laboratory Testing and Characterization of Properties for the Engineering Plan: Evaluation of Alternative Design Features Engineered Barrier System*.

Design Input Transmittal EBS-NEP-99053.T. Las Vegas, Nevada: CRWMS M&O. ACC: MOL.19990315.0053.

CRWMS M&O 2000a. *Waste Package Emplacement Configurations*. Input Transmittal PA-WP-00009.T. Las Vegas, Nevada: CRWMS M&O. ACC: MOL.20000131.0181.

CRWMS M&O 2000b. *WAPDEG Analysis of Waste Package and Drip Shield Degradation*. Input Transmittal 00087.T. Las Vegas, Nevada: CRWMS M&O. ACC: MOL.20000310.0339.

CRWMS M&O 2000c. *Abstraction of Drift Seepage*. ANL-NBS-MD-000005 REV 00. Las Vegas, Nevada: CRWMS M&O. ACC: MOL.20000322.0671.

CRWMS M&O 2000d. *Seepage Model for PA Including Drift Collapse*. MDL-NBS-HS-000002. Las Vegas, Nevada: CRWMS M&O. Submit to RPC URN-0023.

CRWMS M&O 2000e. *Multiscale Thermohydrologic Model*. ANL-EBS-MD-000049 REV 00. Las Vegas, Nevada: CRWMS M&O. Submit to RPC URN-0019.

CRWMS M&O 2000f. *Water Diversion Model*. ANL-EBS-MD-000028 REV 00. Las Vegas, Nevada: CRWMS M&O. ACC: MOL.20000107.0329.

CRWMS M&O 2000g. *Stress Corrosion Cracking of the Drip Shield, the Waste Package Outer Barrier and the Stainless Steel Structural Material*. Input Transmittal 00218.T. Las Vegas, Nevada: CRWMS M&O. ACC: MOL.20000411.0232.

CRWMS M&O 2000h. *Invert Diffusion Properties Model*. ANL-EBS-MD-000031 REV 00. Las Vegas, Nevada: CRWMS M&O. ACC: MOL.20000203.0694.

CRWMS M&O. 2000i. *Waste Form Colloid-Associated Radionuclide Concentrations Limits: Abstraction and Summary*. Input Transmittal 00175.T. Las Vegas, Nevada: CRWMS M&O. ACC: MOL.20000328.0644.

CRWMS M&O 2000j. *In-Drift Colloids and Concentrations*. ANL-EBS-MD-000042 REV 00. Las Vegas, Nevada: CRWMS M&O. Submit to RPC URN-0196.

CRWMS M&O 2000k. *Drift Degradation Analysis*. ANL-EBS-MD-000027 REV 00. Las Vegas, Nevada: CRWMS M&O. ACC: MOL.20000107.0328.

Freeze, R.A. and Cherry, J.A. 1979. *Groundwater*. Englewood Cliffs, New Jersey: Prentice-Hall. TIC: 217571.

Glass, R.J. and Nicholl, M.J. 1996. *Physics of Gravity-Driven Fingering of Immiscible Fluids Within Porous Media: An Overview of Current Understanding and Selected Complicating Factors*. SAND951278J. Albuquerque, New Mexico: Sandia National Laboratories. TIC: 231436.

Gray, D.E., ed. 1972. "Table 2p-2. Diffusion Coefficients of Concentrated Aqueous Solutions of Electrolytes at 25C." *American Institute of Physics Handbook*. 3rd Edition. Page 2-223. New York, New York: McGraw-Hill Book Company. Copyright Requested Library Tracking Number-247425.

Haltier, E.; Fourest, B.; and David, F. 1990. "Spectroelectrochemical Study of Uranium and Cerium in Carbonate Media ." *Radiochimica Acta*, 51, 107-112. München, Germany: R. Oldenbourg Verlag. TIC: 246868.

Howard, C. 2000. EBS Testing Program Pilot-Scale Testing: ¼ Scale Engineering Demonstration Testing, Canister #3. Three volumes. Scientific Notebook SN-SNL-SCI-013-V1 through V3. ACC: MOL.20000302.0344.

Lide, D.R. and Frederikse, H.P.R., eds. 1997. *CRC Handbook of Chemistry and Physics*. 78th Edition. Boca Raton, Florida: CRC Press. TIC: 243741.

Liu, H.H.; Doughty, C.; and Bodvarsson, G.S. 1998. "An Active Fracture Model for Unsaturated Flow and Transport in Fractured Rocks." *Water Resources Research*, 34, (10), 2633-2646. Washington, D.C.: American Geophysical Union. TIC: 243012.

McCord, J.T.; Stephens, D.B.; and Wilson, J.L. 1991. "Hysteresis and State-Dependent Anisotropy in Modeling Unsaturated Hillslope Hydrologic Processes." *Water Resources Research*, 27, (7), 1501-1508. Washington, D.C.: American Geophysical Union. TIC: 246831.

McCord, J.T.; Gotway, C.A.; and Conrad, S.H. 1997. "Impact of Geologic Heterogeneity on Recharge Estimation Using Environmental Tracers: Numerical Modeling Investigation." *Water Resources Research*, 33, (6), 1229-1240. Washington, D.C.: American Geophysical Union. TIC: 238284.

Millard, A.R. and Hedges, R.E.M. 1996. "A Diffusion-Adsorption Model of Uranium Uptake by Archaeological Bone." *Geochimica et Cosmochimica Acta*, 60, (12), 2139-2152. New York, New York: Pergamon Press. TIC: 246791.

Mills, R. 1973. "Self-Diffusion in Normal and Heavy Water in the Range 1-45°." *The Journal of Physical Chemistry*, 77, (5), 685-688. Washington, D.C.: American Chemical Society. TIC: 246404.

Mills, R., and Lobo, V.M.M. 1989. *Self-Diffusion in Electrolyte Solutions: A Critical Examination of Data Compiled from the Literature*. Physical Sciences Data 36. Amsterdam, Netherlands: Elsevier Science Publishers. On Order Library Tracking Number-L1572.

Mohanty, S.; Cragolino, G.; Ahn, T.; Dunn, D.S.; Lichtner, P.C.; Manteufel, R.D.; and Sridhar, N. 1996. *Engineered Barrier System Performance Assessment Code: Ebspac Version 1.0B Technical Description and User's Manual*. CNWRA 96-011. San Antonio, Texas: Center for Nuclear Waste Regulatory Analyses. TIC: 233382.

Nitao, J.J. 1998. *Reference Manual for the NUFT Flow and Transport Code, Version 2.0*. UCRL-MA-130651. Livermore, California: Lawrence Livermore National Laboratory. TIC: 238072.

Perry, D.L.; Phillips, S.L.; and Chung, J.D. 1988. "Potentiostatic Measurement of the Diffusion Coefficient of UO_2^{2+} in Carbonate Media." *Inorganica Chimica Acta*, 149, 301-304. Lausanne, Switzerland: Elsevier Sequoia SA. TIC: 246806.

Philip, J.R.; Knight, J.H.; and Waechter, R.T. 1989. "Unsaturated Seepage and Subterranean Holes: Conspectus, and Exclusion Problem for Circular Cylindrical Cavities." *Water Resources Research*, 25, (1), 16-28. Washington, D.C.: American Geophysical Union. TIC: 239117.

Rosch, F., and Khalkin, V.A. 1990. "Ion mobilities of Trivalent f-Elements in Aqueous Electrolytes." *Radiochimica Acta*, 51, 101-106. Munich, Germany: R. Oldenbourg Verlag. TIC: 246710.

Tada, H.; Paris, P.C.; and Irwin, G.R. 1973. *The Stress Analysis of Cracks Handbook*. St. Louis, Missouri: Del Research Corporation. TIC: 247050.

Tang, S.S.; Herrera, M.L.; Gordon, B.M.; Gordon, G.M.; and Lu, S. 1999. *Weld Residual Stress Analyses of Closure Lid Welds for the Yucca Mountain Project Potential Waste Packages*. Livermore, California: Lawrence Livermore National Laboratory. ACC: MOL.19991223.0421.

Tsukamoto, M.; Ohe, T.; Fujita, T.; Hesbol, R.; and Hermansson, H-P. 1994. "Diffusion of Neptunium(V) in Loosely Compacted Sodium Bentonite." *Radiochimica Acta*, 66/67, 397-403. München, Germany: R. Oldenbourg Verlag. TIC: 246893.

8.2 CODES, STANDARDS, REGULATIONS, AND PROCEDURES

AP-3.10Q, Rev. 2, ICN 0. *Analyses and Models*. Washington, D.C.: U.S. Department of Energy, Office of Civilian Radioactive Waste Management. ACC: MOL.20000217.0246.

AP-3.14Q Rev. 0, ICN 0. *Transmittal of Input*. Washington, D.C.: U.S. Department of Energy, Office of Civilian Radioactive Waste Management. ACC: MOL.19990701.0621.

DOE (U.S. Department of Energy) 2000. *Quality Assurance Requirements and Description*. DOE/RW-0333P, Rev. 9. Washington, D.C.: U.S. Department of Energy, Office of Civilian Radioactive Waste Management. ACC: MOL.19991028.0012.

Dyer, J.R. 1999. "Revised Interim Guidance Pending Issuance of New U.S. Nuclear Regulatory Commission (NRC) Regulations (Revision 01, July 22, 1999), for Yucca Mountain, Nevada." Letter from Dr. J.R. Dyer (DOE/YMSCO) to Dr. D.R. Wilkins (CRWMS M&O), September 3, 1999, OL&RC:SB-1714, with enclosure, "Interim Guidance Pending Issuance of New NRC Regulations for Yucca Mountain (Revision 01)." ACC: MOL.19990910.0079.

Kotra, J.P.; Lee, M.P.; Eisenberg, N.A.; and DeWispelare, A.R. 1996. *Branch Technical Position on the Use of Expert Elicitation in the High-Level Radioactive Waste Program*. NUREG-1563. Washington, D.C.: U.S. Nuclear Regulatory Commission. TIC: 226832.

NRC (U.S. Nuclear Regulatory Commission) 1998. *Issue Resolution Status Report Key Technical Issue: Thermal Effects on Flow*. Rev.1. Washington, D.C.: U.S. Nuclear Regulatory Commission. ACC: MOL.19990317.0357.

NRC 1999a. *Issue Resolution Status Report Key Technical Issue: Evolution of the Near-Field Environment*. Rev. 2. Washington, D.C.: U.S. Nuclear Regulatory Commission. ACC: MOL.19990810.0640.

NRC 1999b. *Issue Resolution Status Report Key Technical Issue: Container Life and Source Term*. Rev. 2. Washington, D.C.: U.S. Nuclear Regulatory Commission. TIC: 245538.

NLP-2-0, REV. 5, *Determination of Importance Evaluations*, Las Vegas, Nevada: CRWMS M&O. ACC: MOL.19981116.0120.

QAP-2-0, Rev. 5. *Conduct of Activities*. Las Vegas, Nevada: CRWMS M&O. ACC: MOL.19980826.0209.

QAP-2-3, Rev 10, *Classification of Permanent Items*, Las Vegas, Nevada: CRWMS M&O. ACC: MOL.19990316.006.

8.3 SOURCE DATA, LISTED BY DATA TRACKING NUMBER

MO0002SPASDC00.002. Self-Diffusion Coefficient of Water. Submittal date: 02/24/2000.

MO0003SPASEI01.003. Seismic Response. Submittal date: 03/22/2000.

MO0003RIB00071.000. Physical and Chemical Characteristics of Alloy 22. Submittal date: 3/13/00.

SN9908T0872799.004. Tabulated In-Drift Geometric and Thermal Properties Used In Drift-Scale Models for TSPA-SR (Total System Performance Assessment-Site Recommendation). Submittal date: 08/30/1999.

9. ATTACHMENTS

| Attachment | Title |
|------------|--|
| I | Slippage and Overlap Between Adjacent Drip Shields |
| II | Analytic Solution for the Primary Case, $t > T_{fill}$ |

I. SLIPPAGE AND OVERLAP BETWEEN ADJACENT DRIP SHIELDS

The range of values for slippage and overlap between adjacent DSs is calculated for two bounding cases: (1) zero slippage, when the lower connector guide is directly against the outermost connector guide on the connector assembly, and (2) maximum slippage, when the lower connector guide is directly against the innermost connector guide on the connector assembly. Parameter values are based on the drip shield design in CRWMS M&O 1999c and the connector assembly design in CRWMS 1999e. The design configuration, as shown in Figures I.1 and I.2, assumes that the weld or other attachment technique between the connector plate and the DS does not impede slippage or block the relative displacement between adjacent DSs.

The results for these two bounding cases show that the slippage between adjacent DSs varies between 0 mm and 434 mm and the overlap between adjacent DSs varies between 200 mm and 635 mm.

Case 1: Zero slippage

The overlap between adjacent DSs can be calculated as the sum of the following dimensions:

- Distance from edge of the connector assembly to the outermost connector guide 50 mm
 - Width of the connector guide on the connector assembly 25.4 mm
 - Width of the connector guide on the lower DS 25 mm
 - Distance from edge of lower DS to the connector guide 100 mm
- Minimum Overlap 200 mm

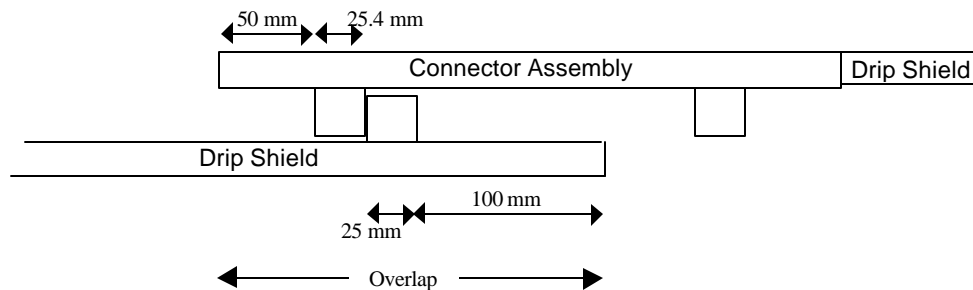


Figure I.1. Minimum Overlap for Adjacent Drip Shields

Case 2: Maximum Slippage

The slippage between adjacent DSs can be calculated as the width of the connector assembly minus the following lengths:

- Width of the connector assembly 610 mm
 - Minus twice the distance from edge of connector assembly to the guide -2 x 50 mm
 - Minus twice the width of the guide on the connector assembly -2 x 25.4 mm
 - Minus the width of the guide on the lower DS -25 mm
- Maximum Slippage 434 mm

The maximum overlap between adjacent DSs can be calculated as follows:

- Width of the connector assembly 610 mm
 - Minus the distance from edge of connector assembly to the guide - 50 mm
 - Minus the width of the guide on the connector assembly - 25.4 mm
 - Plus the distance from the edge of the lower shield to the guide + 100 mm
- Maximum Overlap 635 mm

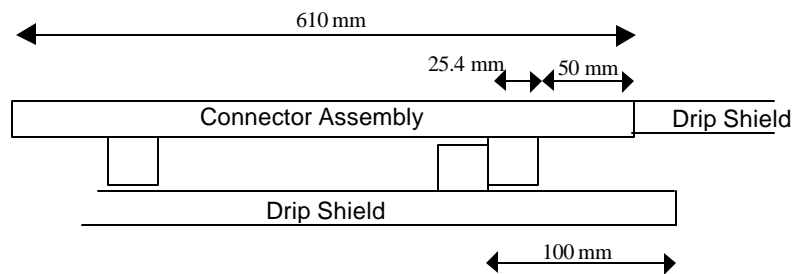


Figure I.2. Maximum Overlap for Adjacent Drip Shields

II. ANALYTIC SOLUTION FOR THE PRIMARY CASE, $t > T_{fill}$

For $t > T_{fill}$, the mass balance within the WP is given by:

$$\dot{m} = Df - q_{out} \frac{m(t)}{V_{tub}}, \quad (\text{Eq. 6.6.1-6})$$

or rearranging terms and using the condition that $q_{out} = q_{in}$,

$$\dot{m} + \frac{q_{in}}{V_{tub}} m(t) = Df. \quad (\text{Eq. II-1})$$

Multiply Equation II-1 by the integrating factor $e^{\frac{q_{in}}{V_{tub}} t}$,

$$\dot{m} e^{\frac{q_{in}}{V_{tub}} t} + \frac{q_{in}}{V_{tub}} e^{\frac{q_{in}}{V_{tub}} t} m(t) = Df e^{\frac{q_{in}}{V_{tub}} t}. \quad (\text{Eq. II-2})$$

or

$$\frac{d}{dt} \left(m(t) e^{\frac{q_{in}}{V_{tub}} t} \right) = Df e^{\frac{q_{in}}{V_{tub}} t}. \quad (\text{Eq. II-3})$$

Integrating Equation II-3 from time T_{fill} to time t :

$$m(t) e^{\frac{q_{in}}{V_{tub}} t} - m(T_{fill}) e^{\frac{q_{in}}{V_{tub}} T_{fill}} = \int_{T_{fill}}^t Df e^{\frac{q_{in}}{V_{tub}} dt}, \quad (\text{Eq. II-4})$$

$$m(t) e^{\frac{q_{in}}{V_{tub}} t} - m(T_{fill}) e^{\frac{q_{in}}{V_{tub}} T_{fill}} = \left(\frac{Df V_{tub}}{q_{in}} \right) \left(e^{\frac{q_{in}}{V_{tub}} t} - e^{\frac{q_{in}}{V_{tub}} T_{fill}} \right) \quad (\text{Eq. II-5})$$

The initial condition for Equation II-5, corresponding to $t = T_{fill}$, is determined by conditions at the end of the fill period. From Equation 6.6.1-2, the mass of radioisotope dissolved within the liquid at time T_{fill} is given by:

$$m(T_{fill}) = Df T_{fill} = Df \frac{V_{tub}}{q_{in}}. \quad (\text{Eq. II-6})$$

It follows that

$$m(t) e^{\frac{q_{in}}{V_{tub}} t} - m(T_{fill}) e^{\frac{q_{in}}{V_{tub}} T_{fill}} = m(T_{fill}) \left(e^{\frac{q_{in}}{V_{tub}} t} - e^{\frac{q_{in}}{V_{tub}} T_{fill}} \right) \quad (\text{Eq. II-7})$$

$$m(t)e^{\frac{q_{in}-t}{V_{tub}}} = m(T_{fill}) \left(e^{\frac{q_{in}-t}{V_{tub}}} \right) \quad (\text{Eq. II-8})$$

and therefore

$$m(t) = m(T_{fill}) = DfT_{fill}, \quad (\text{Eq. II-9})$$

if Equation II-8 is to hold at all values of the time, t . Equation II-9 is the same as Equation 6.6.1-7 in Section 6.6.1.